Supporting Information

Two- and three-dimensional β,β'-*N*-heterocycle fused porphyrins: concise construction, singlet oxygen production and electrocatalytic hydrogen evolution reaction

Yan Fan,[a] Zhiming Zeng,[a] Hui Shu,[a] Mingbo Zhou,*[a] Ling Xu,[a] Yutao, Rao,[a] Tingting Gu,[b] Xu Liang,[b] Weihua Zhu,[b] and Jianxin Song*[a]

[a] Key Laboratory of Chemical Biology & Traditional Chinese Medicine Research (Ministry of Education), Key Laboratory of the Assembly and Application of Organic Functional Molecules of Hunan Province, Hunan Normal University, Changsha 410081, P. R. China.
E-mail: zhoumingbo@hnnu.edu.cn and jxsong@hunnu.edu.cn
[b] School of Chemistry and Chemical Engineering, Jiangsu University, Zhenjiang 212013, P. R. China

Table of Contents

Instrumentation and Materials

^{1}H NMR (500 MHz) and ^{13}C NMR (126 MHz) spectra were taken on a Bruker AVANCE-500 spectrometer, and chemical shifts were reported as the delta scale in ppm. The residual peak of $CDCl_3$ was used as internal reference for ^{1}H NMR (δ = 7.26 ppm) and the solvent $CDCl_3$ was used as internal reference for ^{13}C NMR (δ = 77.0 ppm). UV/Vis absorption spectra were recorded on a Shimadzu UV-3600 spectrometer. MALDI-TOF mass spectra were obtained with a Bruker ultrafle Xtreme MALDI-TOF/TOF spectrometer with matrix. X-Ray data were taken on a Bruker SMART APEX X-Ray diffractometer equipped with a large area CCD detector. Cyclic voltammetry was performed in a three-electrode cell using the Chi-730D electrochemistry station. Compounds **1M-2Br**, **1M-4Br**, **1M-8Br** and **2c-2f** were prepared according to the literature procedure[S1, S2]. Unless otherwise noted, materials obtained from commercial suppliers were used without further purification.

General Procedures

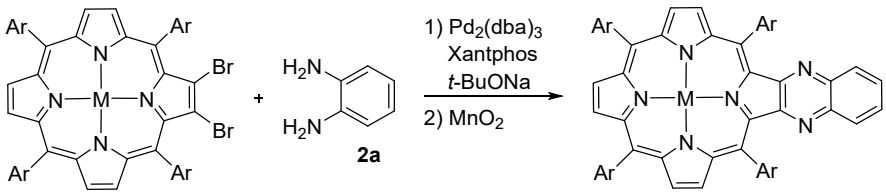

M = Ni, **1Ni-2Br**
M = Zn, **1Zn-2Br**
M = 2H, **1H-2Br**

M = Ni, **3Ni**
M = Zn, **3Zn**
M = 2H, **3H**

Synthesis of 3Ni, **3Zn**, **3H**: A *p*-Xylene solution (3 mL) of **1M-2Br** (0.05 mmol), $Pd_2(dba)_3$ (9.2 mg, 0.01 mmol), Xantphos (11.6 mg, 0.02 mmol), 1,2-diaminobenzene **2a** (5.4 mg, 0.05 mmol), *t*-BuONa (28.8 mg, 0.3 mmol) was degassed through three freeze-pump-thaw cycles, and the reaction flask was purged with argon. The resulting mixture was stirred at reflux for 48 h. Then the reaction mixture was diluted with $CHCl_3$, washed with water, and dried over anhydrous sodium sulfate. After removal of the solvent in vacuo, the residue of the reaction was dissolved in CH_2Cl_2 (20 mL). Then, MnO_2 (173.9 mg, 2.0 mmol) was added to the solution. After stirring at room temperature for 4 h, the reaction mixture was passed through short Celite® pad to remove the solids of MnO_2, concentrated in vacuo, and purified by silica gel column chromatography eluting with CH_2Cl_2/hexane. Recrystallization from CH_2Cl_2/MeOH afforded **3Ni** (38.3 mg, 0.03 mmol, 63% yield), **3Zn** (17.2 mg, 0.014 mmol, 28% yield) and **3H** (15.2 mg, 0.013 mmol, 26% yield), respectively.

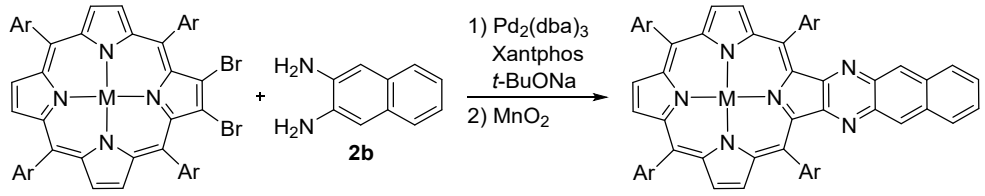

M = Ni, **1Ni-2Br**
M = Zn, **1Zn-2Br**
M = 2H, **1H-2Br**

M = Ni, **4Ni**
M = Zn, **4Zn**
M = 2H, **4H**

Synthesis of 4Ni, **4Zn**, **4H**：Replacing **2a** with **2b** (7.9 mg, 0.05 mmol), the procedures of synthesis of **4Ni**, **4Zn**, **4H** are the same with that of synthesis of **3Ni**. Recrystallization from CH_2Cl_2/MeOH afforded **4Ni** (24.2 mg, 0.019 mmol, 38% yield), **4Zn** (7.0 mg, 0.0055 mmol, 11% yield) and **4H** (3.7 mg, 0.003 mmol, 6% yield), respectively.

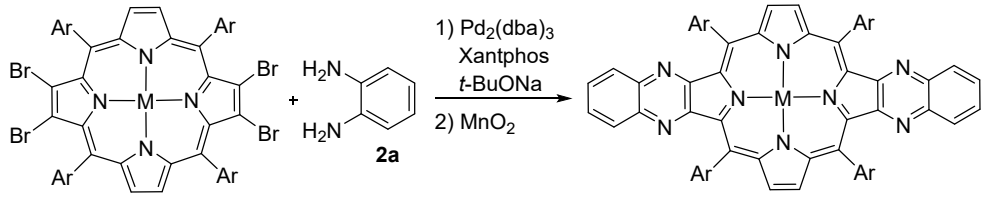

M = Ni, **1Ni-4Br**
M = Zn, **1Zn-4Br**
M = 2H, **1H-4Br**

M = Ni, **5Ni**
M = Zn, **5Zn**
M = 2H, **5H**

Synthesis of 5Ni, **5Zn**, **5H**： A *p*-Xylene solution (3 mL) of **1M-4Br** (0.05 mmol), $Pd_2(dba)_3$ (9.2 mg, 0.01 mmol), Xantphos (11.6 mg, 0.02 mmol), 1,2-diaminobenzene **2a** (9.7 mg, 0.09 mmol), *t*-BuONa (28.8 mg, 0.3 mmol) was degassed through three freeze-pump-thaw cycles, and the reaction flask was purged with argon. The resulting mixture was stirred at reflux for 48 h. Then the reaction mixture was diluted with $CHCl_3$, washed with water, and dried over anhydrous sodium sulfate. After removal of the solvent in vacuo, the residue of the reaction was dissolved in CH_2Cl_2 (20 mL). Then, MnO_2 (173.9 mg, 2.0 mmol) was added to the solution. After stirring at room temperature for 4 h, the reaction mixture was passed through short Celite® pad to remove the solids of MnO_2, concentrated in vacuo, and purified by silica gel column chromatography eluting with CH_2Cl_2/hexane. Recrystallization from CH_2Cl_2/MeOH afforded **5Ni** (22.1 mg, 0.017 mmol, 37% yield), **5Zn** (19.2 mg, 0.014 mmol, 32% yield), **5H** (10.3 mg, 0.0081 mmol, 18% yield), respectively.

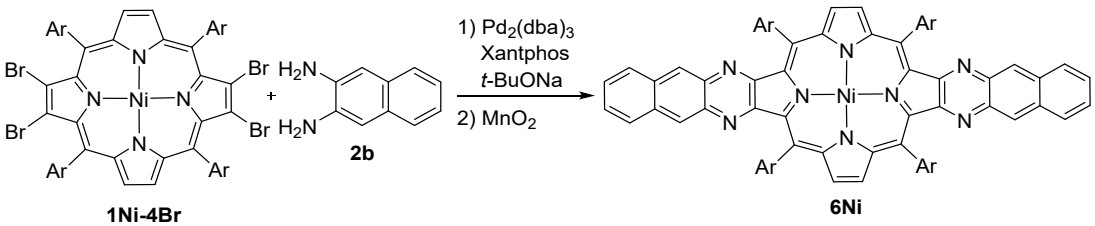

1Ni-4Br

6Ni

Synthesis of 6Ni: Replacing **2a** with **2b** (14.2 mg, 0.09 mmol), the procedures of synthesis of **6Ni** is the same with that of synthesis of **5Ni**. Recrystallization from CH_2Cl_2/MeOH afforded **6Ni** (11.5 mg, 0.0081 mmol, 18% yield).

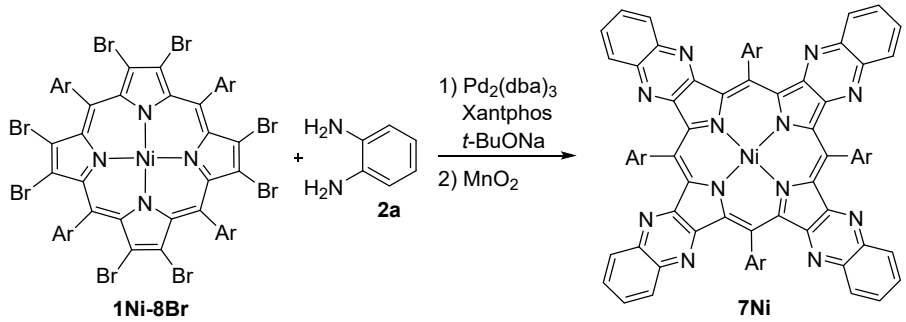

Synthesis of 7Ni: A *p*-Xylene solution (3 mL) of **1Ni-8Br** (87.7 mg, 0.05 mmol), $Pd_2(dba)_3$ (9.2 mg, 0.01 mmol), Xantphos (11.6 mg, 0.02 mmol), 1,2-diaminobenzene **2a** (19.5 mg, 0.18 mmol), *t*-BuONa (57.7 mg, 0.6 mmol) was degassed through three freeze-pump-thaw cycles, and the reaction flask was purged with argon. The resulting mixture was stirred at reflux for 48 h. Then the reaction mixture was diluted with $CHCl_3$, washed with water, and dried over anhydrous sodium sulfate. After removal of the solvent in vacuo, the residue of the reaction was dissolved in CH_2Cl_2 (20 mL). Then, MnO_2 (173.9 mg, 2.0 mmol) was added to the solution. After stirring at room temperature for 4 h, the reaction mixture was passed through short Celite® pad to remove the solids of MnO_2, concentrated in vacuo, and purified by silica gel column chromatography eluting with CH_2Cl_2/hexane. Recrystallization from CH_2Cl_2/MeOH afforded **7Ni** (17.2 mg, 0.011 mmol, 25% yield).

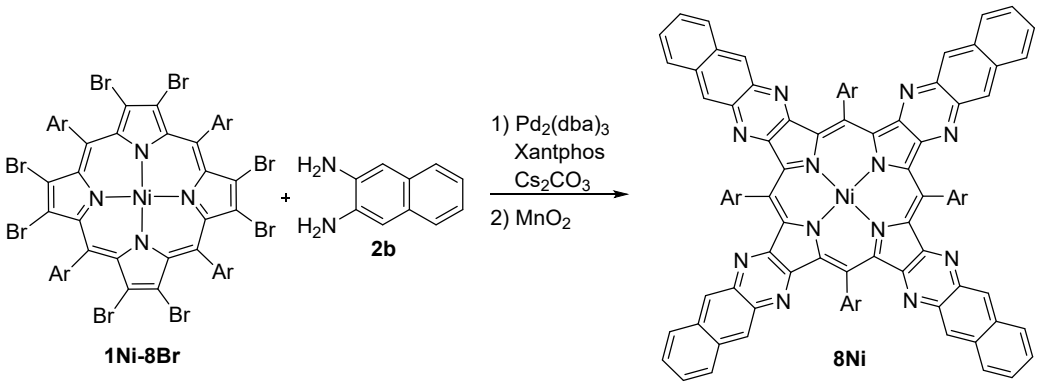

Synthesis of 8Ni: Replacing **2a** with **2b** (28.4mg, 0.18 mmol), the procedure of synthesis of **8Ni** is the same with that of synthesis of **7Ni**. Recrystallization from CH_2Cl_2/MeOH afforded **8Ni** (6.2 mg, 0.0036 mmol, 8% yield).

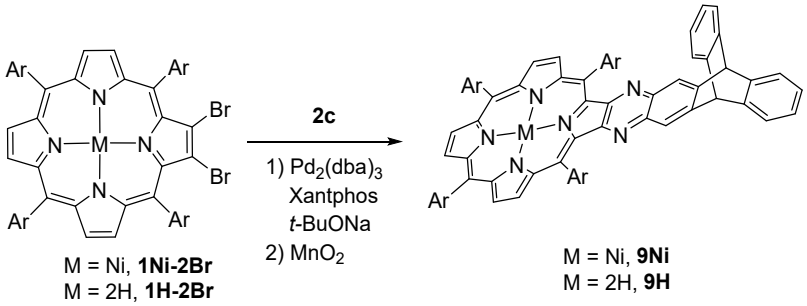

Synthesis of 9Ni: A *p*-Xylene solution (3 mL) of **1Ni-2Br** (64.0 mg, 0.05 mmol), $Pd_2(dba)_3$ (9.2 mg, 0.01 mmol), Xantphos (11.6 mg, 0.02 mmol), **2c** (14.2 mg, 0.05 mmol), *t*-BuONa (28.8 mg, 0.3 mmol)，was degassed through three freeze-pump-thaw cycles, and the reaction flask was purged with argon. The resulting mixture was stirred at reflux for 48 h. Then the reaction mixture was diluted with $CHCl_3$, washed with water, and dried over anhydrous sodium sulfate. After removal of the solvent in vacuo, the residue of the reaction was dissolved in CH_2Cl_2 (20 mL). Then, MnO_2 (173.9 mg, 2.0 mmol) was added to the solution. After stirring at room temperature for 4 h, the reaction mixture was passed through short Celite® pad to remove the solids of MnO_2, concentrated in vacuo, and purified by silica gel column chromatography eluting with CH_2Cl_2/hexane. Recrystallization from CH_2Cl_2/MeOH afforded **9Ni** (49.3 mg, 0.035 mmol, 70% yield).

Synthesis of 9H: 9Ni (15.6 mg, 0.011 mmol) was dissolved in CH_2Cl_2 (10 mL) and concentrated sulfuric acid (0.4 mL) was added. After stirring at room temperature for 6 h, the reaction mixture was washed with water, Na_2CO_3 aq., and water. The crude product was extracted with CH_2Cl_2, and the organic extract was dried over anhydrous sodium sulfate. Evaporation of the solvent followed by silica-gel column chromatography (CH_2Cl_2/hexane as an eluent) and recrystallization with CH_2Cl_2/MeOH provided **9H** (14.2 mg, 0.011 mmol, 95% yield).

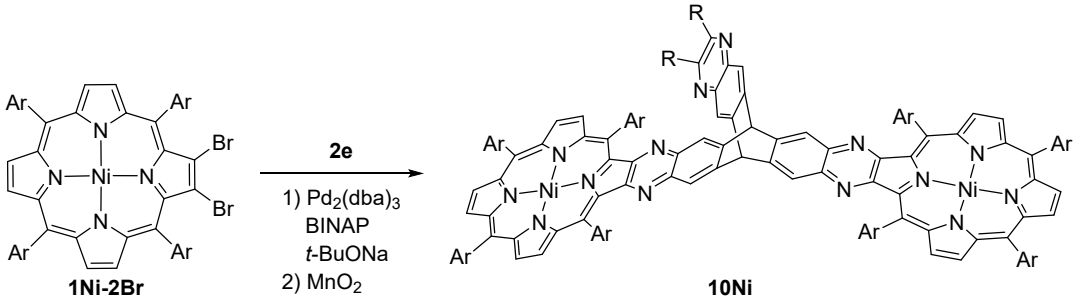

Synthesis of 10Ni: A *p*-Xylene solution (3 mL) of **1Ni-2Br** (64.0 mg, 0.05 mmol), $Pd_2(dba)_3$ (9.2 mg, 0.01 mmol), BINAP (12.5 mg, 0.02 mmol), **2e** (14.5 mg, 0.025 mmol), *t*-BuONa (57.7 mg, 0.6 mmol) was degassed through three freeze-pump-thaw cycles, and the reaction flask was purged with argon. The resulting mixture was stirred at reflux for 48 h. Then the reaction mixture was diluted with $CHCl_3$, washed with water, and dried over anhydrous sodium sulfate. After stirring at room temperature for 4 h, the reaction mixture was passed through short Celite® pad to remove the solids of MnO_2, concentrated in vacuo, and purified by silica gel column chromatography eluting with CH_2Cl_2/hexane. Recrystallization from CH_2Cl_2/MeOH afforded **10Ni** (15.4 mg, 0.0055 mmol, 22% yield).

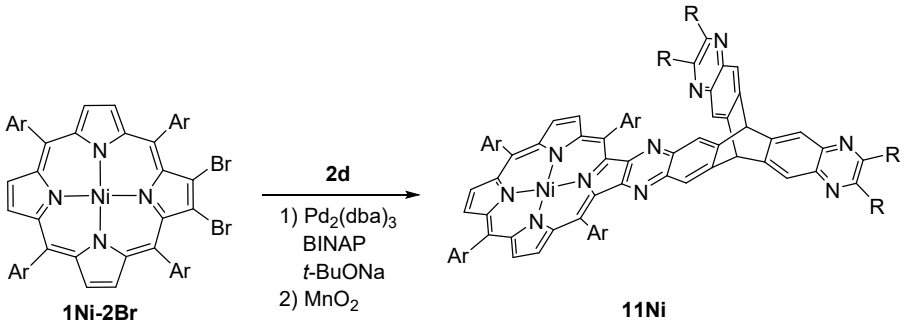

Synthesis of 11Ni: A *p*-Xylene solution (3 mL) of **1Ni-2Br** (64.0 mg, 0.05 mmol), $Pd_2(dba)_3$ (9.2 mg, 0.01 mmol), BINAP (12.5 mg, 0.02 mmol), **2d** (40.7 mg, 0.05 mmol), *t*-BuONa (28.8 mg, 0.3 mmol) was degassed through three freeze-pump-thaw cycles, and the reaction flask was purged with argon. The resulting mixture was stirred at reflux for 48 h. Then the reaction mixture was diluted with $CHCl_3$, washed with water, and dried over anhydrous sodium sulfate. After stirring at room temperature for 4 h, the reaction mixture was passed through short Celite® pad to remove the solids of MnO_2, concentrated in vacuo, and purified by silica gel column chromatography eluting with CH_2Cl_2/hexane. Recrystallization from CH_2Cl_2/MeOH afforded **11Ni** (20.2 mg, 0.011 mmol, 21% yield).

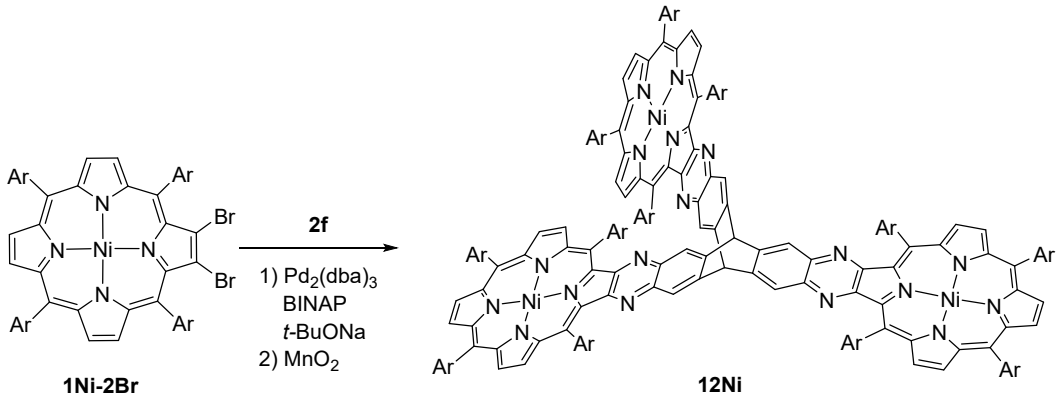

Synthesis of 12Ni: A *p*-Xylene solution (3 mL) of **1Ni-2Br** (64.0 mg, 0.05 mmol), $Pd_2(dba)_3$ (9.2 mg, 0.01 mmol), BINAP (12.5 mg, 0.02 mmol), **2f** (17.7 mg, 0.025 mmol), *t*-BuONa (57.7 mg, 0.6 mmol), triethylamine (0.1 mL) was degassed through three freeze-pump-thaw cycles, and the reaction flask was purged with argon. The resulting mixture was stirred at reflux for 48 h. Then the reaction mixture was diluted with $CHCl_3$, washed with water, and dried over anhydrous sodium sulfate. After stirring at room temperature for 4 h, the reaction mixture was passed through short Celite® pad to remove the solids of MnO_2, concentrated in vacuo, and purified by silica gel column chromatography eluting with CH_2Cl_2/hexane. Recrystallization from CH_2Cl_2/MeOH afforded **12Ni** (6.8 mg, 0.0018 mmol, 11% yield).

Synthesis of 12H: 12Ni (15.6 mg, 0.0042 mmol) was dissolved in CH_2Cl_2 (10 mL) and concentrated sulfuric acid (0.4 mL) was added. After stirring at room temperature for 6 h, the reaction mixture was washed with water, Na_2CO_3 aq., and water. The crude product was extracted with CH_2Cl_2, and the organic extract was dried over anhydrous sodium sulfate. Evaporation of the solvent followed by silica-gel column chromatography (CH_2Cl_2/hexane as an eluent) and recrystallization with CH_2Cl_2/MeOH provided **12H** (11.9 mg, 0.0034 mmol, 80% yield).

Synthesis of 12Zn: 12H (10 mg, 0.0075 mmol) was added to a round-bottomed 50-mL flask and dissolved in CH_2Cl_2 (6 mL). An excess amount of saturated zinc(II) acetate in methanol was added. After stirring for 4 h, the complete metalation was confirmed by TLC. The reaction mixture was passed through a short silica-gel column, evaporated and recrystallized from CH_2Cl_2/MeOH to give **12Zn** (9.9 mg, 0.0071 mmol, 95%).

Compound Data

3Ni[3]: ^{1}H NMR (500 MHz, $CDCl_3$): δ = 8.91 (d, 2H, *J* = 4.90 Hz, *β*-H), 8.77 (d, 2H, *J* = 4.90 Hz, *β*-H), 8.68 (s, 2H, *β*-H), 7.84 (br, 4H, Ar-H), 7.81 (br, 4H, *quinoxaline*-H and Ar-H), 7.75 (br, 2H, quinoxaline-H), 7.70 (br, 6H, Ar-H), 1.46 (br, 36H, *t*-Bu-H), 1.42 (br, 36H, *t*-Bu-H) ppm; ^{13}C NMR (126 MHz, $CDCl_3$): δ = 150.88, 149.20, 149.13, 143.92, 141.86, 141.06, 140.60, 139.37, 139.06, 133.36, 133.07, 131.65, 131.26, 130.25, 128.92, 128.30, 127.65, 122.14, 121.29, 120.77, 116.66, 35.00, 34.92, 31.79, 31.68 ppm; HR-MS (MALDI-TOF-MS): *m/z* = 1220.6861 $[M]^+$, calcd for $(C_{82}H_{94}N_6Ni)^+$ = 1220.6893; λ_{max} (ε $[M^{-1}cm^{-1}]$) = 406 (54525), 444 (55815), 556 (6826), 600 (7396).

3Zn[3]: ^{1}H NMR (500 MHz, $CDCl_3$): δ = 9.05 (d, 2H, *J* = 4.65 Hz, *β*-H), 9.00 (d, 2H, *J* = 4.65 Hz, *β*-H), 8.90 (s, 2H, *β*-H), 8.09 (d, 4H, *J* = 1.85 Hz, Ar-H), 7.96 (d, 4H, *J* = 1.85 Hz, Ar-H), 7.92 (s, 2H, Ar-H), 7.91 (dd, 2H, *J* = 6.45, 3.45 Hz, *quinoxaline*-H), 7.80 (br, 4H, Ar-H and *quinoxaline*-H), 1.53 (s, 36H, *t*-Bu-H), 1.48 (s, 36H, *t*-Bu-H) ppm; HR-MS (MALDI-TOF-MS): *m/z* = 1226.6839 $[M]^+$, calcd for $(C_{82}H_{94}N_6Zn)^+$ = 1226.6831; λ_{max} (ε $[M^{-1}cm^{-1}]$) = 415 (75239), 440 (80714), 530 (5105), 567 (10901), 610 (9176).

3H[3]: ^{1}H NMR (500 MHz, $CDCl_3$): δ = 9.07 (d, 2H, *J* = 4.90 Hz, *β*-H), 8.99 (d, 2H, *J* = 4.90 Hz, *β*-H), 8.79 (s, 2H, *β*-H), 8.10 (d, 4H, *J* = 1.85 Hz, Ar-H), 7.97 (br, 4H, Ar-H), 7.93 (s, 2H, Ar-H), 7.83 (br, 4H, Ar-H and *quinoxaline*-H), 7.74 (dd, 2H, *J* = 6.40, 3.35 Hz, *quinoxaline*-H), 1.53 (s, 36H, *t*-Bu-H), 1.48 (s, 36H, *t*-Bu-H), -2.51 (s, 2H, NH) ppm; HR-MS (MALDI-TOF-MS): *m/z* = 1164.7668 $[M]^+$, calcd for $(C_{82}H_{96}N_6)^+$ = 1164.7696; λ_{max} (ε $[M^{-1}cm^{-1}]$) = 430 (132681), 528 (11734), 562 (4508), 597 (6396).

4Ni: ^{1}H NMR (500 MHz, $CDCl_3$): δ = 8.82 (d, 2H, *J* = 4.65 Hz, *β*-H), 8.72 (d, 2H, *J* = 4.60 Hz, *β*-H), 8.63 (s, 2H, *β*-H), 8.40 (s, 2H, *quinoxaline*-H), 8.13 (m, 2H, *quinoxaline*-H), 7.85 (m, 6H, Ar-H and quinoxaline-H), 7.72 (m, 6H, Ar-H and quinoxaline-H), 7.56 (m, 2H, *quinoxaline*-H), 1.46 (br, 72H, *t*-Bu-H) ppm; ^{13}C NMR (126 MHz, $CDCl_3$): δ = 151.86, 149.31, 149.14, 144.26, 144.23, 141.86, 141.84, 140.30, 139.25, 139.23, 138.95, 138.13, 133.66, 133.52, 133.14, 131.40, 131.00, 128.51, 128.32, 128.21, 127.60, 125.97,.122.63, 121.30, 120.85, 116.17, 34.99, 34.94, 31.80, 31.67 ppm; HR-MS (MALDI-TOF-MS): *m/z* =

1270.6967 $[M]^+$, calcd for $(C_{86}H_{96}N_6Ni)^+$ = 1270.7050; λ_{max} (ε [$M^{-1}cm^{-1}$]) = 349 (36978), 420 (153332), 472 (59371), 634 (14488).

4Zn: ^{1}H NMR (500 MHz, $CDCl_3$): δ = 9.01 (d, 2H, *J* = 4.85 Hz, *β*-H), 8.98 (d, 2H, *J* = 4.50 Hz, *β*-H), 8.86 (s, 2H, *β*-H), 8.49 (s, 2H, *quinoxaline*-H), 8.20 (m, 2H, *quinoxaline*-H), 8.09 (d, 4H, *J* = 1.5 Hz, Ar-H), 7.99 (s, 6H, Ar-H), 7.79 (s, 2H, Ar-H), 7.60 (m, 2H, *quinoxaline*-H), 1.53 (br, 36H, *t*-Bu-H), 1.51 (br, 36H, *t*-Bu-H) ppm; ^{13}C NMR (126 MHz, $CDCl_3$): δ = 152.95, 151.80, 149.66, 148.97, 148.64, 142.35, 141.65, 141.49, 138.14, 133.49, 132.43, 131.44, 131.26, 129.26, 128.63, 128.60, 128.20, 125.93, 125.21, 120.93, 120.64, 118.34, 35.07, 35.03, 31.94, 31.78 ppm; HR-MS (MALDI-TOF-MS): *m/z* = 1276.7101 $[M]^+$, calcd for $(C_{86}H_{96}N_6Zn)^+$ = 1276.6988; λ_{max} (ε [$M^{-1}cm^{-1}$]) = 395 (60291), 429 (185265), 472 (64002), 545 (10082), 587 (13829), 636 (20224).

4H: ^{1}H NMR (500 MHz, $CDCl_3$): δ = 9.07 (d, 2H, *J* = 4.85 Hz, *β*-H), 8.99 (d, 2H, *J* = 4.85 Hz, *β*-H), 8.78 (s, 2H, *β*-H), 8.42 (s, 2H, *quinoxaline*-H), 8.17 (m, 2H, *quinoxaline*-H), 8.11 (s, 4H, Ar-H), 8.01 (br, 6H, Ar-H), 7.81 (s, 2H, Ar-H), 7.58 (m, 2H, *quinoxaline*-H), 1.53 (br, 36H, *t*-Bu-H), 1.51 (br, 36H, *t*-Bu-H), -2.35 (s, 2H, NH) ppm; ^{13}C NMR (126 MHz, $CDCl_3$): δ = 154.78, 153.51, 149.06, 148.80, 146.33, 141.10, 140.88, 139.80, 137.96, 137.92, 134.06, 133.51, 129.51, 128.71, 128.56, 128.44, 128.10, 128.01, 125.88, 123.00, 121.09, 120.88, 117.55, 35.06, 35.03, 31.91, 31.75 ppm; HR-MS (MALDI-TOF-MS): *m/z* = 1214.7865 $[M]^+$, calcd for $(C_{86}H_{98}N_6)^+$ = 1214.7853; λ_{max} (ε [$M^{-1}cm^{-1}$]) = 430 (184363), 537 (14799), 609 (10171).

5Ni[3]: ^{1}H NMR (500 MHz, $CDCl_3$): δ = 8.96 (s, 4H, *β*-H), 7.82 (br, 8H, *quinoxaline*-H and Ar-H), 7.75 (br, 12H, *quinoxaline*-H and Ar-H), 1.43 (br, 72H, *t*-Bu-H) ppm; ^{13}C NMR (125 MHz, $CDCl_3$): δ = 150.34, 149.31, 141.57, 141.08, 138.47, 132.36, 131.89, 130.27, 129.00, 127.53, 120.95, 118.67, 34.93, 31.77 ppm; ^{13}C NMR (126 MHz, $CDCl_3$): δ = 150.32, 149.28, 141.55, 141.06, 138.45, 132.34, 131.87, 130.25, 128.97, 127.51, 120.94, 118.65, 34.92, 31.77 ppm; HR-MS (MALDI-TOF-MS): *m/z* = 1322.7009 $[M]^+$, calcd for $(C_{88}H_{96}N_8Ni)^+$ = 1322.7111; λ_{max} (ε [$M^{-1}cm^{-1}$]) = 357 (53577), 402 (49841), 461 (106709), 549 (6076), 617 (7746), 659.(16475).

5Zn[3]: ^{1}H NMR (500 MHz, $CDCl_3$): δ = 9.12 (s, 4H, *β*-H), 8.00 (br, 8H, Ar-H), 7.95 (m, 8H, *quinoxaline*-H and Ar-H), 7.81 (br, 4H, *quinoxaline*-H), 1.50 (s, 72H, *t*-Bu-H) ppm; HR-MS (MALDI-TOF-MS): *m/z* = 1328.7080 $[M]^+$, calcd for $(C_{88}H_{96}N_8Zn)^+$ = 1328.7049; λ_{max} (ε [$M^{-1}cm^{-1}$]) = 343 (33752), 399 (82493), 459 (153398), 551 (7480), 603 (8044), 626 (9433), 653 (34013).

5H[3]: ^{1}H NMR (500 MHz, $CDCl_3$): δ = δ 9.10 (s, 4H, *β*-H), 8.00 (br, 8H, Ar-H), 7.95 (br, 4H, Ar-H,), 7.86 (m, 4H, *quinoxaline*-H), 7.76 (m, 4H, *quinoxaline*-H), 1.50 (br, 72H, *t*-Bu-H), -2.47 (s, 2H, NH) ppm; HR-MS (MALDI-TOF-MS): *m/z* = 1266.7923 $[M]^+$, calcd for $(C_{88}H_{98}N_8)^+$ = 1266.7914; λ_{max} (ε [$M^{-1}cm^{-1}$]) = 347 (33609), 445 (219791), 532 (19851), 612 (9962), 667 (8269).

6Ni: ^{1}H NMR (500 MHz, $CDCl_3$): δ = 8.90 (s, 4H, *β*-H), 8.44 (br, 4H, Ar-H), 8.16 (m, 4H, *quinoxaline*-H), 7.89 (br, 4H, *quinoxaline*-H), 7.77 (d, 8H, *J* = 1.65 Hz, Ar-H), 7.58 (m, 4H, *quinoxaline*-H), 1.48 (br, 72H, *t*-Bu-H) ppm; ^{13}C NMR (126 MHz, $CDCl_3$): δ = 151.13, 149.40, 141.56, 138.31, 138.12, 133.54, 132.62, 131.65, 128.50, 128.30, 127.46, 125.99, 121.04, 118.58, 34.95, 31.78 ppm; HR-MS (MALDI-TOF-MS): *m/z* = 1422.7351 $[M]^+$, calcd for $(C_{96}H_{100}N_8Ni)^+$ = 1422.7424; λ_{max} (ε [$M^{-1}cm^{-1}$]) = 336 (26007), 394 (72803), 482 (79325), 666 (7691), 725 (14032).

7Ni: ^{1}H NMR (500 MHz, $CDCl_3$): δ = 7.95 (m, 8H, *quinoxaline*-H), 7.88 (br, 4H, Ar-H), 7.79 (m, 8H, *quinoxaline*-H), 7.69 (br, 8H, Ar-H), 1.41 (br, 72H, *t*-Bu-H) ppm; ^{13}C NMR (126 MHz, $CDCl_3$): δ = 150.76, 149.36, 140.79, 136.52, 131.20, 130.33, 129.25, 127.21, 121.25, 117.68, 34.90, 31.89 ppm; HR-MS (MALDI-TOF-MS): *m/z* = 1526.7696 $[M]^+$, calcd for $(C_{100}H_{100}N_{12}Ni)^+$ = 1526.7547; λ_{max} (ε [$M^{-1}cm^{-1}$]) = 356 (76173), 422 (39986), 514 (68641), 649 (10905), 701 (39157).

8Ni: ^{1}H NMR (500 MHz, $CDCl_3$): δ = 8.56 (s, 8H, *quinoxaline*-H), 8.15 (m, 8H, *quinoxaline*-H), 7.80 (s, 4H, Ar-H), 7.74 (br, 8H, Ar-H), 7.57 (m, 8H, *quinoxaline*-H), 1.46 (br, 72H, *t*-Bu-H) ppm; ^{13}C NMR (126 MHz, $CDCl_3$): δ = 151.27, 149.60, 137.81, 136.30, 133.76, 131.42, 128.59, 128.53, 127.20, 126.15, 121.44, 117.42, 34.98, 31.94 ppm; HR-MS (MALDI-TOF-MS): *m/z* = 1726.8268 $[M]^+$, calcd for $(C_{116}H_{108}N_{12}Ni)^+$ = 1726.8173; λ_{max} (ε [$M^{-1}cm^{-1}$]) = 321 (53664), 384 (74720), 489 (82880), 561 (26955), 796 (34240).

9Ni: ^{1}H NMR (500 MHz, $CDCl_3$): δ = 8.88 (d, 2H, *J* = 5.05 Hz, *β*-H), 8.76 (d, 2H, *J* = 4.95 Hz, *β*-H), 8.71 (s, 2H, *β*-H), 7.85 (d, 6H, *J* = 2.05 Hz, Ar-H), 7.71 (m, 8H, triptycene aromatic C-H and Ar-H), 7.51 (br, 4H, triptycene aromatic C-H), 7.10 (br, 4H, triptycene aromatic C-H), 5.65 (s, 2H, triptycene aliphatic C-H), 1.47 (br, 72H, *t*-Bu-H) ppm; ^{13}C NMR (126 MHz, $CDCl_3$): δ = 150.50, 149.07, 149.03, 145.31, 144.08, 143.79, 141.70, 140.49, 140.08, 139.36, 139.04, 133.31, 133.00, 131.59, 131.27, 128.29, 127.67, 125.88, 123.93, 123.52, 121.86, 121.21, 120.62, 116.51, 53.81, 34.97, 34.90, 31.80, 31.66 ppm; HR-MS (MALDI-TOF-MS): *m/z* = 1396.7403 $[M]^+$, calcd for $(C_{96}H_{102}N_6Ni)^+$ = 1396.7519; λ_{max} (ε $[M^{-1}cm^{-1}]$) = 370 (96405), 408 (216154), 450 (290126), 556 (35041), 599 (31051).

9H: ^{1}H NMR (500 MHz, $CDCl_3$): δ = 9.02 (d, 2H, *J* = 4.95 Hz, *β*-H), 8.97 (d, 2H, *J* = 4.95 Hz, *β*-H), 8.77 (s, 2H, *β*-H), 8.08 (d, 4H, *J* = 1.85 Hz, Ar-H), 7.96 (br, 2H, Ar-H), 7.93 (d, 4H, *J* = 1.80 Hz, Ar-H), 7.79 (s, 2H, triptycene aromatic C-H), 7.66 (s, 2H, Ar-H), 7.51 (m, 4H, triptycene aromatic C-H), 7.08 (m, 4H, triptycene aromatic C-H), 5.65 (s, 2H, triptycene aliphatic C-H), 1.52 (br, 36H, *t*-Bu-H), 1.49 (br, 36H, *t*-Bu-H), -2.57 (s, 2H, NH) ppm; ^{13}C NMR (126 MHz, $CDCl_3$): δ = 154.73, 152.45, 148.74, 146.04, 145.15, 144.28, 141.17, 140.93, 139.74, 139.66, 137.97, 134.08, 129.57, 128.49, 128.20, 127.86, 125.79, 123.90, 122.56, 121.03, 120.68, 118.15, 53.86, 35.05, 34.99, 34.91, 34.91, 31.75 ppm; HR-MS (MALDI-TOF-MS): *m/z* = 1340.8214 $[M]^+$, calcd for $(C_{96}H_{104}N_6)^+$ = 1340.8322; λ_{max} (ε $[M^{-1}cm^{-1}]$) = 369 (29536), 436 (196265), 527 (16223), 599 (8536).

10Ni: ^{1}H NMR (500 MHz, $CDCl_3$): δ = 8.96 (d, 4H, *J* = 5.05 Hz, *β*-H), 8.80 (d, 4H, *J* = 4.95 Hz, *β*-H), 8.73 (s, 4H, *β*-H), 8.27 (s, 2H, triptycene aromatic C-H), 7.96 (s, 4H, triptycene aromatic C-H), 7.90 (br, 4H, Ar-H,), 7.86 (br, 8H, Ar-H), 7.73 (s, 12H, Ar-H and Ar-H), 7.48 (d, 4H, *J* = 8.55 Hz, Ar-H), 6.91 (d, 4H, *J* = 8.55 Hz, Ar-H), 6.10 (s, 2H, triptycene aliphatic C-H), 3.86 (s, 6H, OMe-H), 1.53 (br, 72H, *t*-Bu-H), 1.49 (br, 72H, *t*-Bu-H) ppm; ^{13}C NMR (126 MHz, $CDCl_3$): δ = 160.15, 152.83, 150.80, 149.19, 149.09, 144.04, 143.67, 142.95, 141.74, 140.53, 140.35, 139.27, 139.00, 133.11, 131.71, 131.29, 131.21, 128.27, 127.76, 124.58, 123.56, 122.00, 121.26, 120.54, 116.63, 113.79, 55.31, 53.31, 34.97, 31.89, 31.64 ppm; HR-MS (MALDI-TOF-MS): *m/z* = 2803.4625 $[M]^+$, calcd for $(C_{188}H_{202}N_{14}Ni_2O_2)^+$ = 2803.4842; λ_{max} (ε $[M^{-1}cm^{-1}]$) = 411 (212123), 455 (193363), 560 (31516), 602 (26809).

11Ni: ^{1}H NMR (500 MHz, $CDCl_3$): δ = 8.87 (d, 2H, *J* = 4.95 Hz, *β*-H), 8.73 (d, 2H, *J* = 5.05 Hz, *β*-H), 8.67 (s, 2H, *β*-H), 8.22 (s, 4H, triptycene aromatic C-H), 7.86 (s, 2H, triptycene aromatic C-H), 7.83 (m, 6H, Ar-H) , 7.68 (m, 6H, Ar-H), 7.43 (d, 8H, *J* = 8.50 Hz, Ar-H), 6.85 (d, 8H, *J* = 8.50 Hz, Ar-H), 6.04 (s, 2H, triptycene aliphatic C-H), 3.82 (s, 12H, OMe-H), 1.44 (br, 72H, *t*-Bu-H) ppm; ^{13}C NMR (126 MHz, $CDCl_3$): δ = 160.13, 152.78, 150.76, 149.18, 149.07, 143.80, 143.72, 142.90, 141.75, 140.55, 140.27, 139.27, 138.94, 133.05, 131.64, 131.60, 131.30, 131.19, 128.27, 127.65, 124.51, 123.59, 121.98, 121.24, 120.70, 116.66, 113.76, 55.32, 53.30, 53.27, 34.96, 34.93, 31.81 ppm; HR-MS (MALDI-TOF-MS): *m/z* = 1924.9280 $[M]^+$, calcd for $(C_{128}H_{126}N_{10}NiO_4)^+$ = 1924.9317; λ_{max} (ε $[M^{-1}cm^{-1}]$) = 408 (141070), 453 (119086), 522 (11061), 559 (17416), 600 (15644).

12Ni: ^{1}H NMR (500 MHz, $CDCl_3$): δ = 8.90 (d, 6H, *J* = 4.95 Hz, *β*-H), 8.75 (d, 6H, *J* = 4.95 Hz, *β*-H), 8.67 (s, 6H, *β*-H), 7.93 (s, 6H, triptycene aromatic C-H), 7.84 (br, 6H, Ar-H), 7.80 (br, 12H, Ar-H), 7.68 (br, 18H, Ar-H), 6.04 (s, 2H, triptycene aliphatic C-H), 1.50 (br, 108H, *t*-Bu-H), 1.44 (br, 108H, *t*-Bu-H) ppm; ^{13}C NMR (126 MHz, $CDCl_3$): δ = 150.82, 149.13, 149.07, 143.60, 143.06, 141.68, 140.47, 139.23, 139.01, 133.17, 133.03, 131.70, 131.23, 128.89, 128.23, 127.85, 124.58, 121.98, 121.25, 120.25, 116.53, 35.00, 34.96, 31.94, 31.64 ppm; HR-MS (MALDI-TOF-MS): *m/z* = 3682.0347 $[M]^+$, calcd for $(C_{248}H_{278}N_{18}Ni_3)^+$ = 3682.0367; λ_{max} (ε $[M^{-1}cm^{-1}]$) = 376 (163718), 412 (431665), 461 (416424), 560 (69076), 601 (55064).

12H: ^{1}H NMR (500 MHz, $CDCl_3$): δ = 9.03 (d, 6H, *J* = 5.15 Hz, *β*-H), 8.99 (d, 6H, *J* = 5.20 Hz, *β*-H), 8.78 (s, 6H, *β*-H), 8.12 (s, 6H, triptycene aromatic C-H), 8.09 (br, 12H, Ar-H), 7.99 (br, 12H, Ar-H), 7.92 (s, 6H, Ar-H), 7.80 (s, 6H, Ar-H), 6.08 (s, 2H, triptycene aliphatic C-H), 1.61 (br, 108H, *t*-Bu-H), 1.53 (br, 108H, *t*-Bu-H), -2.57 (s, 6H, NH) ppm; ^{13}C NMR (126 MHz, $CDCl_3$): δ = 154.79, 152.80, 148.80, 148.75, 145.74, 143.36, 141.11, 141.04, 140.14, 139.66, 138.02, 134.12, 129.56, 128.57, 128.28, 127.89, 124.79, 122.66, 121.04, 120.38, 118.12, 53.56, 35.11, 35.04, 32.09, 31.74 ppm; HR-MS (MALDI-TOF-MS): *m/z* = 3514.2580 $[M]^+$, calcd for $(C_{248}H_{284}N_{18})^+$ = 3514.2776; λ_{max} (ε $[M^{-1}cm^{-1}]$) = 373 (43167), 441 (259426), 529 (25957), 565 (10392), 600 (15847).

12Zn: ^{1}H NMR (500 MHz, $CDCl_3$): δ = 8.97 (s, 12H, *β*-H), 8.87 (s, 6H, *β*-H), 8.11 (s, 6H, triptycene aromatic C-H), 8.07 (d, 12H, *J* = 1.85 Hz, Ar-H), 7.99 (br, 6H, Ar-H), 7.96 (d, 12H, *J* = 1.85 Hz, Ar-H), 7.77 (br, 6H, Ar-H), 6.13 (s, 2H, triptycene aliphatic C-H), 1.51 (br, 216H, *t*-Bu-H) ppm; ^{13}C NMR (126 MHz, $CDCl_3$): δ = 152.62, 150.67, 149.91, 149.12, 148.73, 148.59, 143.32, 141.64, 140.48, 132.33, 131.59, 131.52, 129.35, 128.37, 124.71, 120.90, 120.14, 118.87, 35.12, 35.05, 32.12, 31.76 ppm; HR-MS (MALDI-TOF-MS): *m/z* = 3700.0282 $[M]^+$, calcd for $(C_{248}H_{278}N_{18}Zn_3)^+$ = 3700.0181; λ_{max} (ε $[M^{-1}cm^{-1}]$) = 370 (116868), 423 (528138), 450 (540609), 532 (39181), 571 (95129), 612 (69093).

NMR Spectra of Compounds

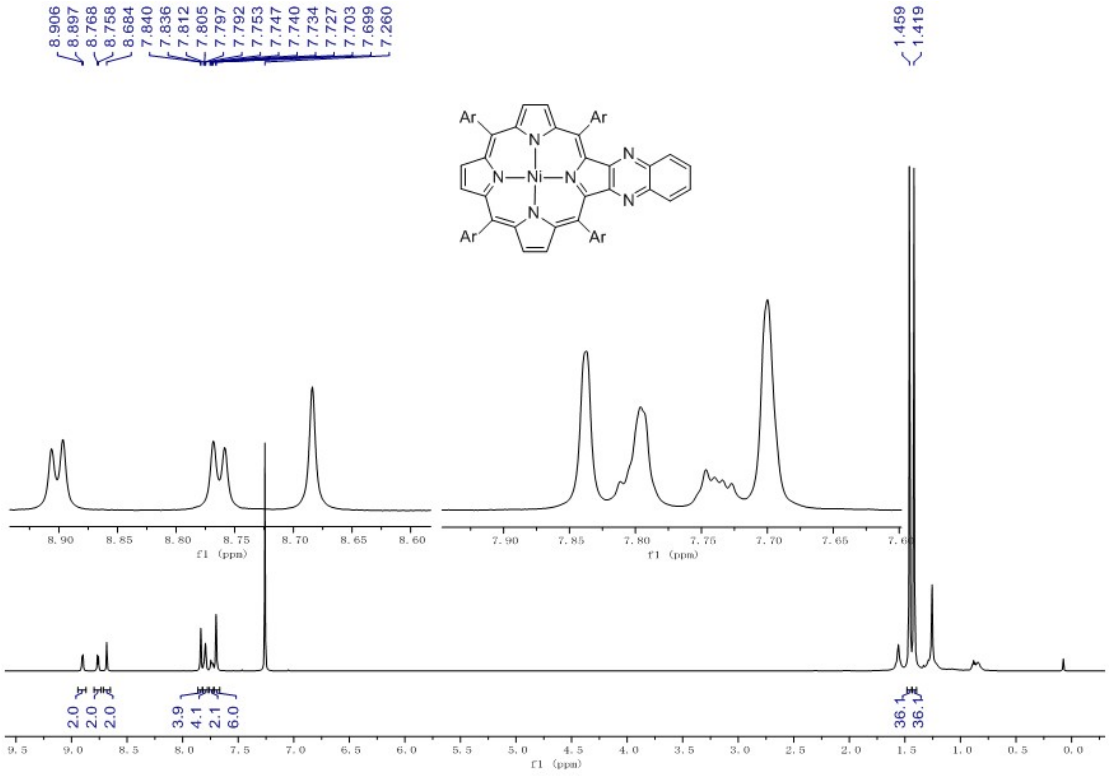

Figure S1. ^{1}H NMR spectrum of **3Ni** in $CDCl_3$ at 298 K

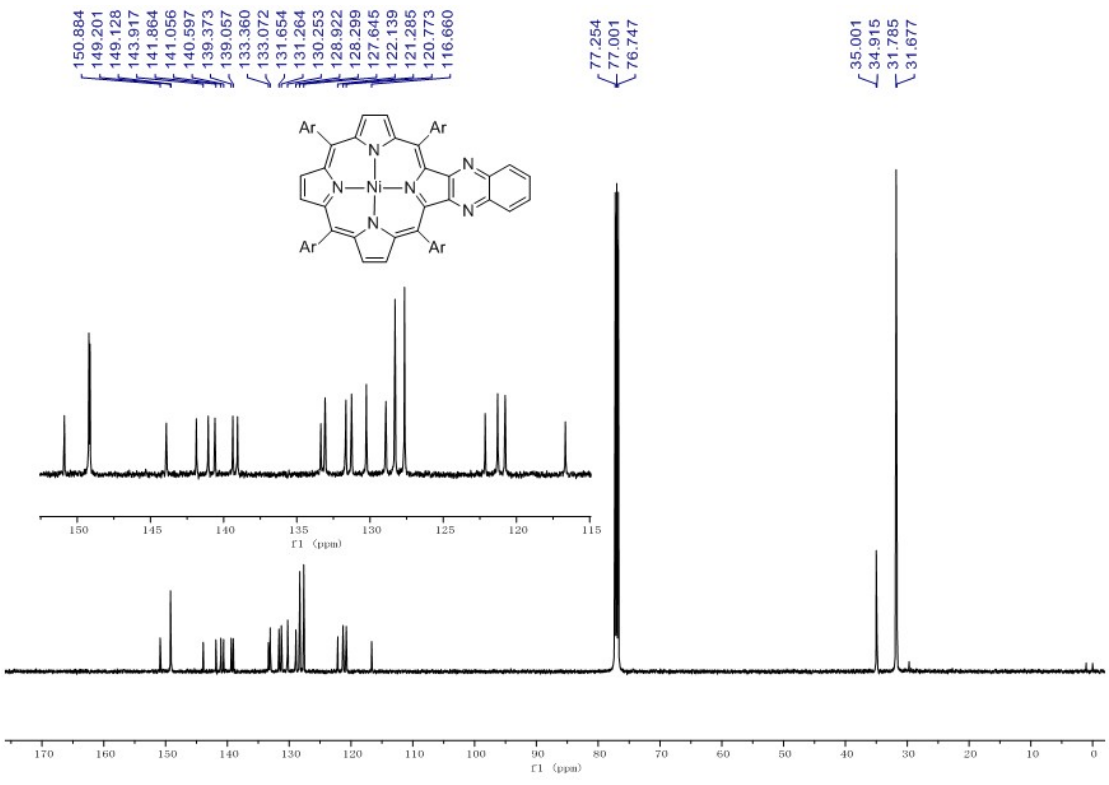

Figure S2. ^{13}C NMR spectrum of **3Ni** in $CDCl_3$ at 298 K

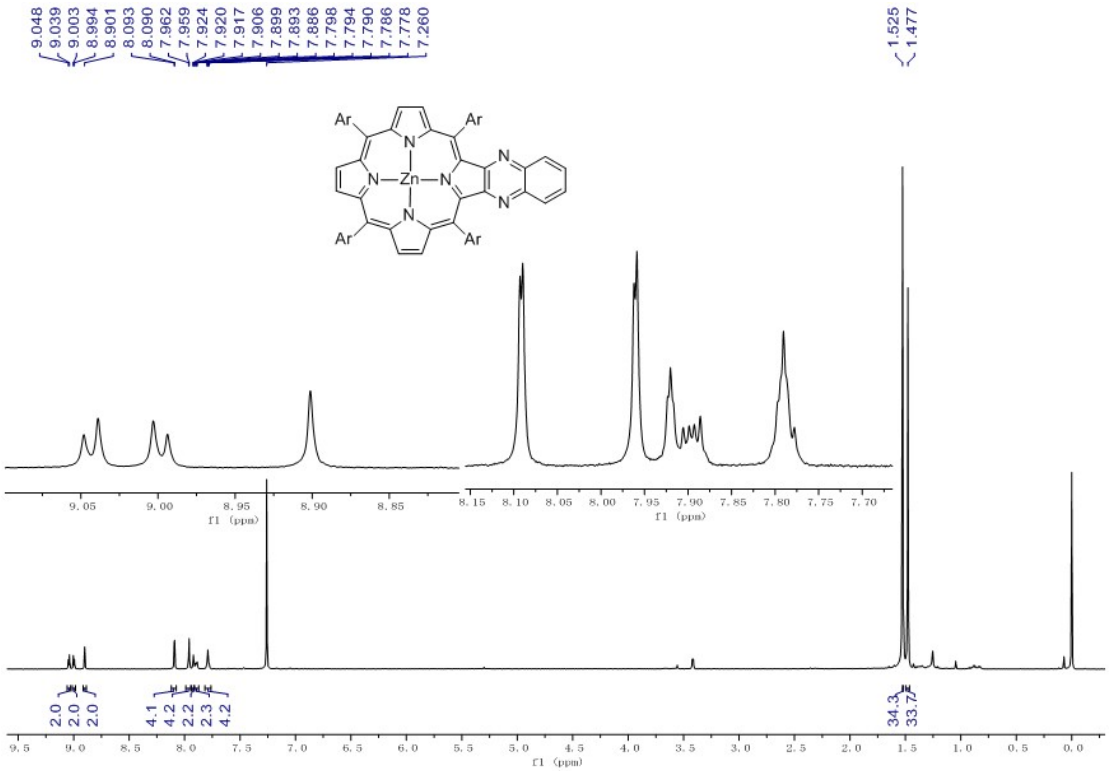

Figure S3. ^{1}H NMR spectrum of **3Zn** in $CDCl_3$ at 298 K

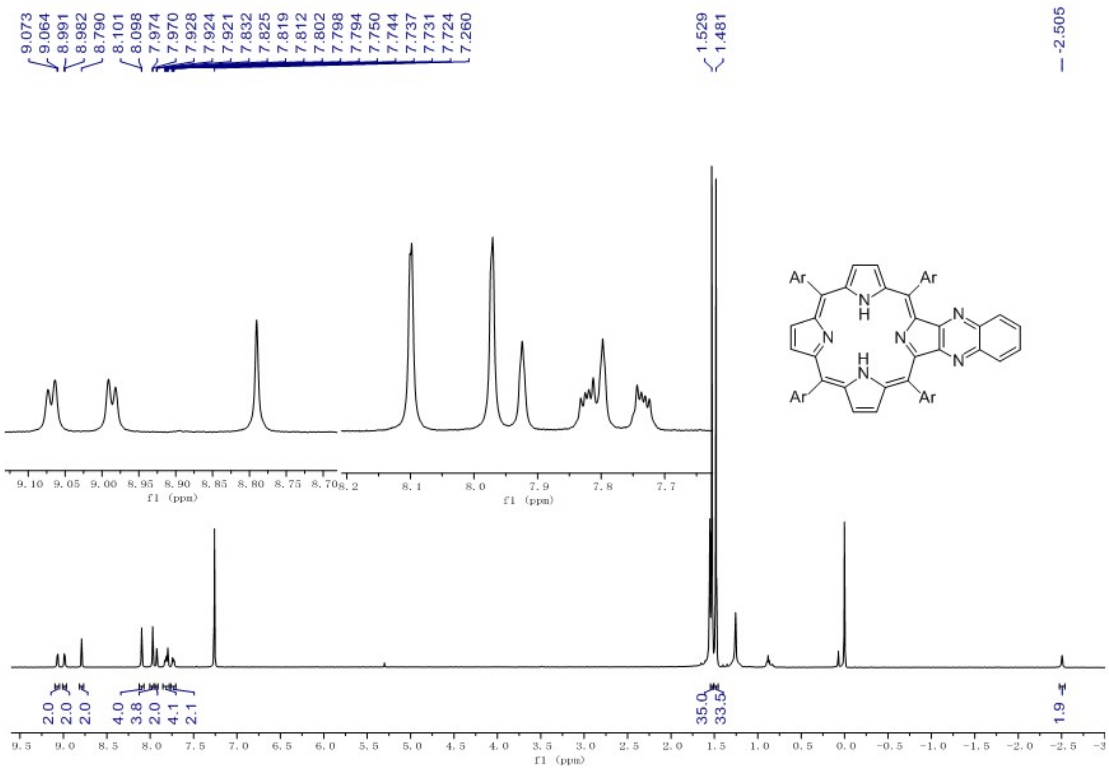

Figure S4. ^{1}H NMR spectrum of **3H** in $CDCl_3$ at 298 K

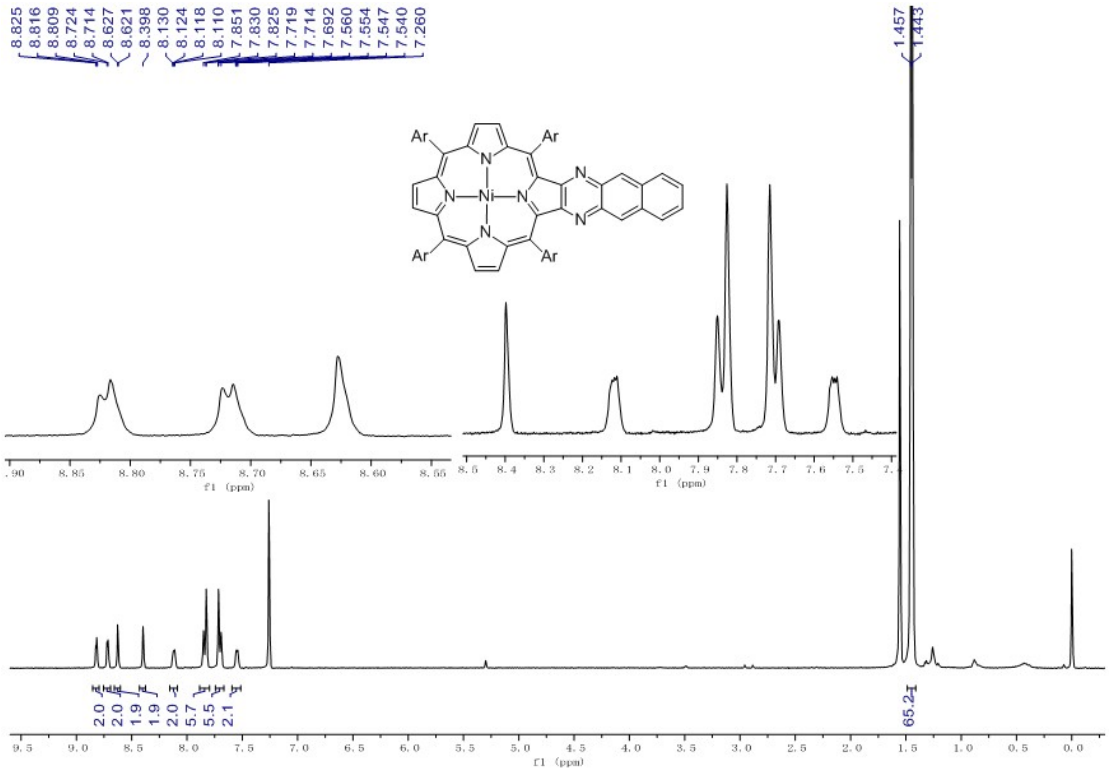

Figure S5. ^{1}H NMR spectrum of **4Ni** in $CDCl_3$ at 298 K

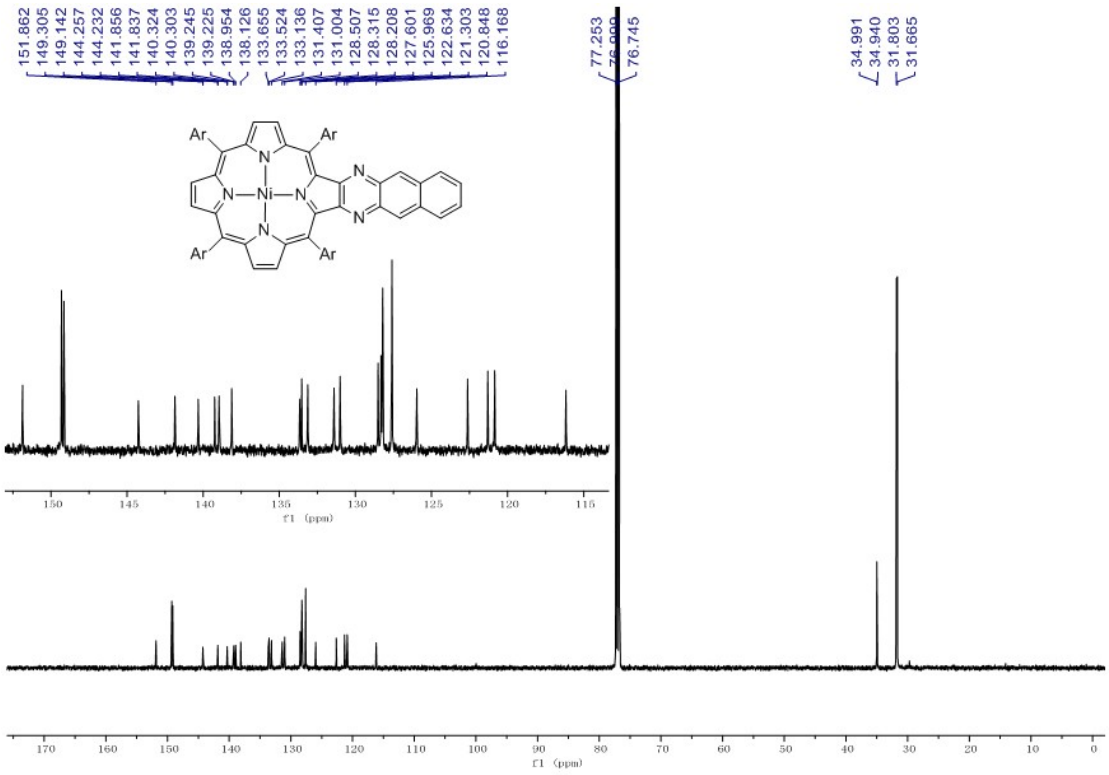

Figure S6. ^{13}C NMR spectrum of **4Ni** in $CDCl_3$ at 298 K

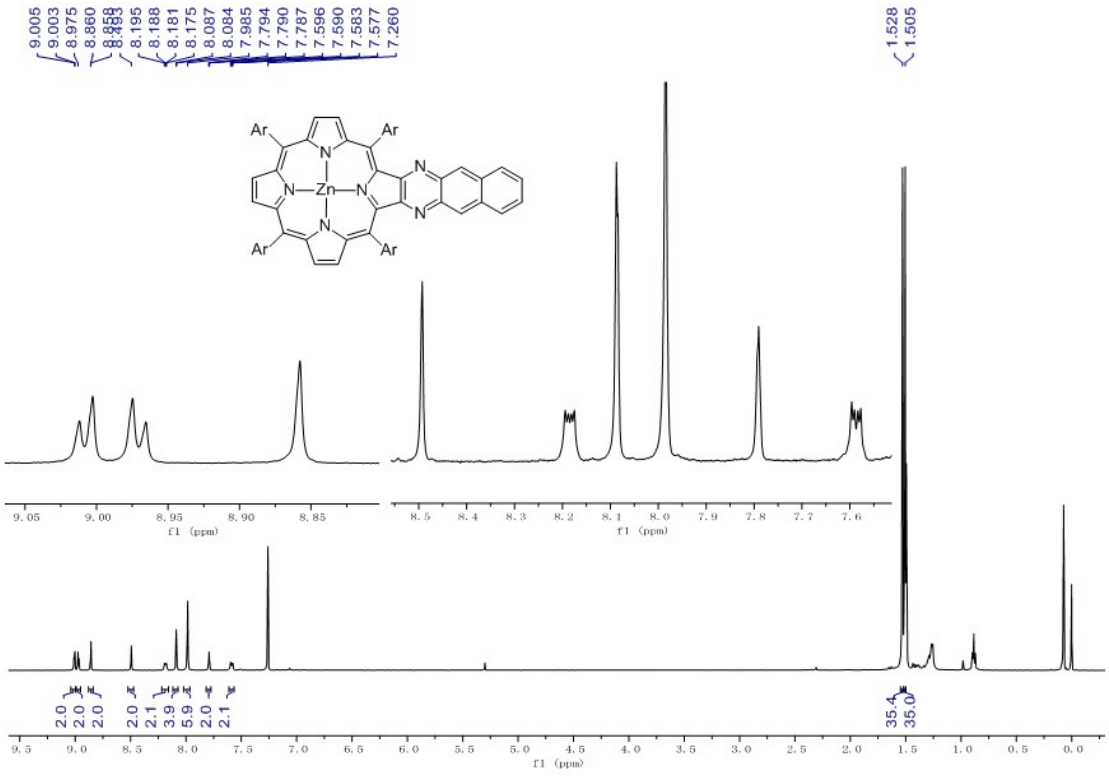

Figure S7. ^{1}H NMR spectrum of **4Zn** in $CDCl_3$ at 298 K

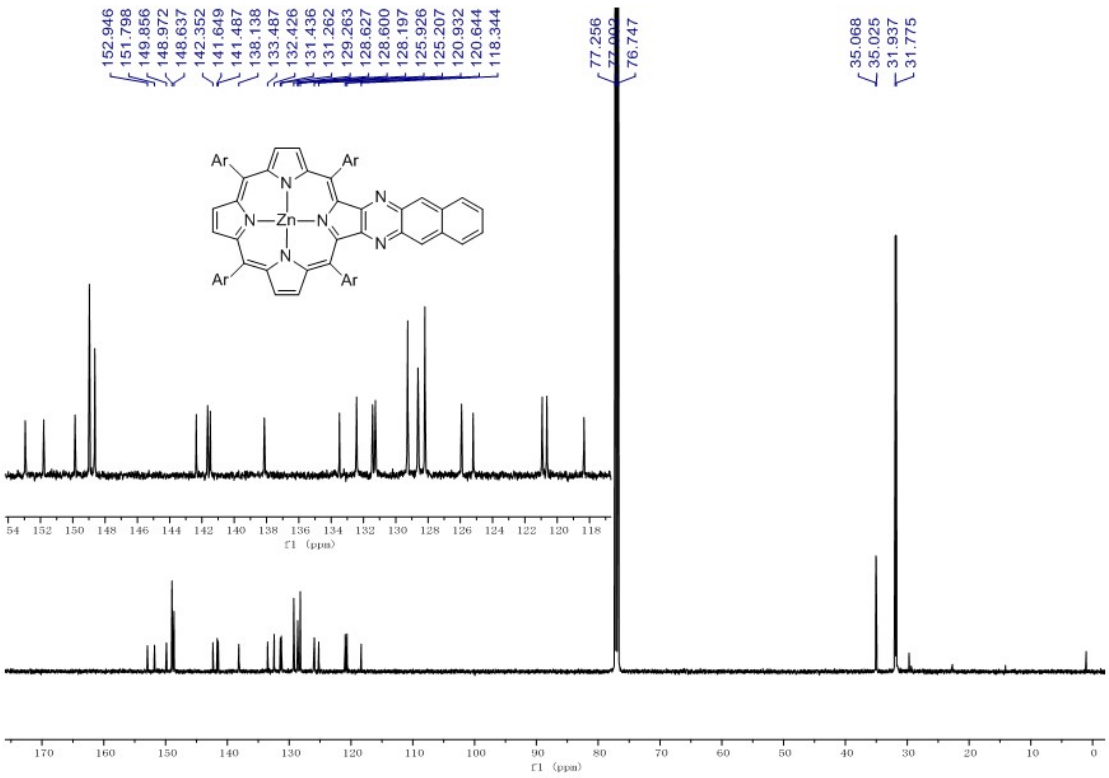

Figure S8. ^{13}C NMR spectrum of **4Zn** in $CDCl_3$ at 298 K

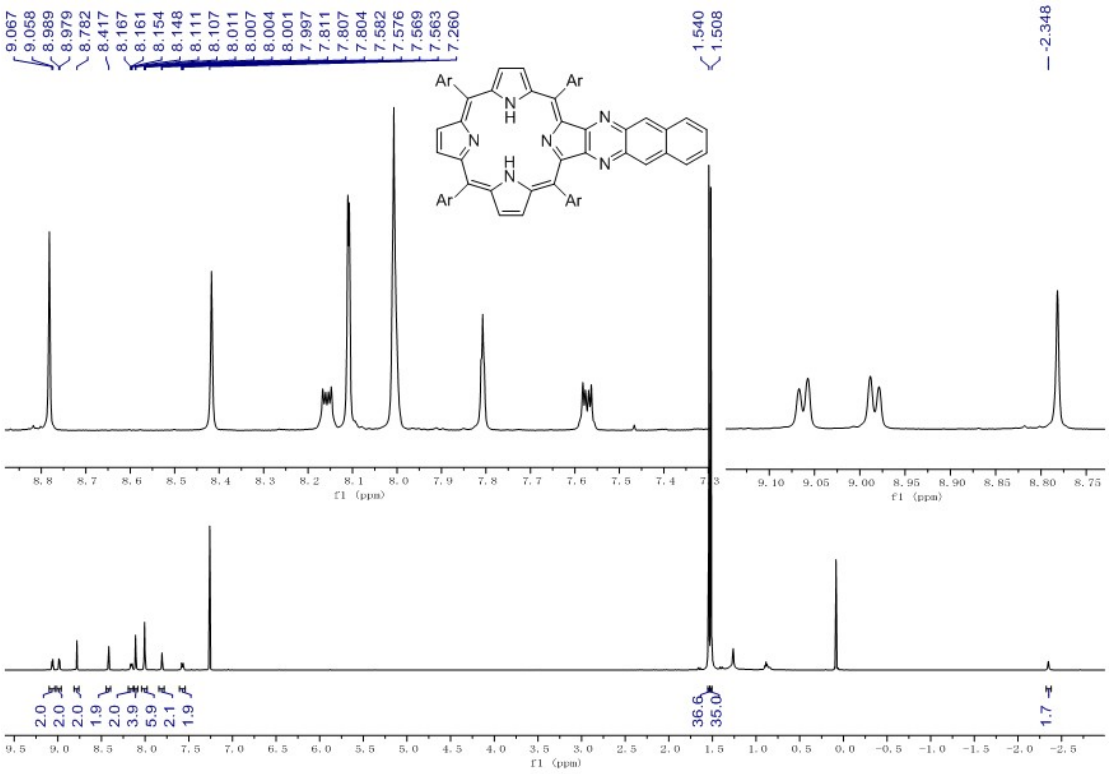

Figure S9. ^{1}H NMR spectrum of **4H** in $CDCl_3$ at 298 K

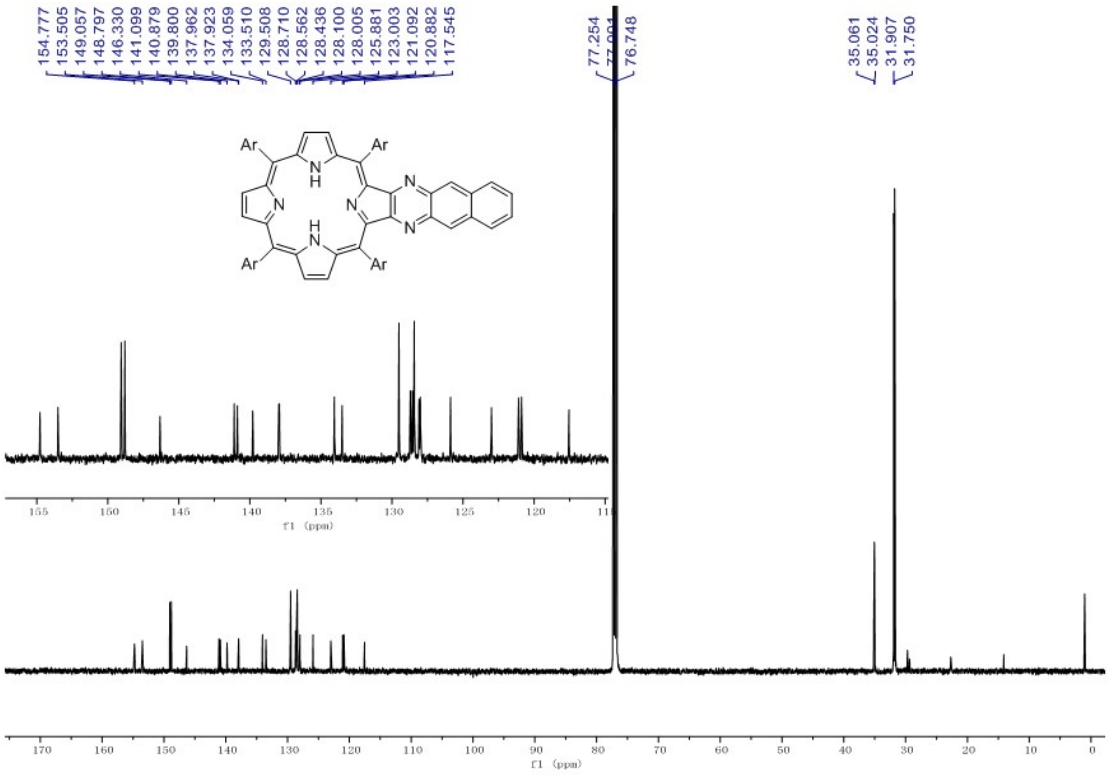

Figure S10. ^{13}C NMR spectrum of **4H** in $CDCl_3$ at 298 K

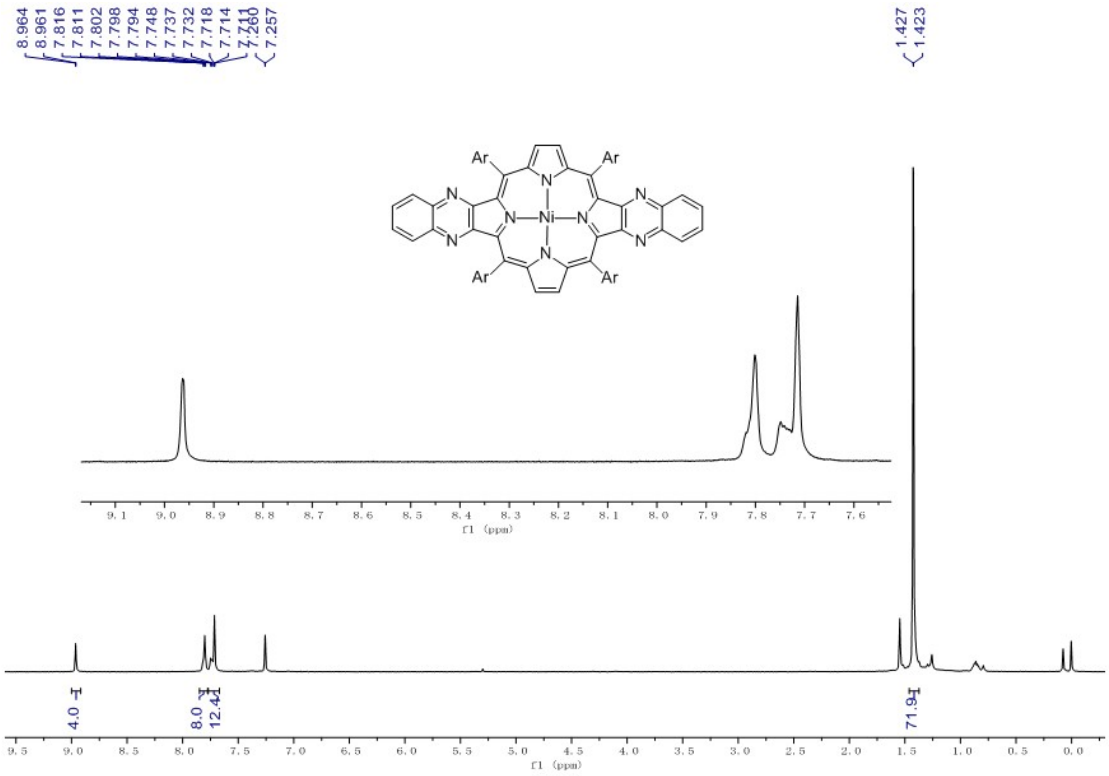

Figure S11. ^{1}H NMR spectrum of **5Ni** in $CDCl_3$ at 298 K

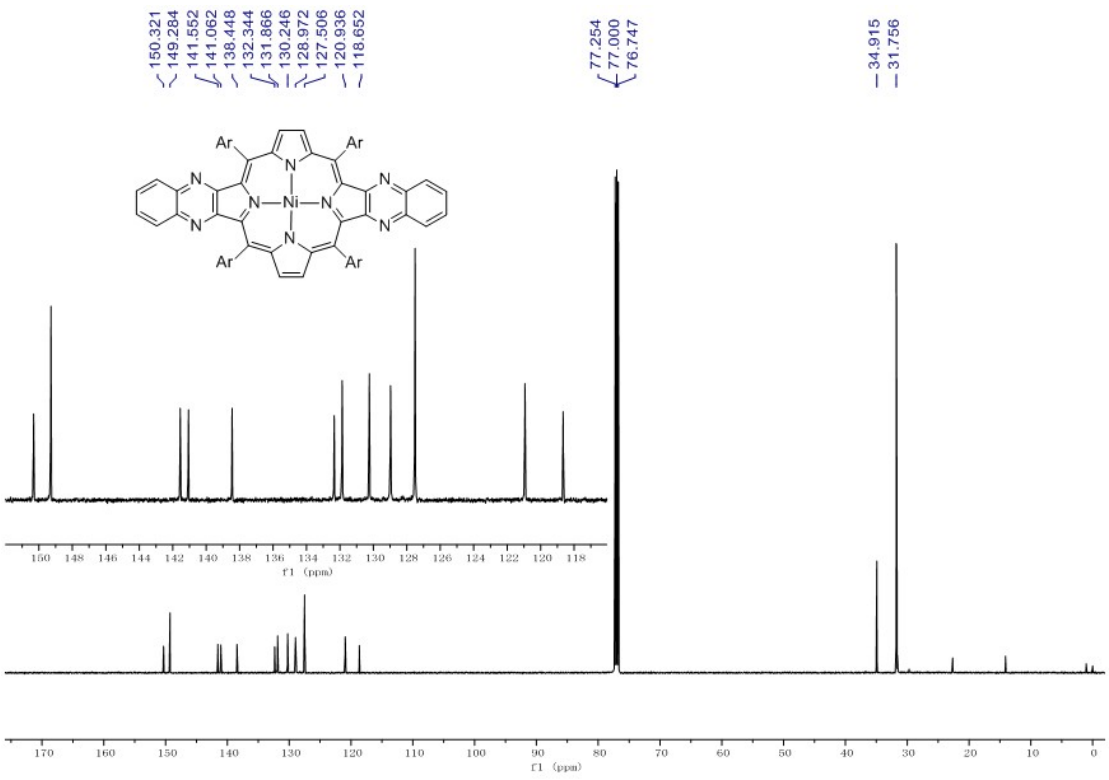

Figure S12. ^{13}C NMR spectrum of **5Ni** in $CDCl_3$ at 298 K

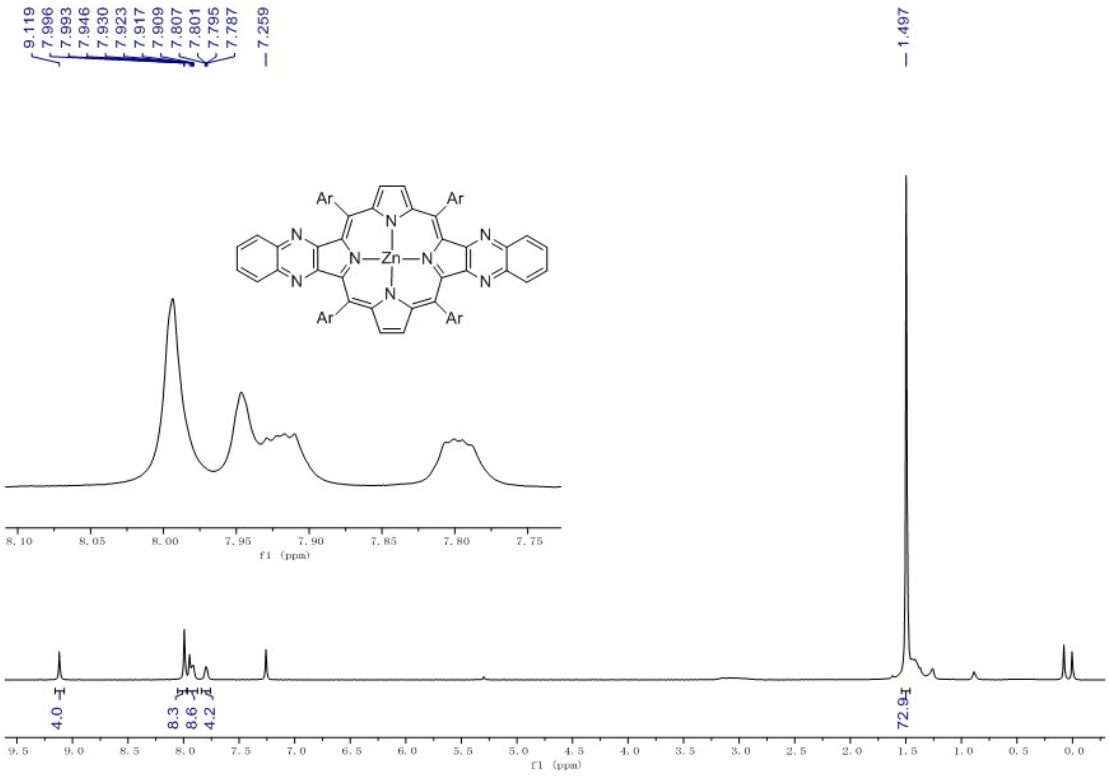

Figure S13. ^{1}H NMR spectrum of **5Zn** in $CDCl_3$ at 298 K

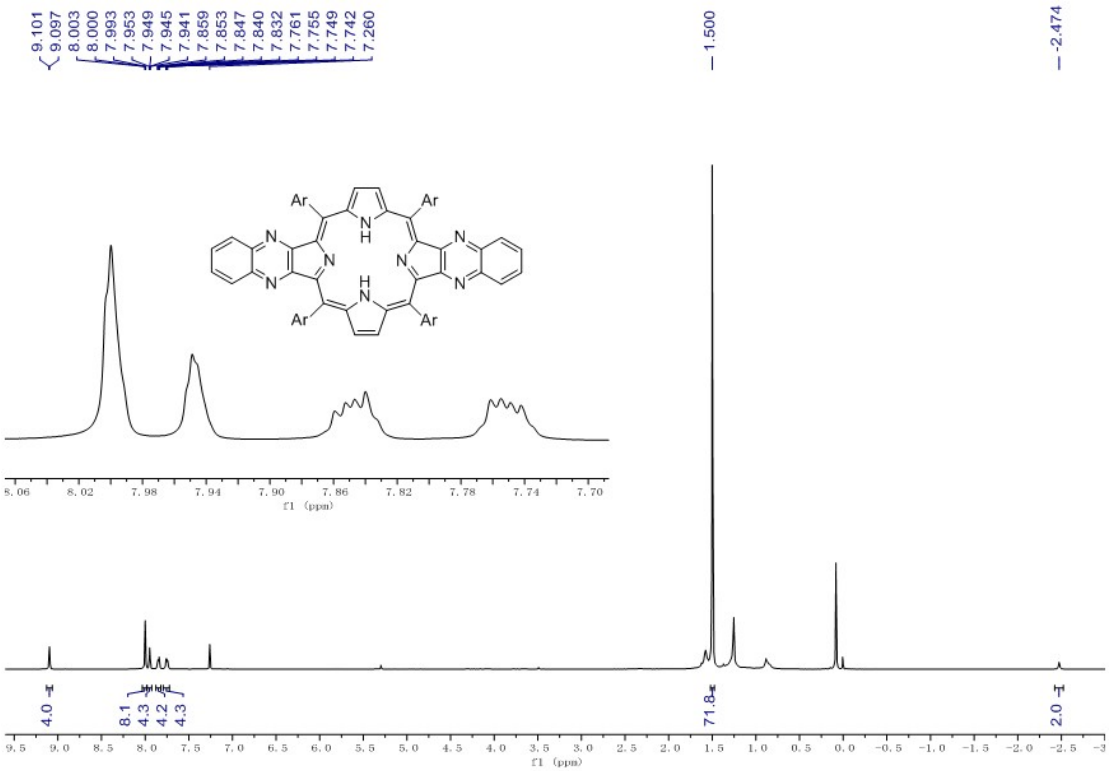

Figure S14. ^{1}H NMR spectrum of **5H** in $CDCl_3$ at 298 K

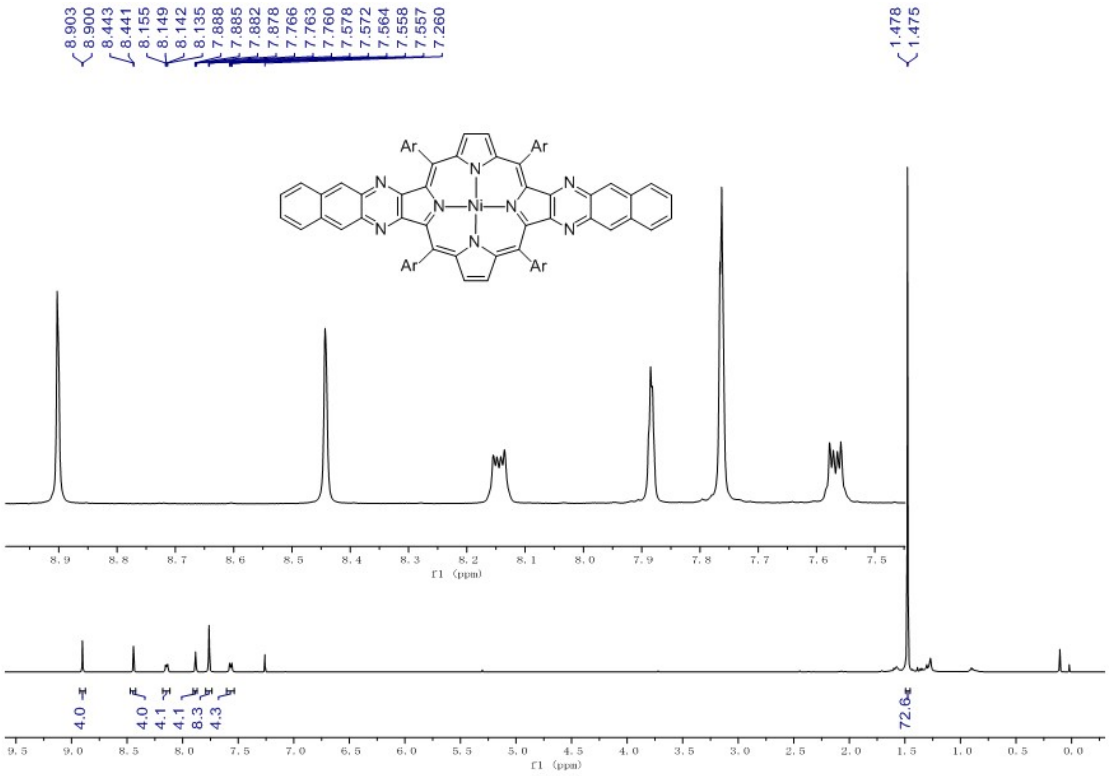

Figure S15. ^{1}H NMR spectrum of **6Ni** in $CDCl_3$ at 298 K

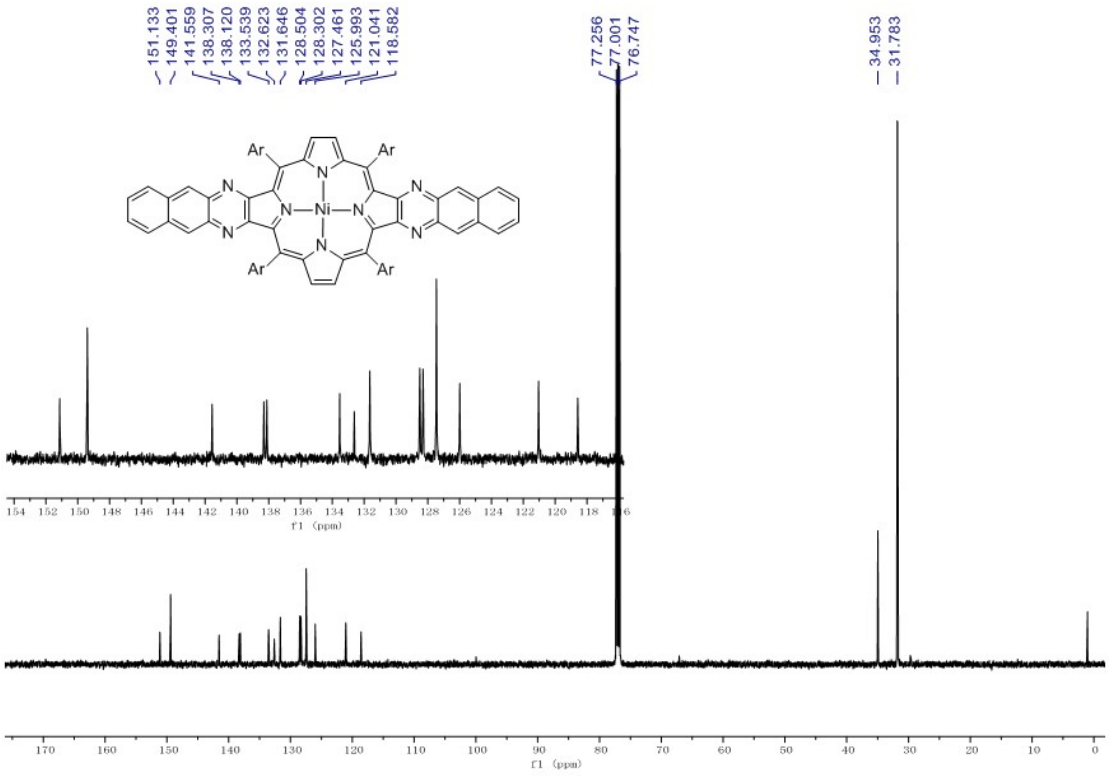

Figure S16. ^{13}C NMR spectrum of **6Ni** in $CDCl_3$ at 298 K

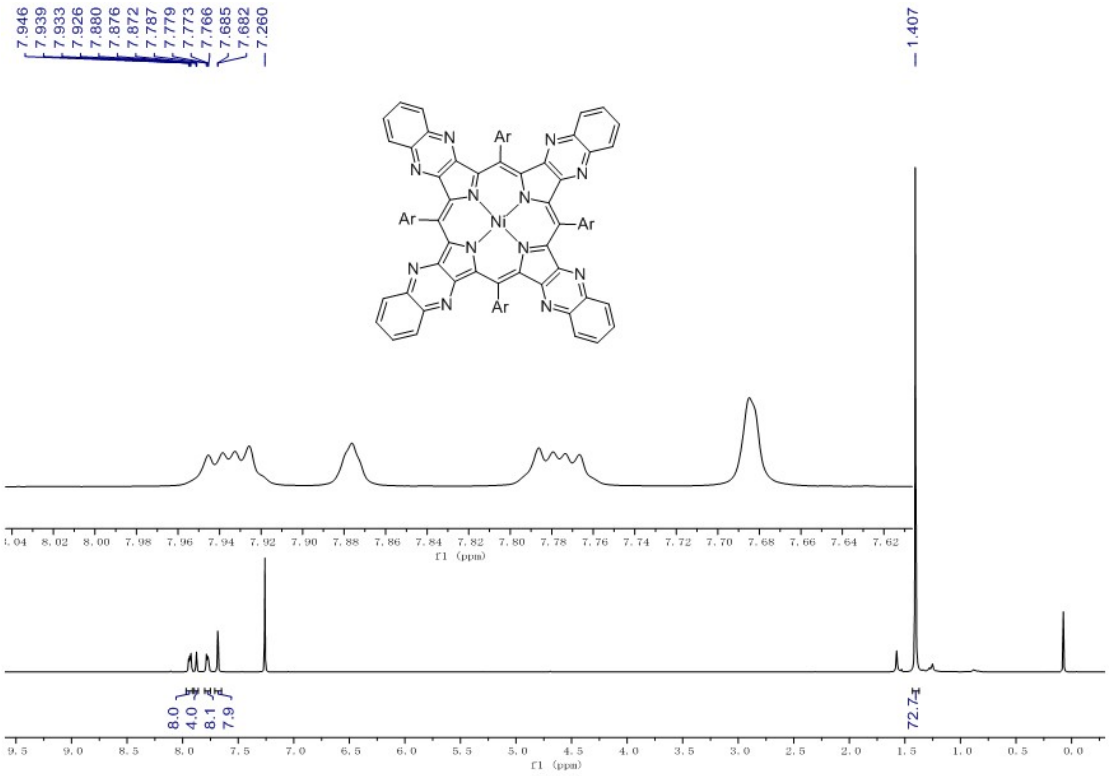

Figure S17. ^{1}H NMR spectrum of **7Ni** in $CDCl_3$ at 298 K

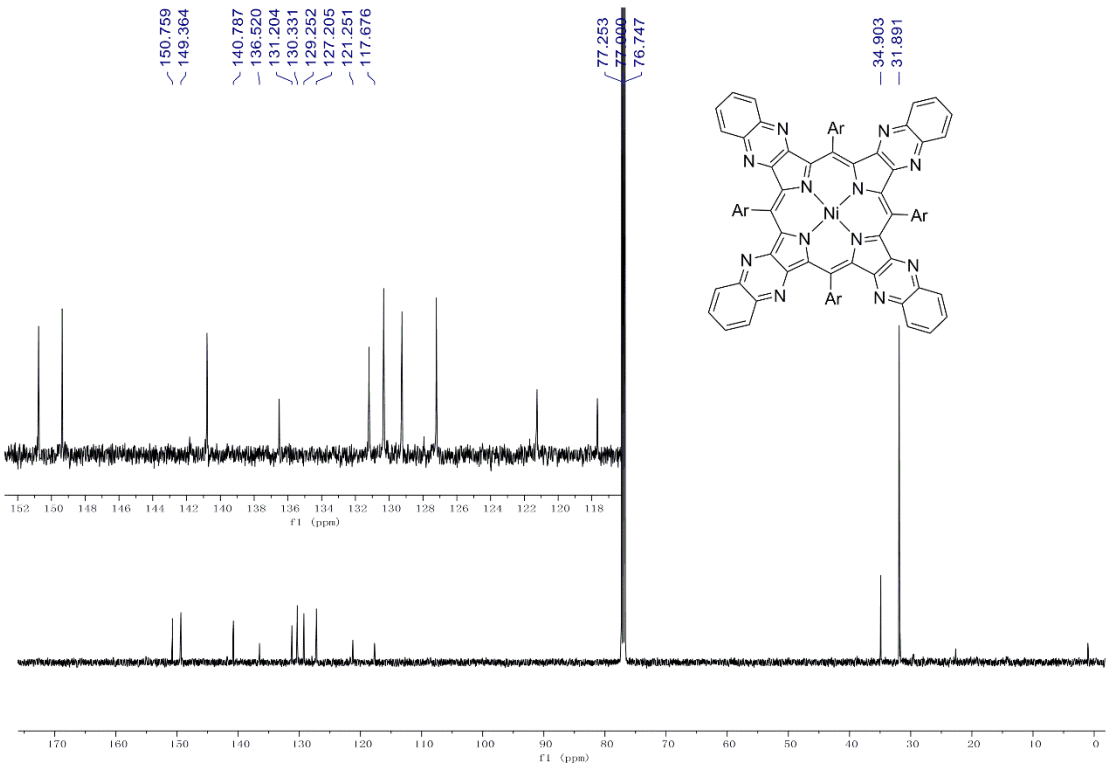

Figure S18. ^{13}C NMR spectrum of **7Ni** in $CDCl_3$ at 298 K

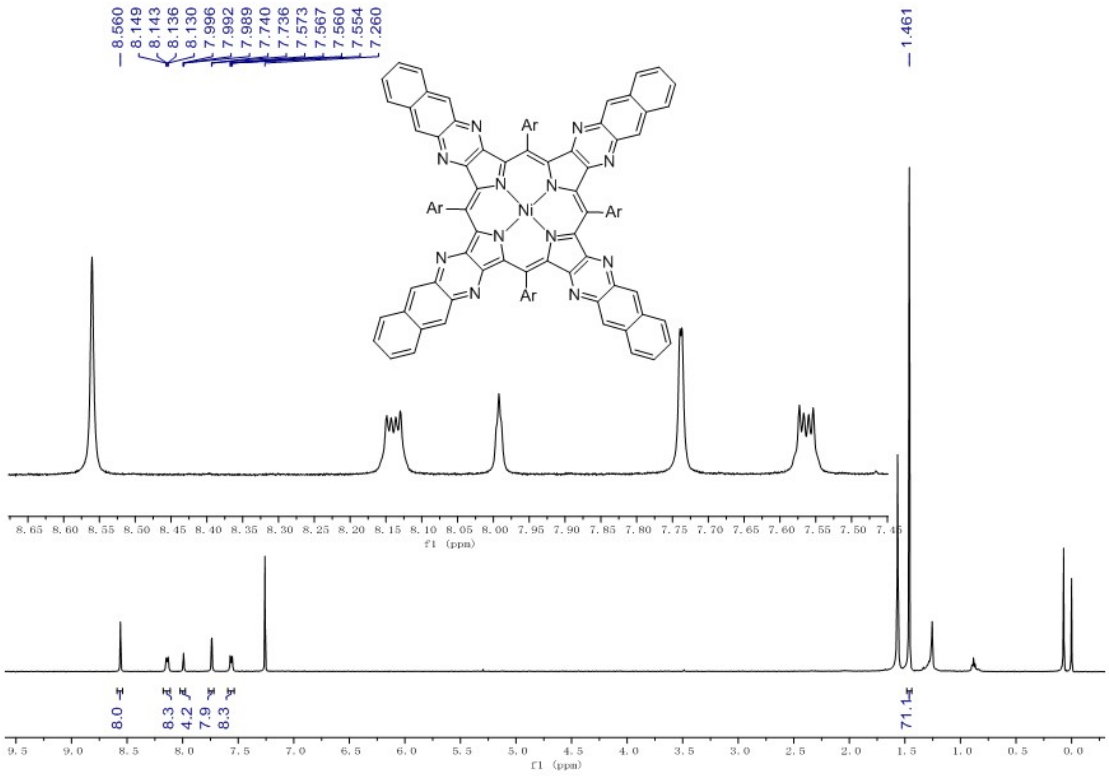

Figure S19. ^{1}H NMR spectrum of **8Ni** in $CDCl_3$ at 298 K

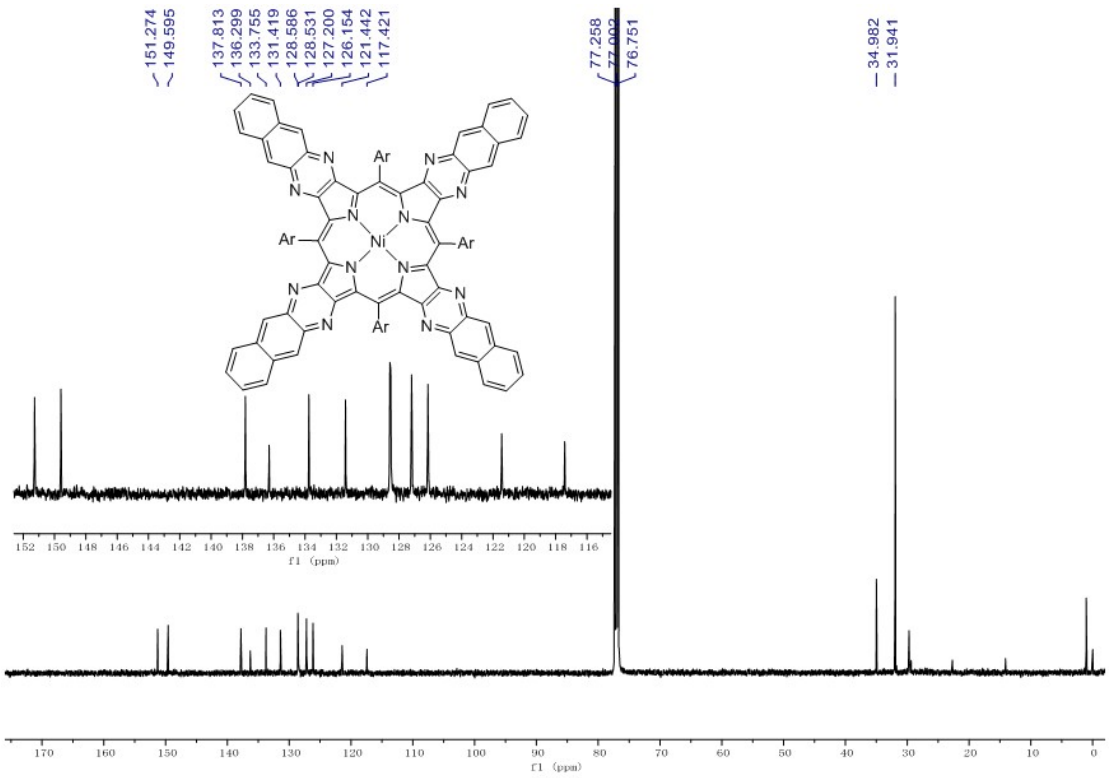

Figure S20. ^{13}C NMR spectrum of **8Ni** in $CDCl_3$ at 298 K

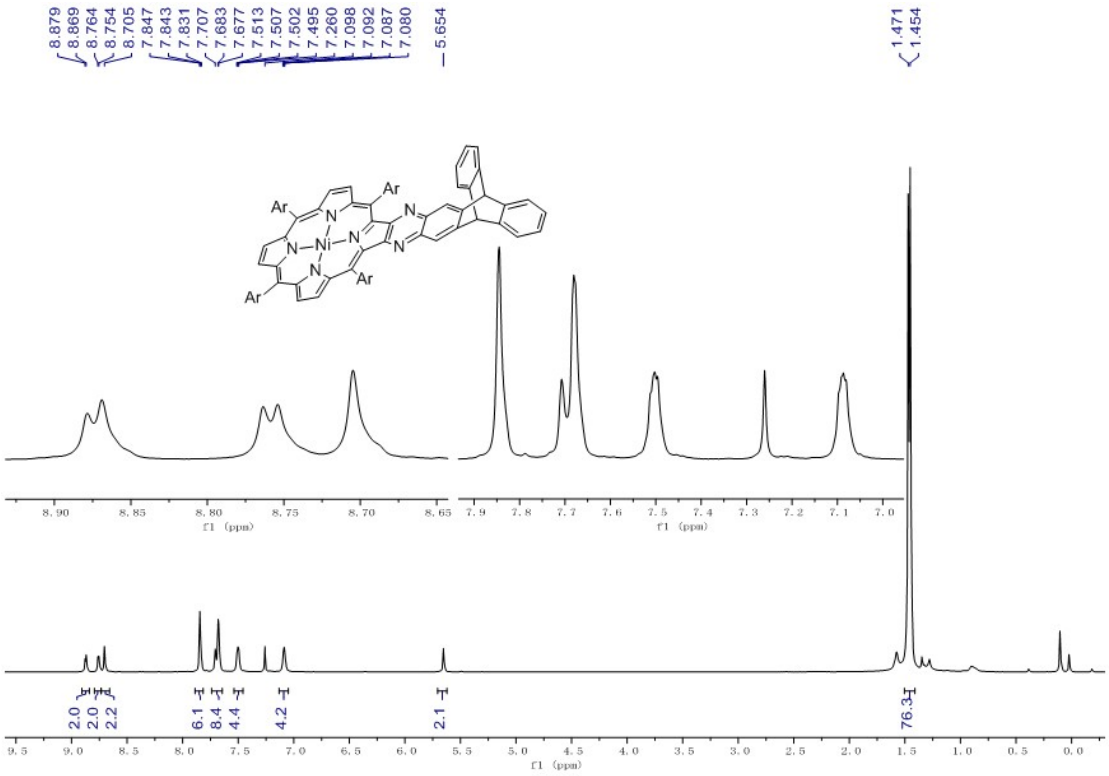

Figure S21. ^{1}H NMR spectrum of **9Ni** in $CDCl_3$ at 298 K

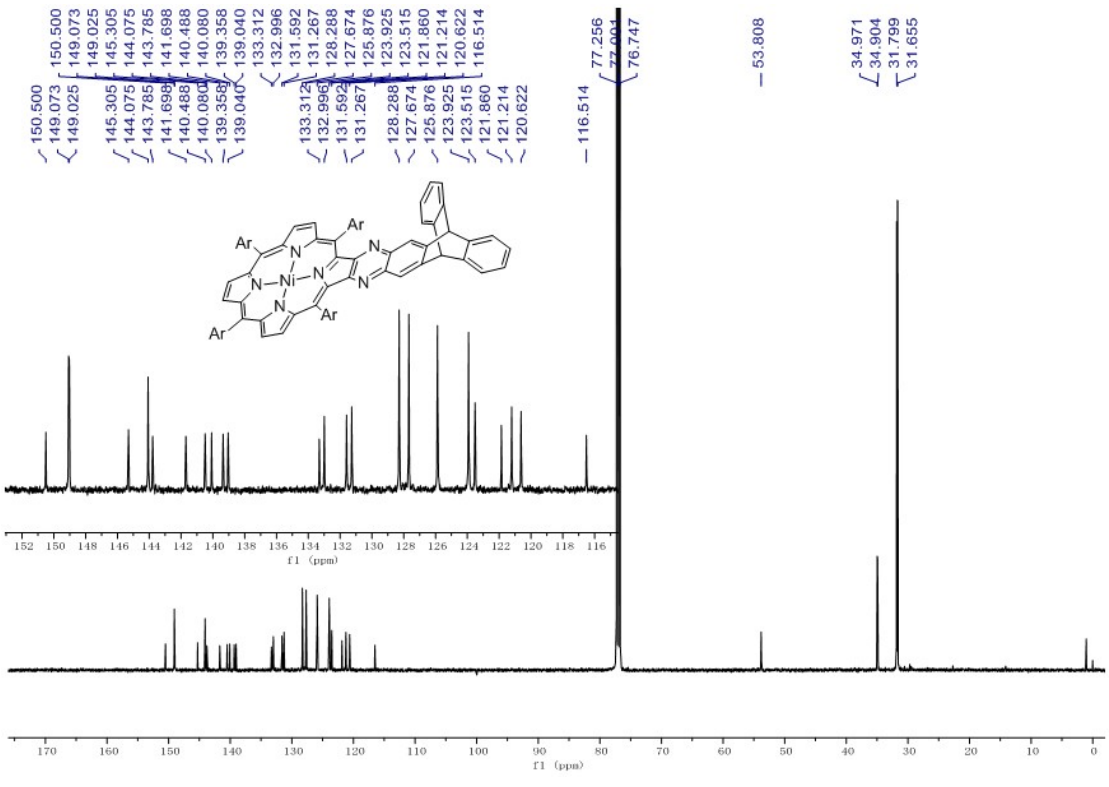

Figure S22. ^{13}C NMR spectrum of **9Ni** in $CDCl_3$ at 298 K

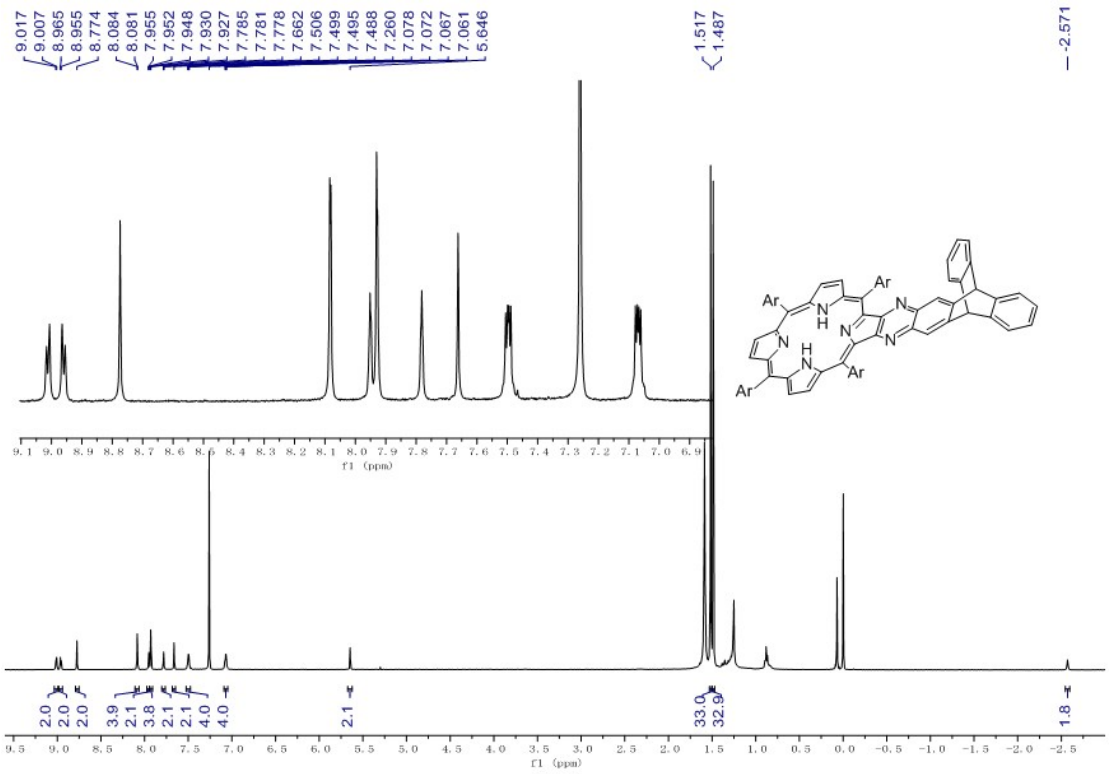

Figure S23. ^{1}H NMR spectrum of **9H** in $CDCl_3$ at 298 K

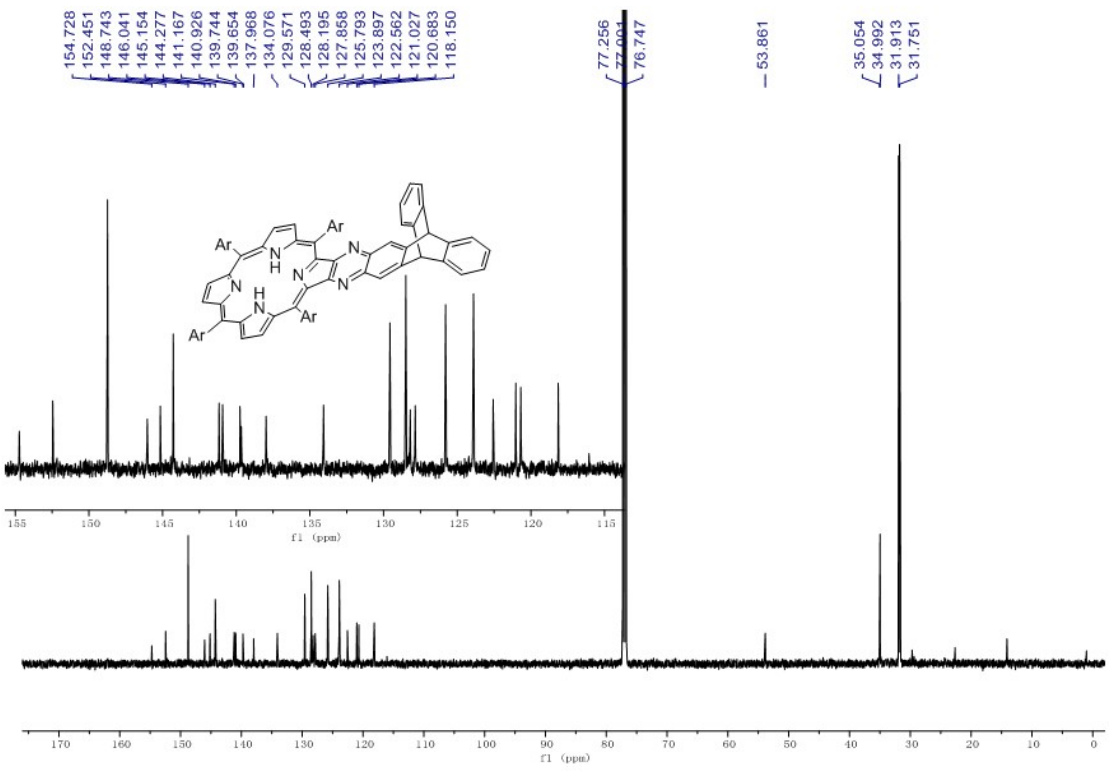

Figure S24. ^{13}C NMR spectrum of **9H** in $CDCl_3$ at 298 K

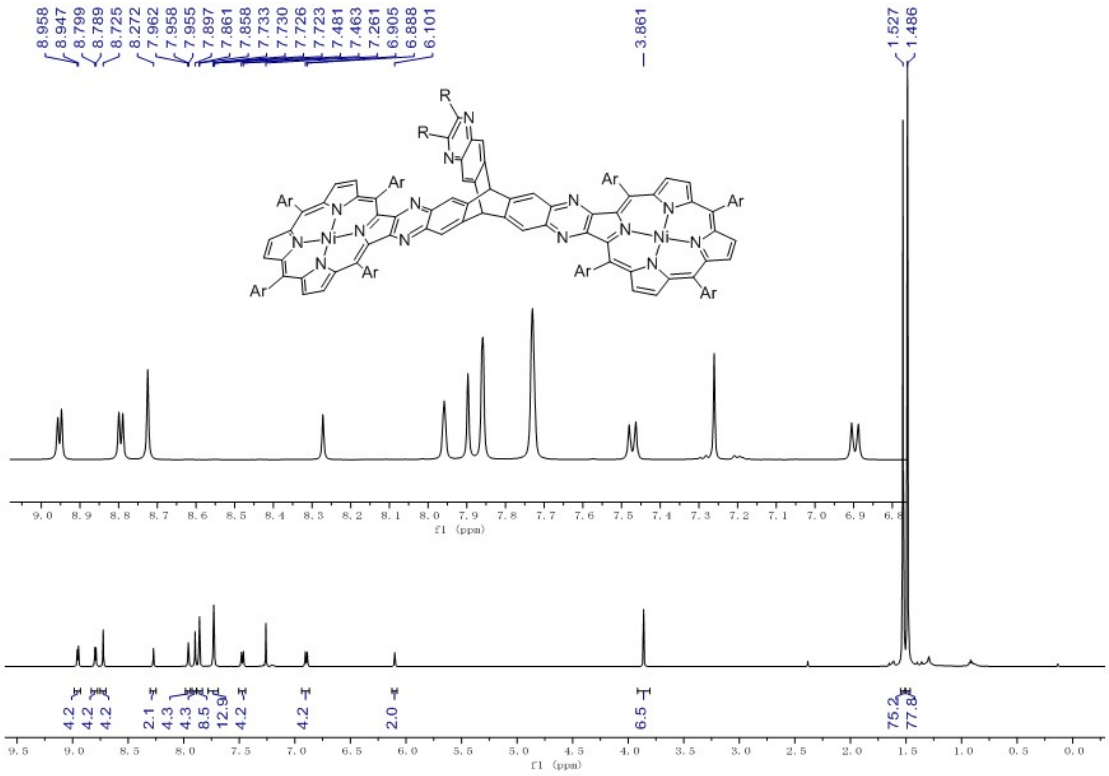

Figure S25. ^{1}H NMR spectrum of **10Ni** in $CDCl_3$ at 298 K

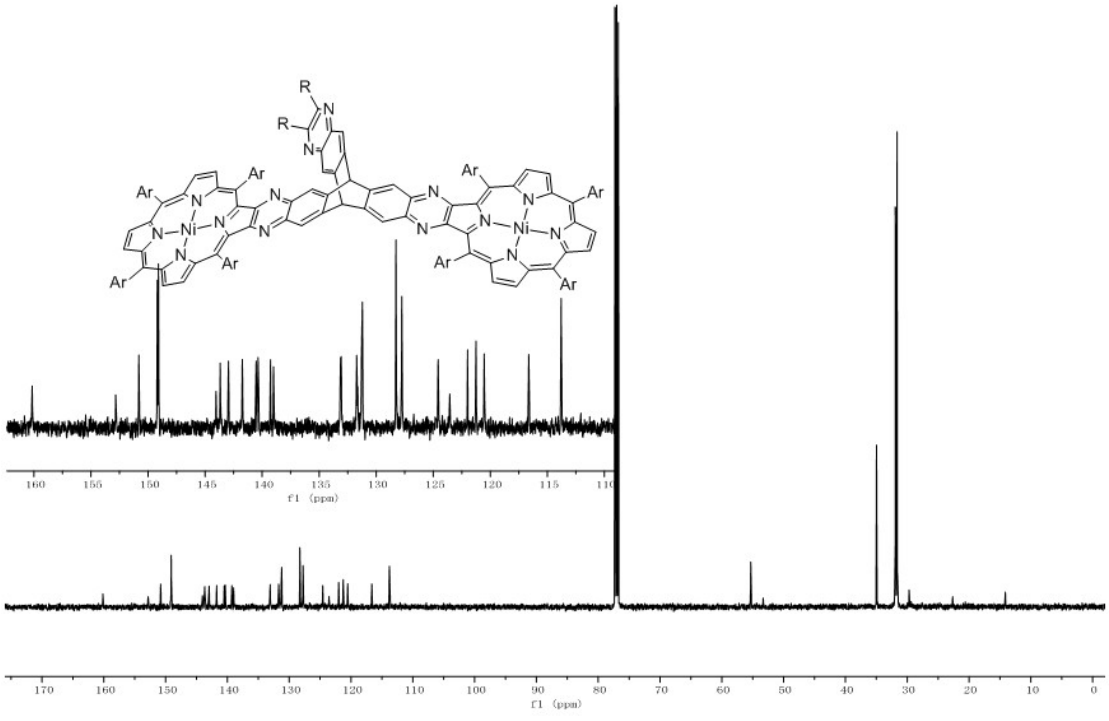

Figure S26. ^{13}C NMR spectrum of **10Ni** in $CDCl_3$ at 298 K.

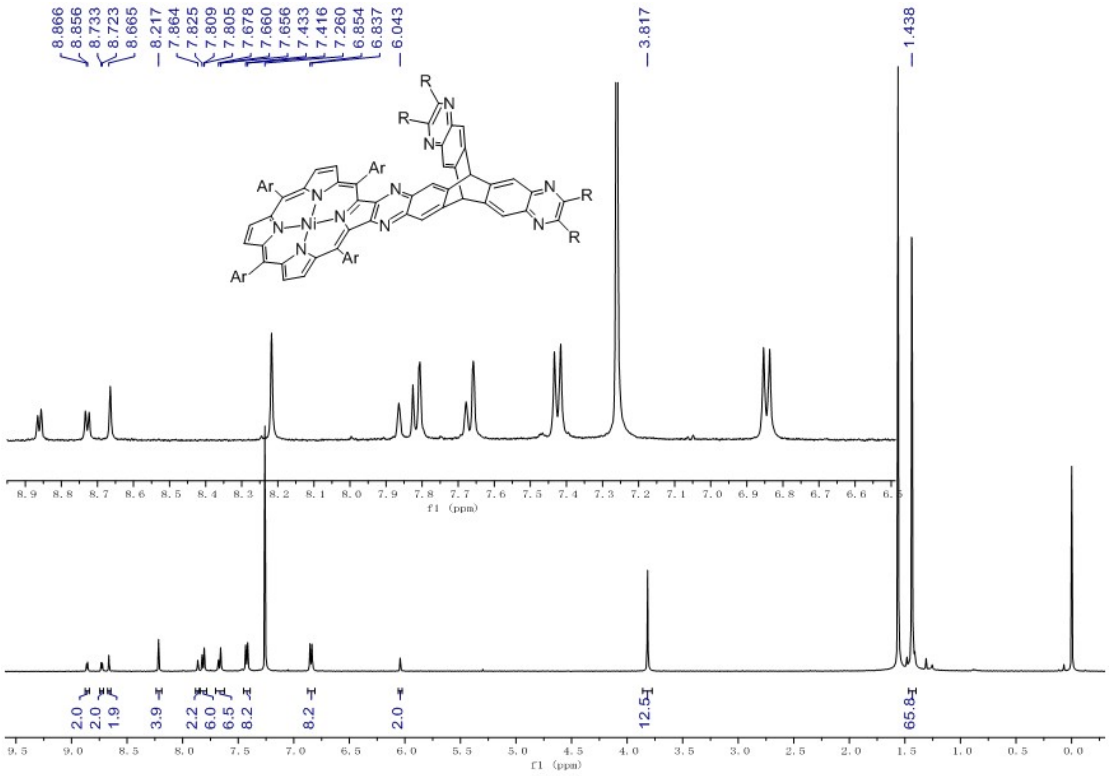

Figure S27. ^{1}H NMR spectrum of **11Ni** in $CDCl_3$ at 298 K

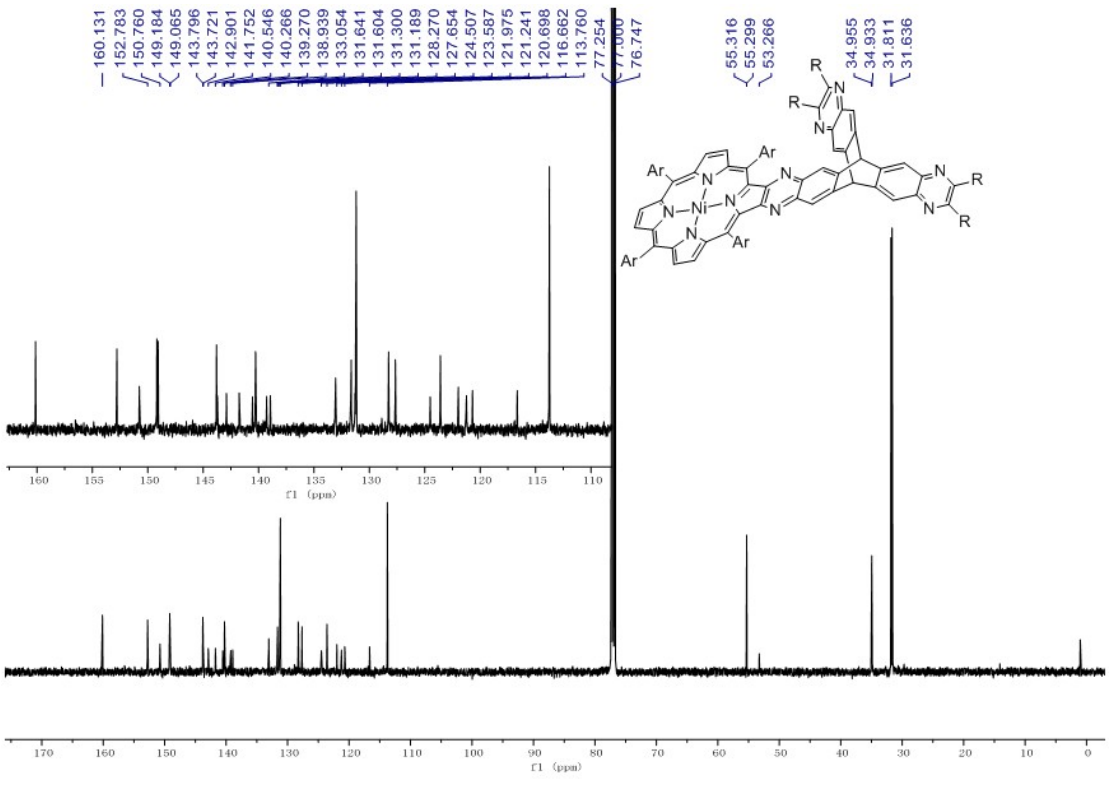

Figure S28. ^{13}C NMR spectrum of **11Ni** in $CDCl_3$ at 298 K

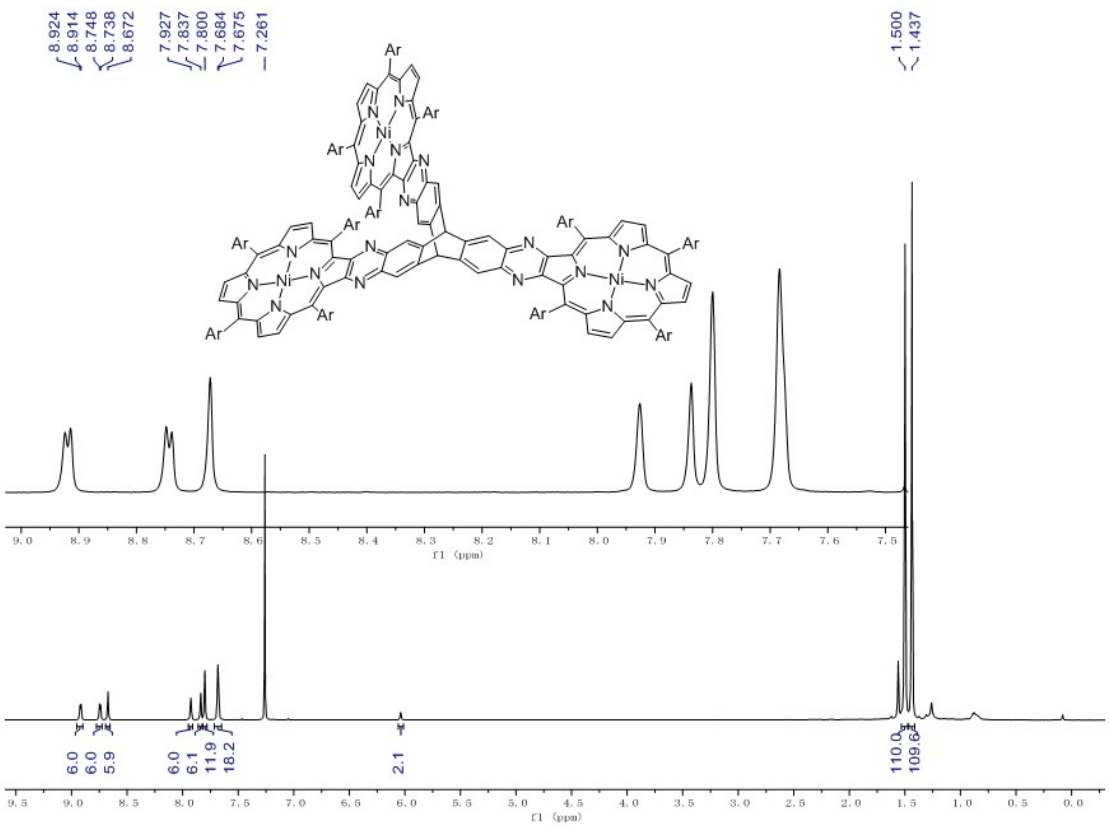

Figure S29. ^{1}H NMR spectrum of **12Ni** in $CDCl_3$ at 298 K

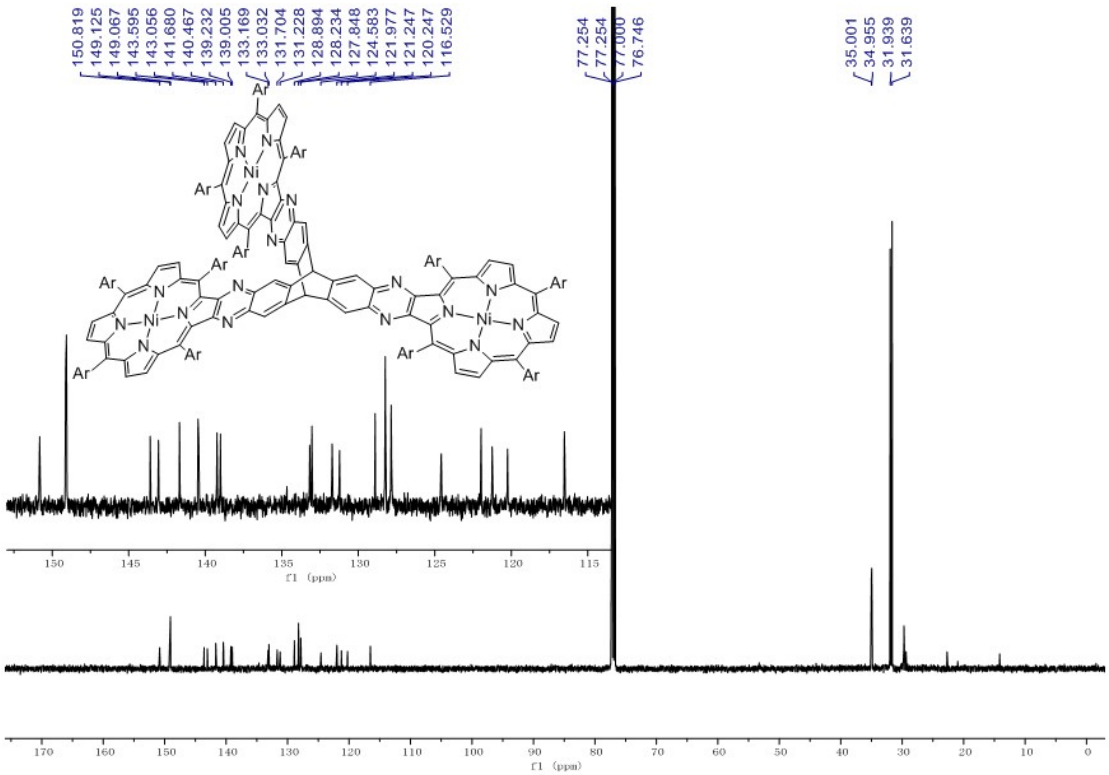

Figure S30. ^{13}C NMR spectrum of **12Ni** in $CDCl_3$ at 298 K

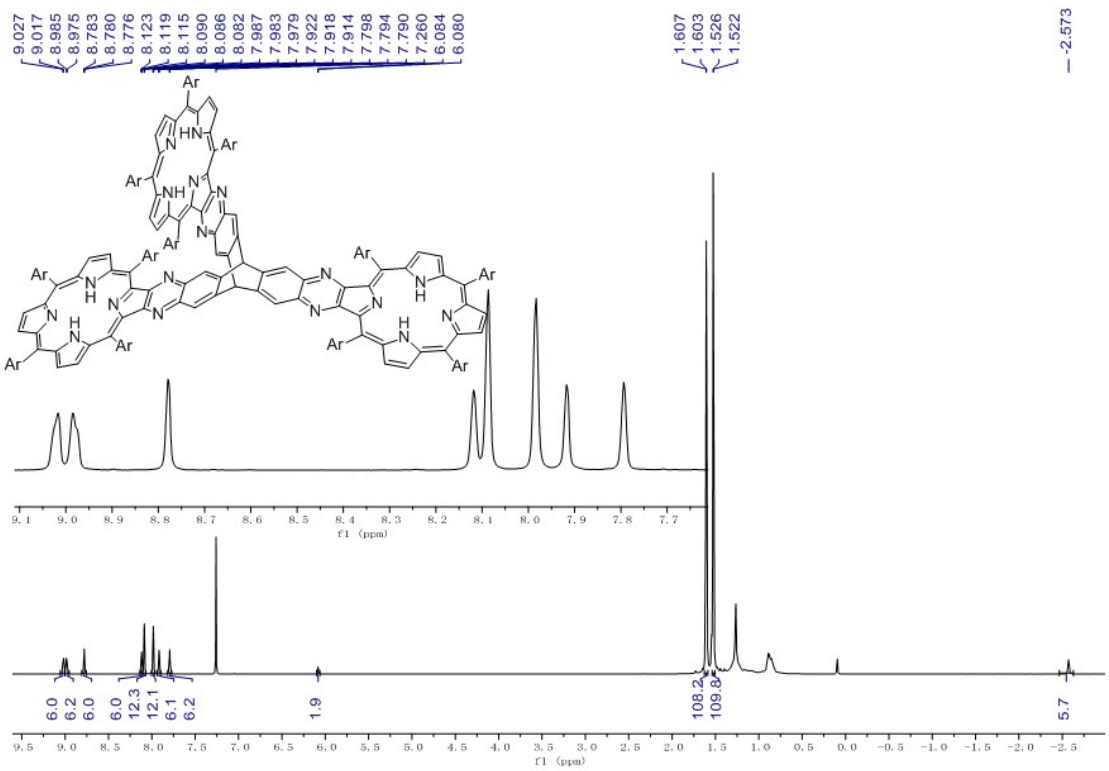

Figure S31. ^{1}H NMR spectrum of **12H** in $CDCl_3$ at 298 K

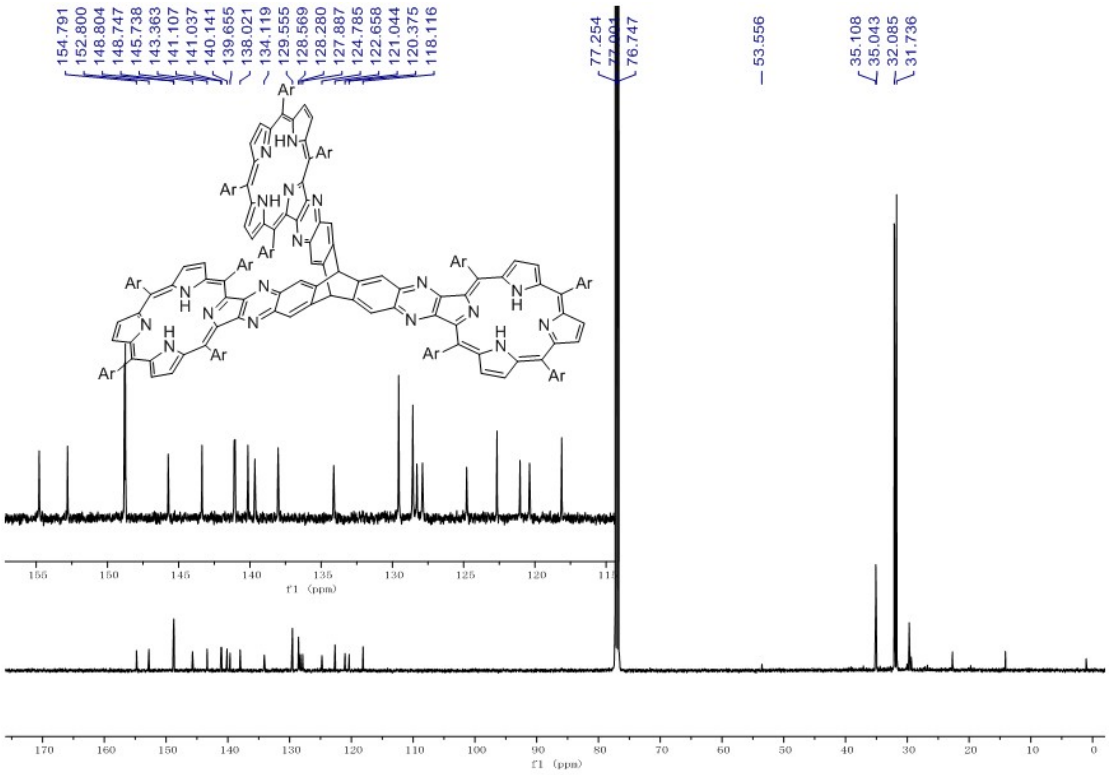

Figure S32. ^{13}C NMR spectrum of **12H** in $CDCl_3$ at 298 K

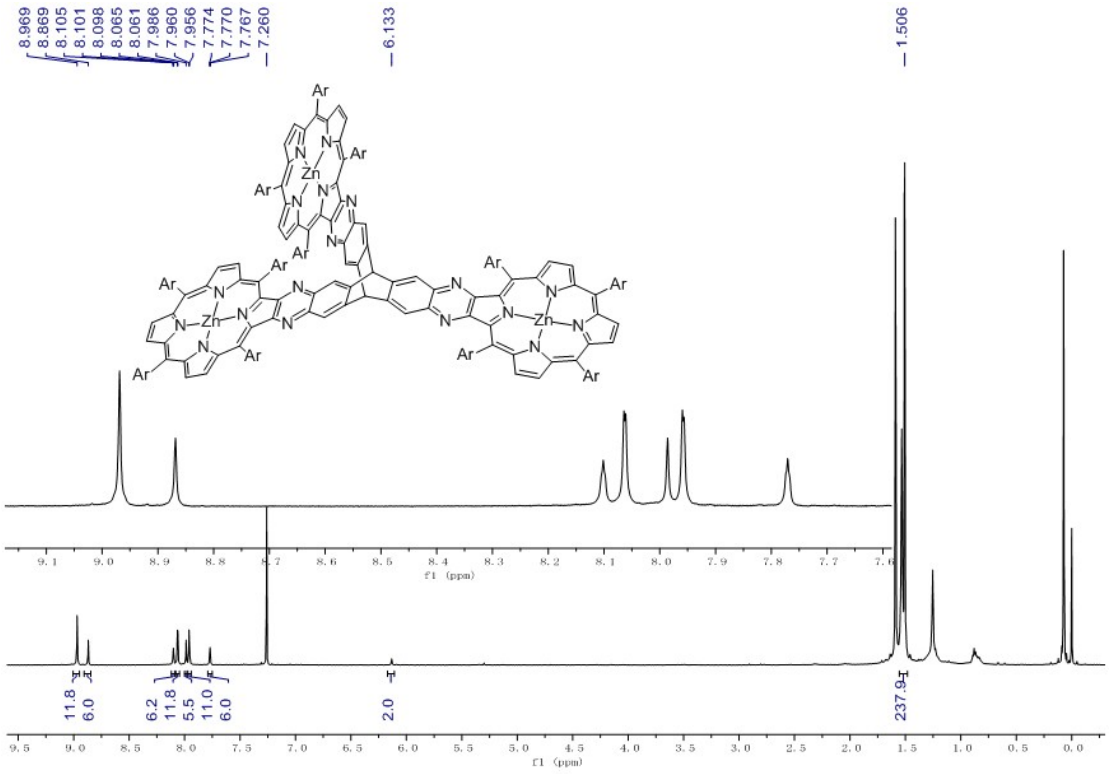

Figure S33. ^{1}H NMR spectrum of **12Zn** in $CDCl_3$ at 298 K

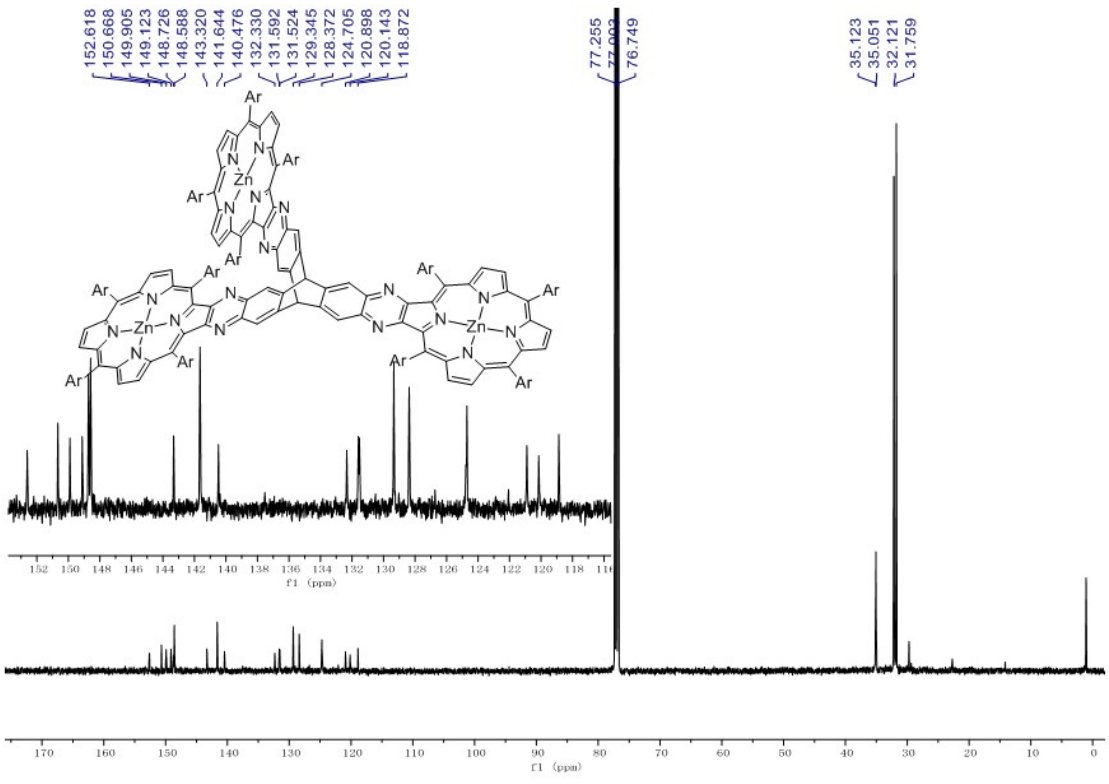

Figure S34. ^{13}C NMR spectrum of **12Zn** in $CDCl_3$ at 298 K

UV/Vis Absorption Spectra

Table S1. UV/Vis absorption data

Compound	λ/nm	Compound	λ/nm
3Ni	406, 444, 556, 600	**7Ni**	356, 422, 514, 649, 701
3H	430, 528, 562, 597	**8Ni**	321, 384, 489, 561, 796
3Zn	415, 440, 530, 567, 610	**9Ni**	370, 408, 450, 556, 599
4Ni	349, 420, 472, 634	**9H**	369, 436, 527, 599
4H	430, 537, 609	**10Ni**	411, 455, 560, 602
4Zn	395, 429, 472, 545, 587, 636	**11Ni**	408, 453, 522, 559, 600
5Ni	357, 402, 461, 549, 617, 659	**12Ni**	376, 412, 461, 560, 601
5H	347, 445, 532, 612, 667	**12H**	373, 441, 529, 565, 600
5Zn	343, 399, 459, 551, 603, 626, 653	**12Zn**	370, 423, 450, 532, 571, 612
6Ni	336, 394, 482, 666, 725		

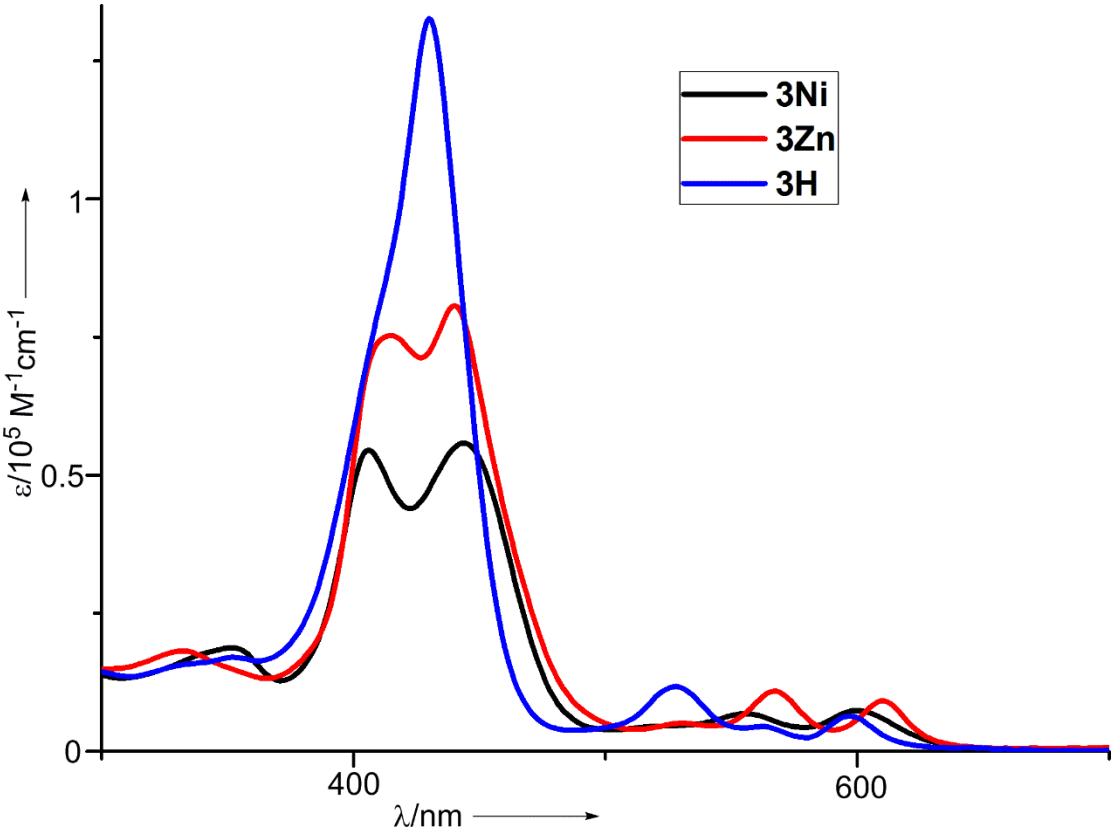

Figure S35. UV/Vis absorption spectra of **3Ni**, **3Zn**, and **3H** in CH_2Cl_2.

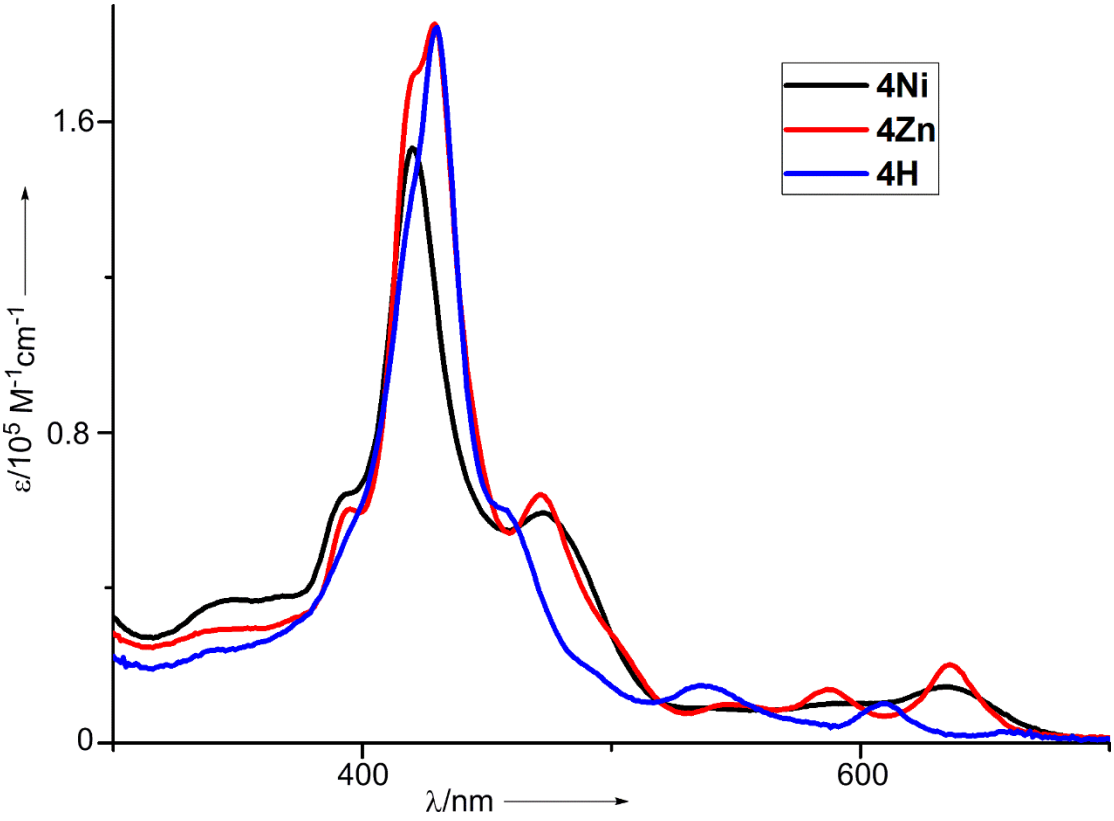

Figure S36. UV/Vis absorption spectra of **4Ni**, **4Zn** and **4H** in CH_2Cl_2.

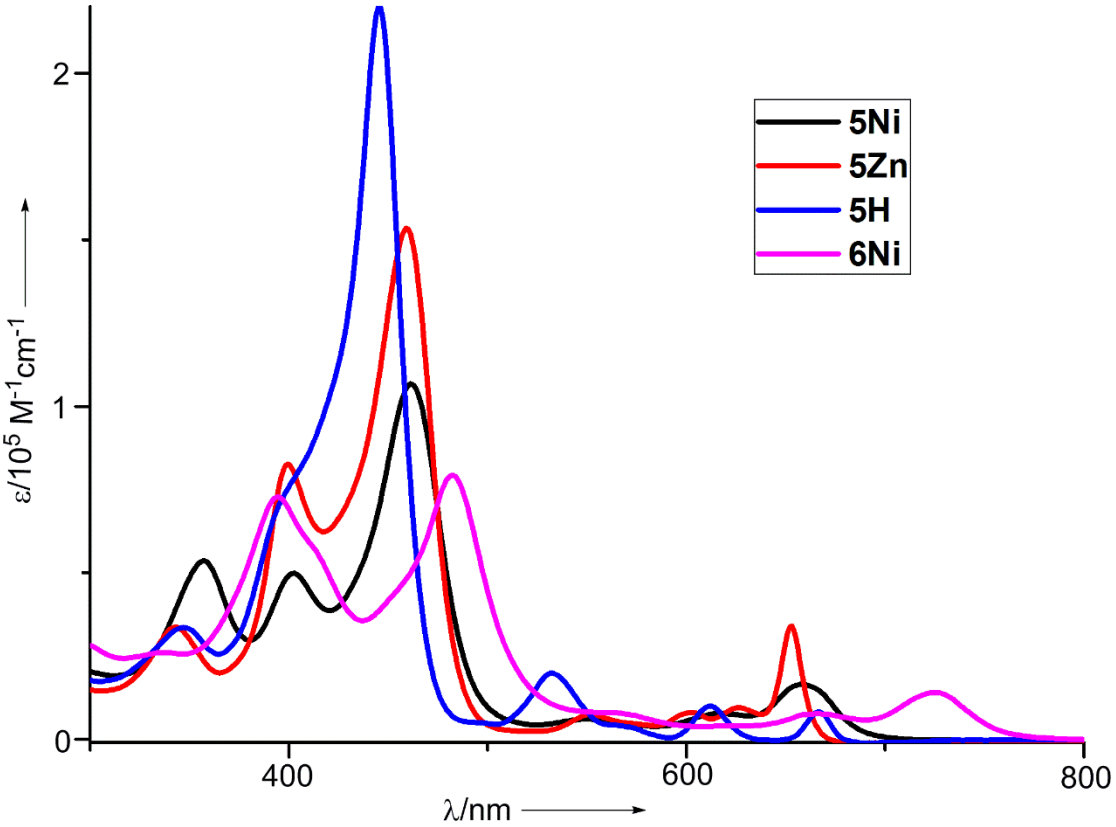

Figure S37. UV/Vis absorption spectra of **5Ni**, **5Zn**, **5H** and **6Ni** in CH_2Cl_2.

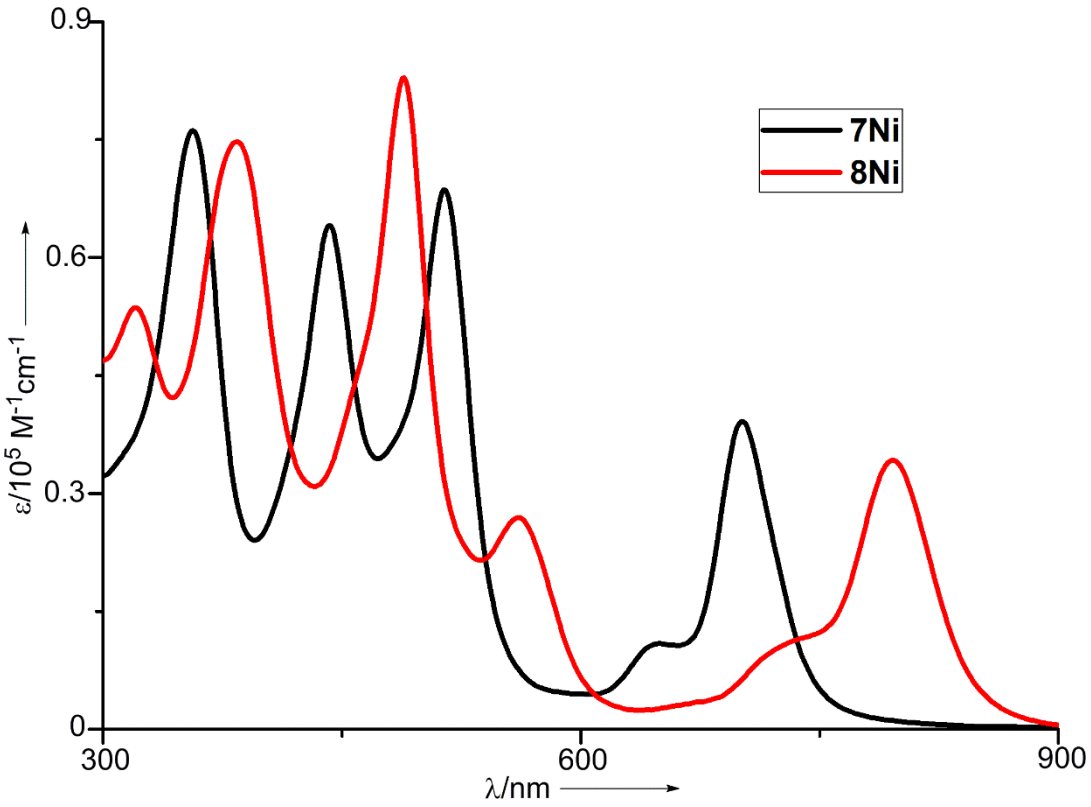

Figure S38. UV/Vis absorption spectra of **7Ni** and **8Ni** in CH_2Cl_2.

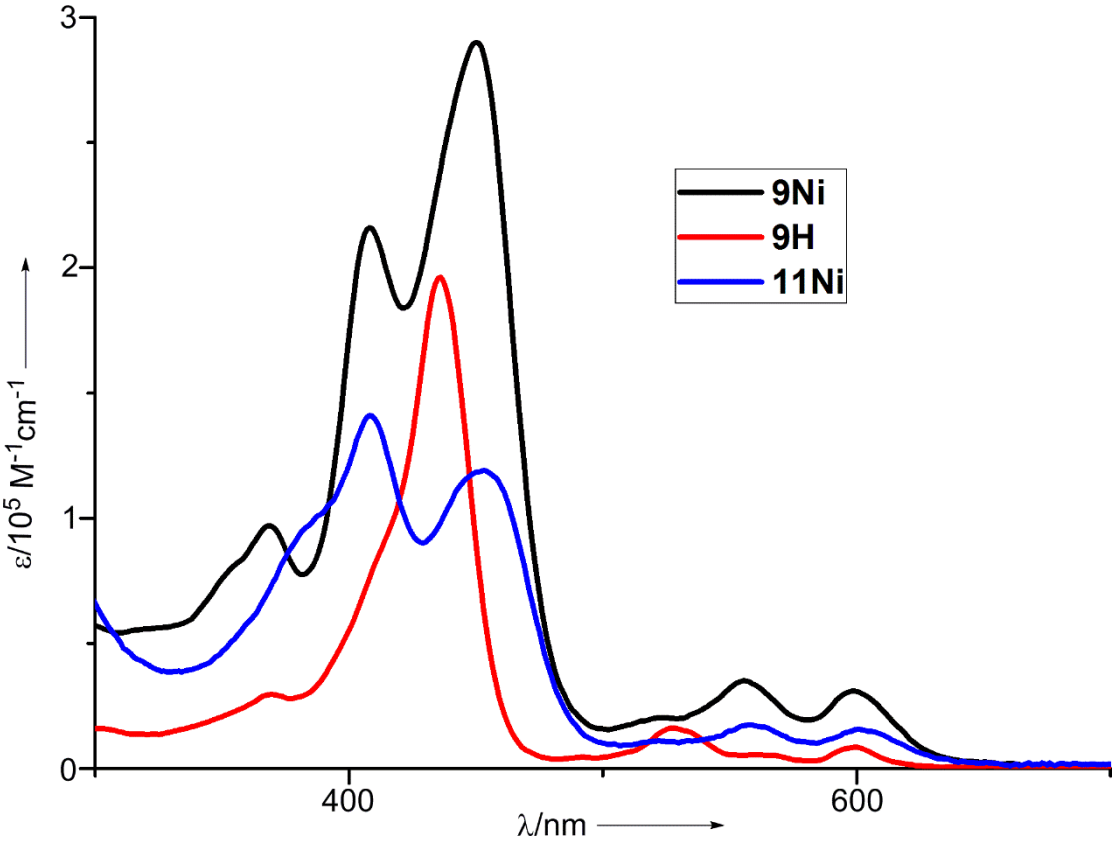

Figure S39. UV/Vis absorption spectra of **9Ni**, **9H** and **11Ni** in CH_2Cl_2.

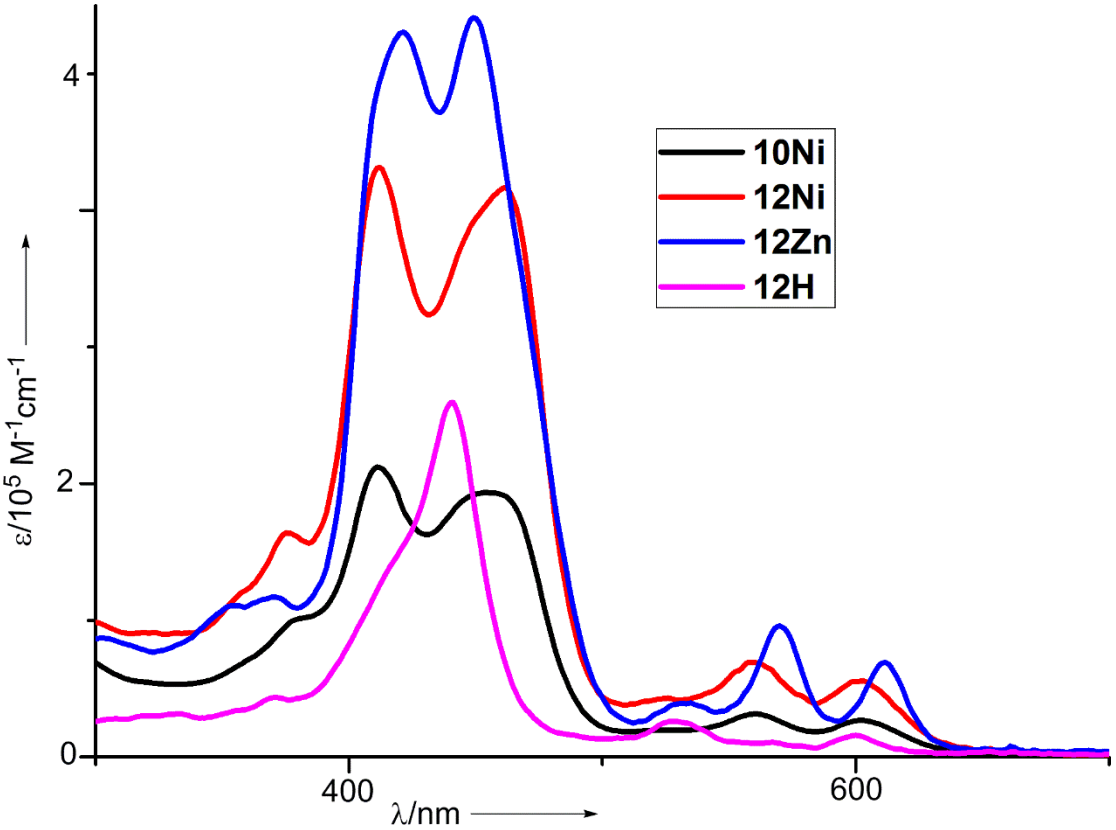

Figure S40. UV/Vis absorption spectra of **10Ni**, **12Ni**, **12Zn** and **12H** in CH_2Cl_2.

Electrochemical Data

Table S2. CV and DPV of **3Ni**, **4Ni**, **5Ni**, **7Ni**, **8Ni**, **9Ni** and **12Ni** in CH_2Cl_2 with 0.1 M tetra-*n*-butylammonium perchlorate (TBAP). Working electrode: glassy carbon; Counter electrode: Pt wire; Reference electrode: Ag/AgCl.

Compound	$E_{ox.1}$	$E_{red.1}$	$E_{red.2}$	ΔE_{HL}
3Ni	0.99	–1.09	–1.54	2.08
4Ni	0.97	–1.02	–1.35	1.99
5Ni	0.95	–0.96	–1.38	1.91
6Ni	0.91	–0.86	–1.24	1.77
7Ni	0.92	–0.85	–1.39	1.77
8Ni	0.72	–0.77	–1.21	1.49
9Ni	0.98	–1.09	–1.56	2.07
12Ni	1.04	–1.07	–1.95	2.11

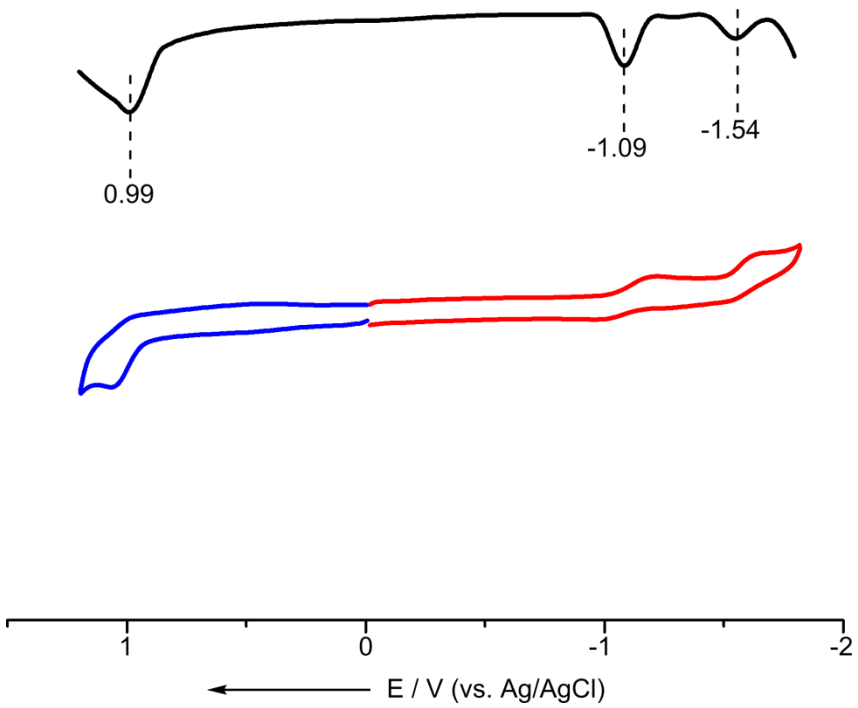

Figure S41. Cyclic voltammogram and differential pulse voltammogram of **3Ni**.

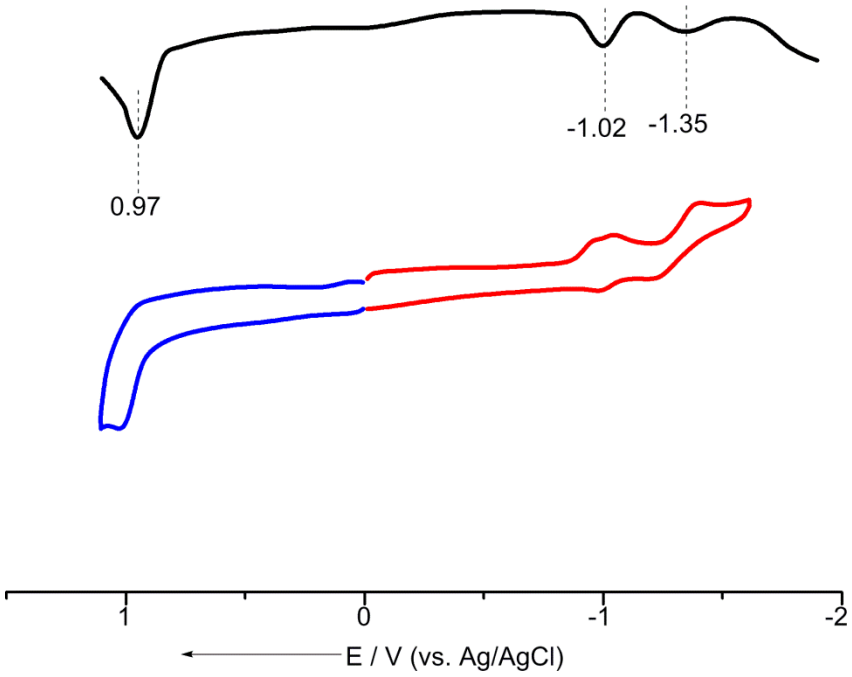

Figure S42. Cyclic voltammogram and differential pulse voltammogram of **4Ni**.

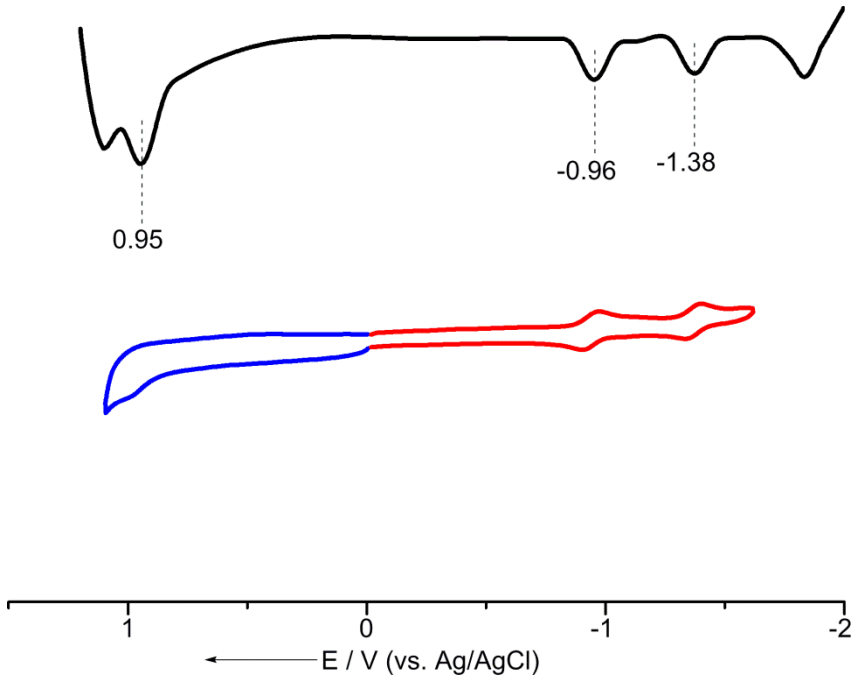

Figure S43. Cyclic voltammogram and differential pulse voltammogram of **5Ni**.

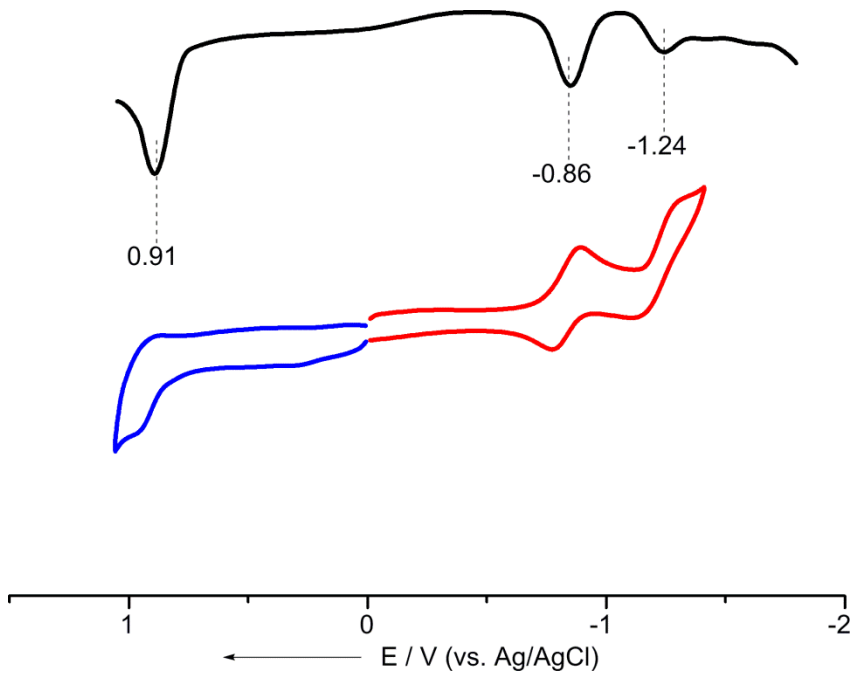

Figure S44. Cyclic voltammogram and differential pulse voltammogram of **6Ni**.

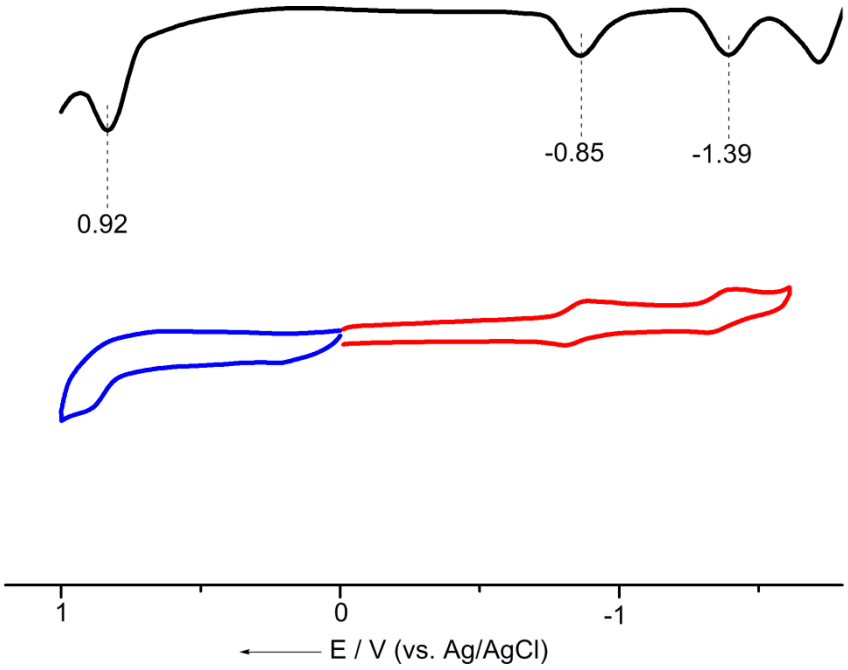

Figure S45. Cyclic voltammogram and differential pulse voltammogram of **7Ni**.

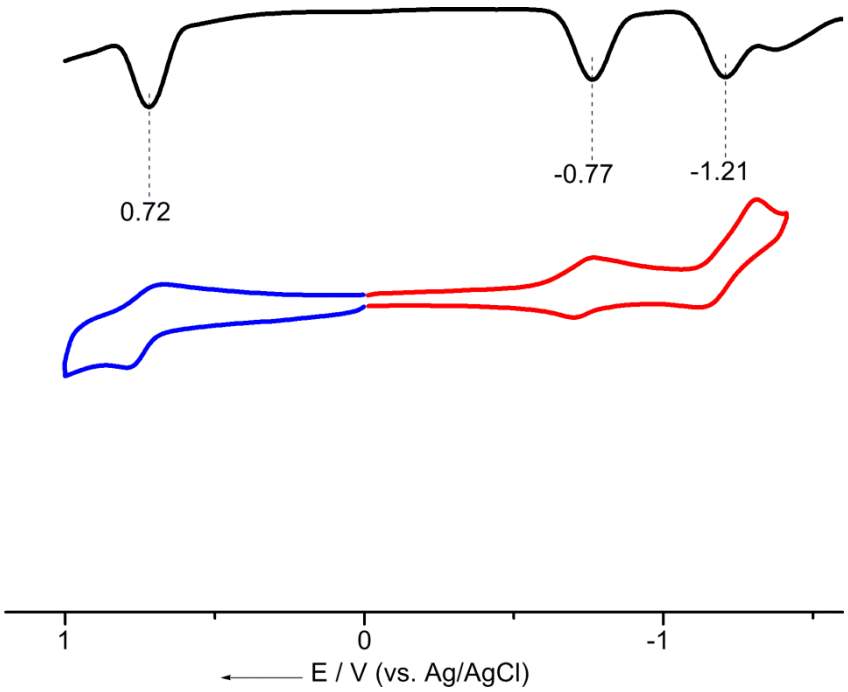

Figure S46. Cyclic voltammogram and differential pulse voltammogram of **8Ni**.

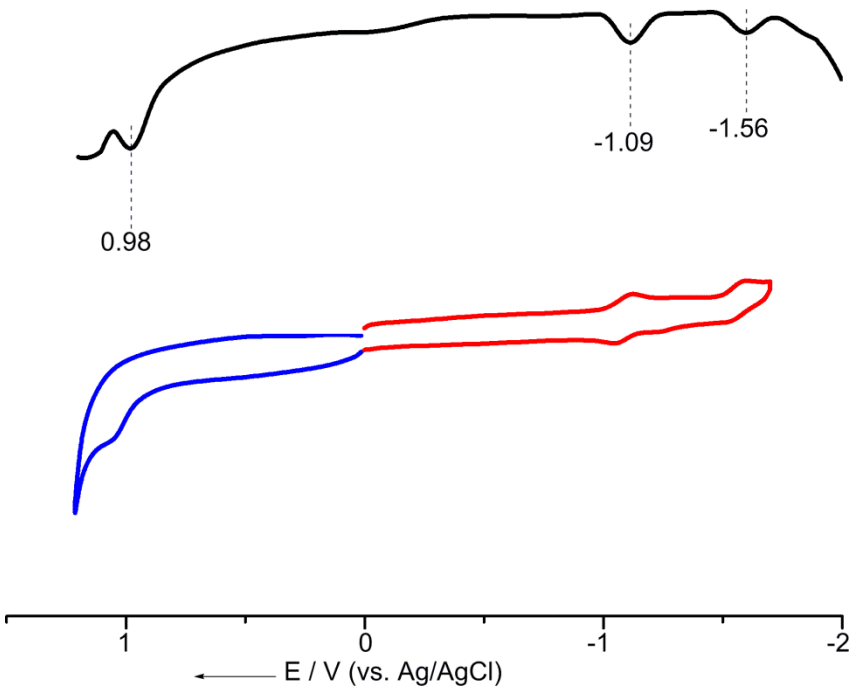

Figure S47. Cyclic voltammogram and differential pulse voltammogram of **9Ni**.

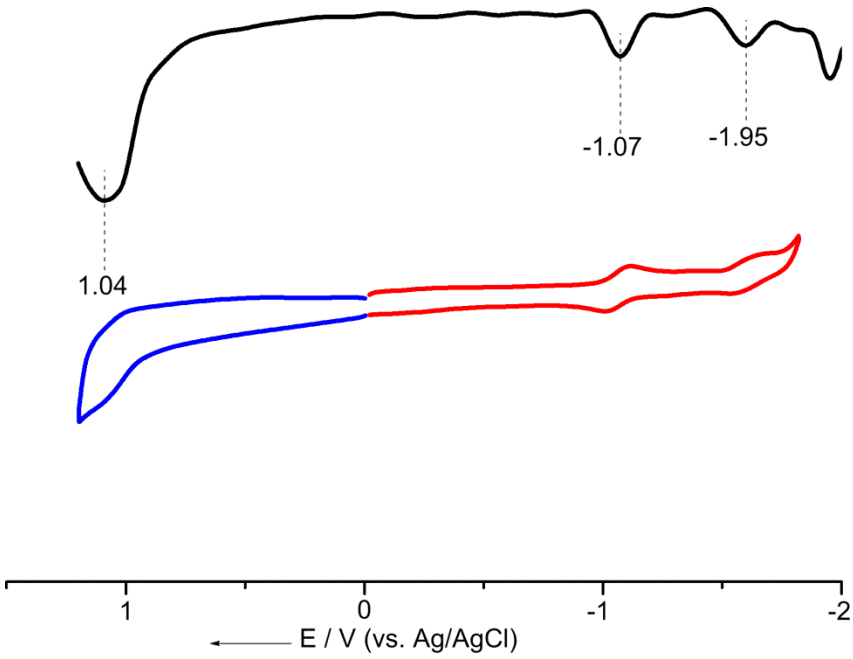

Figure S48. Cyclic voltammogram and differential pulse voltammogram of **12Ni**.

X-Ray Crystal Data

Single crystal of **5Ni**, **6Ni**, and **7Ni** were obtained by slow vapor diffusion of MeCN into a toluene solution. Single crystal of **8Ni** was obtained by slow vapor diffusion of ethanol into a chlorobenzene solution. Single crystal of **9Ni** was obtained by slow vapor diffusion of methanol into a toluene solution. Single crystal of **10Ni** was obtained by slow vapor diffusion of dimethylcarbinol into a *p*-xylene solution. Single crystal of **12Zn** was obtained by slow vapor diffusion of methanol into and toluene solution mixed with a drop of pyridine.

A suitable crystal of **5Ni**-**10Ni** and **12Zn** were selected and measured on a SuperNova, Dual, Cu at zero, EosS2 diffractometer. The crystal of **5Ni**, **7Ni**, **8Ni**, **10Ni** and **12Zn** were kept at 100.01(10) K during data collection. The crystal of **6Ni** and **9Ni** were kept at 100.00(11) K, 100.00(10) K during data collection, respectively. Using Olex[4], the structure of **5Ni**-**10Ni** and **12Zn** were solved with the olex2.solve[5] structure solution program using Charge Flipping and refined with the ShelXL[6] refinement package using Least Squares minimisation.

Crystallographic data for **5Ni**-**10Ni** and **12Zn** have been deposited with the Cambridge Crystallographic Data Centre as supplementary publication Nos. CCDC-2061480, 2061483, 2061481, 2061484, 2061485, 2061487 and 2061486, respectively.

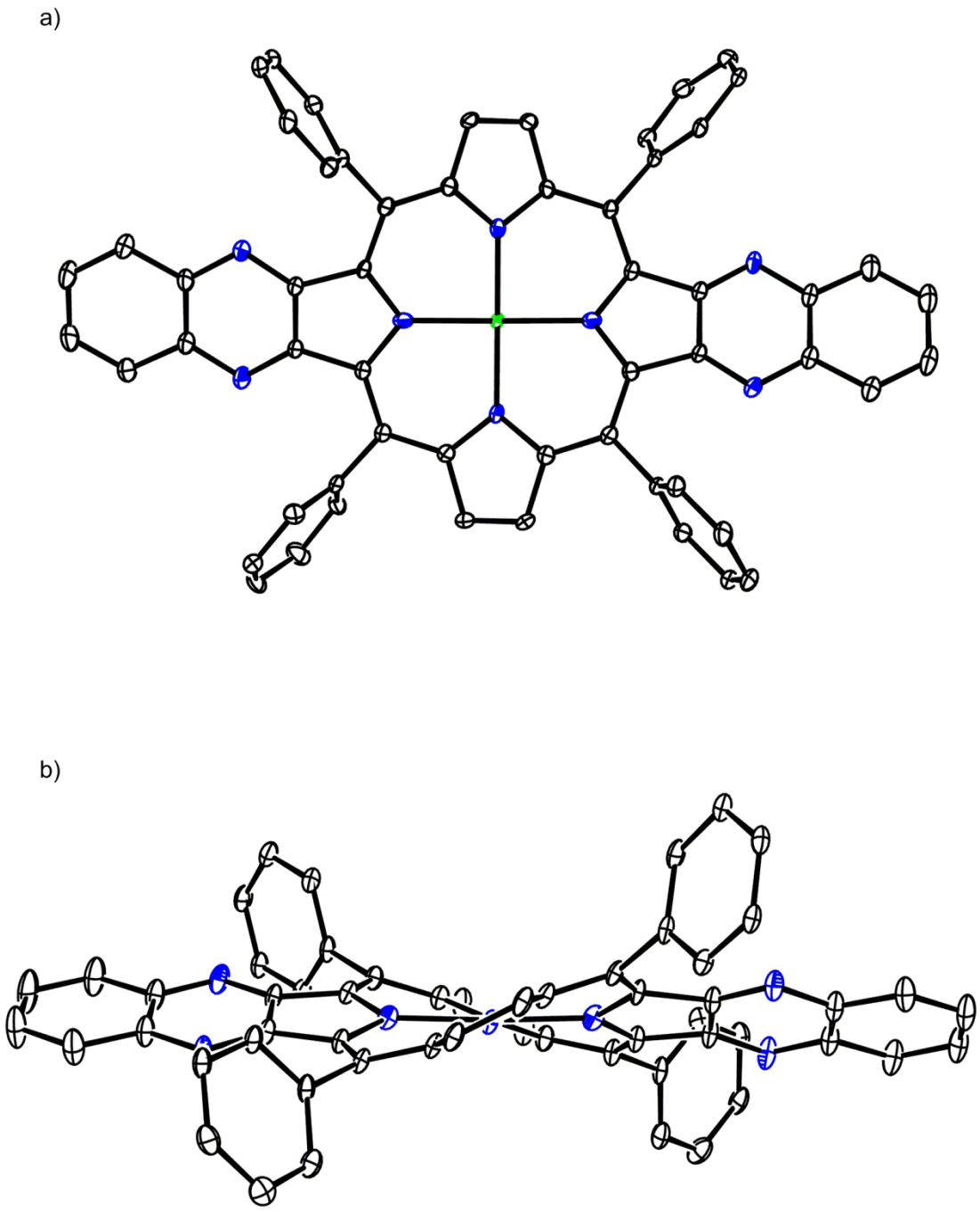

Figure S49. X-ray crystal structure of **5Ni**. (a) Top view, (b) side view. The thermal ellipsoids are 50% probability level. *tert*-Butyl groups and solvent molecules are omitted for clarity.

Table S3. Crystal data and structure refinement for **5Ni**

Identification code	exp_46_sq	
Empirical formula	$C_{88}H_{96}N_8Ni$	
Formula weight	1324.43	
Temperature	100.01(10) K	
Wavelength	1.54184 Å	
Crystal system	Triclinic	
Space group	P-1	
Unit cell dimensions	a = 16.1391(3) Å	α=111.8529(19)°.
	b = 16.8531(4) Å	β=109.1654(17)°.
	c = 20.3578(4) Å	γ= 96.7357(17)°.
Volume	4669.80(18) $Å^3$	
Z	2	
Density (calculated)	0.942 Mg/m^3	
Absorption coefficient	0.605 mm^{-1}	
F(000)	1416	
Crystal size	0.3 x 0.3 x 0.2 mm^3	
Theta range for data collection	4.367 to 66.598°.	
Index ranges	-19<=h<=19, -20<=k<=20, -18<=l<=24	
Reflections collected	48528	
Independent reflections	16484 [R(int) = 0.0555]	
Completeness to theta = 66.598°	100.0 %	
Absorption correction	Semi-empirical from equivalents	
Max. and min. transmission	1.00000 and 0.25268	
Refinement method	Full-matrix least-squares on F^2	
Data / restraints / parameters	16484 / 413 / 969	
Goodness-of-fit on F^2	1.082	
Final R indices [I>2sigma(I)]	R1 = 0.0723, wR2 = 0.1992	
R indices (all data)	R1 = 0.0800, wR2 = 0.2067	
Extinction coefficient	n/a	
Largest diff. peak and hole	0.987 and -0.587 e.$Å^{-3}$	

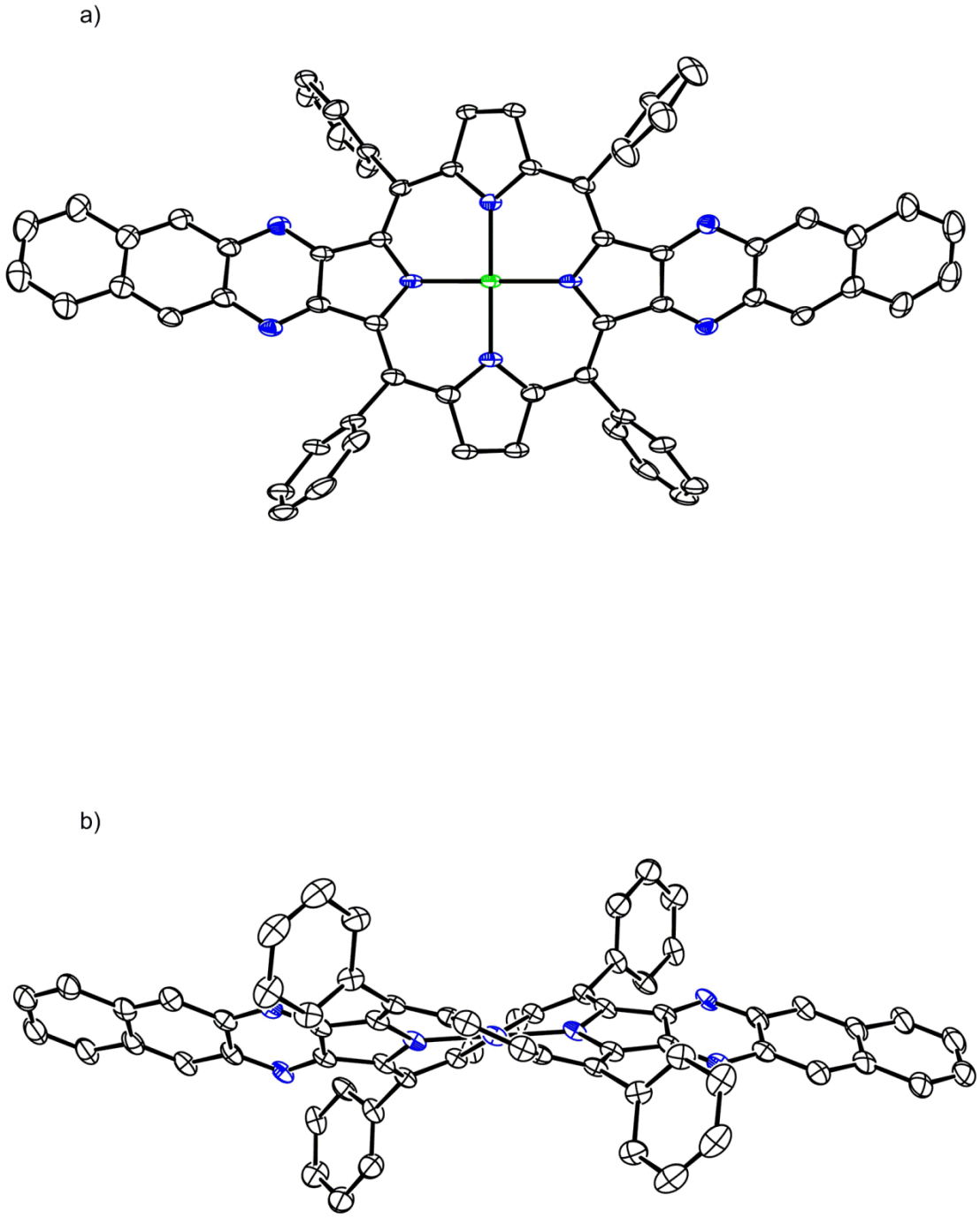

Figure S50. X-ray crystal structure of **6Ni**. (a) Top view, (b) side view. The thermal ellipsoids are 50% probability level. *tert*-Butyl groups and solvent molecules are omitted for clarity.

Table S4. Crystal data and structure refinement for **6Ni**

Identification code	exp_132_sq	
Empirical formula	$C_{96}H_{100}N_8Ni$	
Formula weight	1424.54	
Temperature	100.00(11) K	
Wavelength	1.54184 Å	
Crystal system	Monoclinic	
Space group	I 1 2/a 1	
Unit cell dimensions	a = 17.6246(4) Å	α = 90°.
	b = 17.1567(3) Å	β = 97.990(2)°.
	c = 30.5564(9) Å	γ = 90°.
Volume	9149.9(4) $Å^3$	
Z	4	
Density (calculated)	1.034 Mg/m^3	
Absorption coefficient	0.649 mm^{-1}	
F(000)	3040	
Crystal size	0.3 x 0.01 x 0.01 mm^3	
Theta range for data collection	4.420 to 66.598°.	
Index ranges	-20<=h<=20, -20<=k<=18, -36<=l<=36	
Reflections collected	28976	
Independent reflections	8079 [R(int) = 0.0523]	
Completeness to theta = 66.599°	99.9 %	
Absorption correction	Semi-empirical from equivalents	
Max. and min. transmission	1.00000 and 0.66504	
Refinement method	Full-matrix least-squares on F^2	
Data / restraints / parameters	8079 / 376 / 620	
Goodness-of-fit on F^2	1.033	
Final R indices [I>2sigma(I)]	R1 = 0.0823, wR2 = 0.2363	
R indices (all data)	R1 = 0.0926, wR2 = 0.2500	
Extinction coefficient	n/a	
Largest diff. peak and hole	0.818 and -0.495 $e.Å^{-3}$	

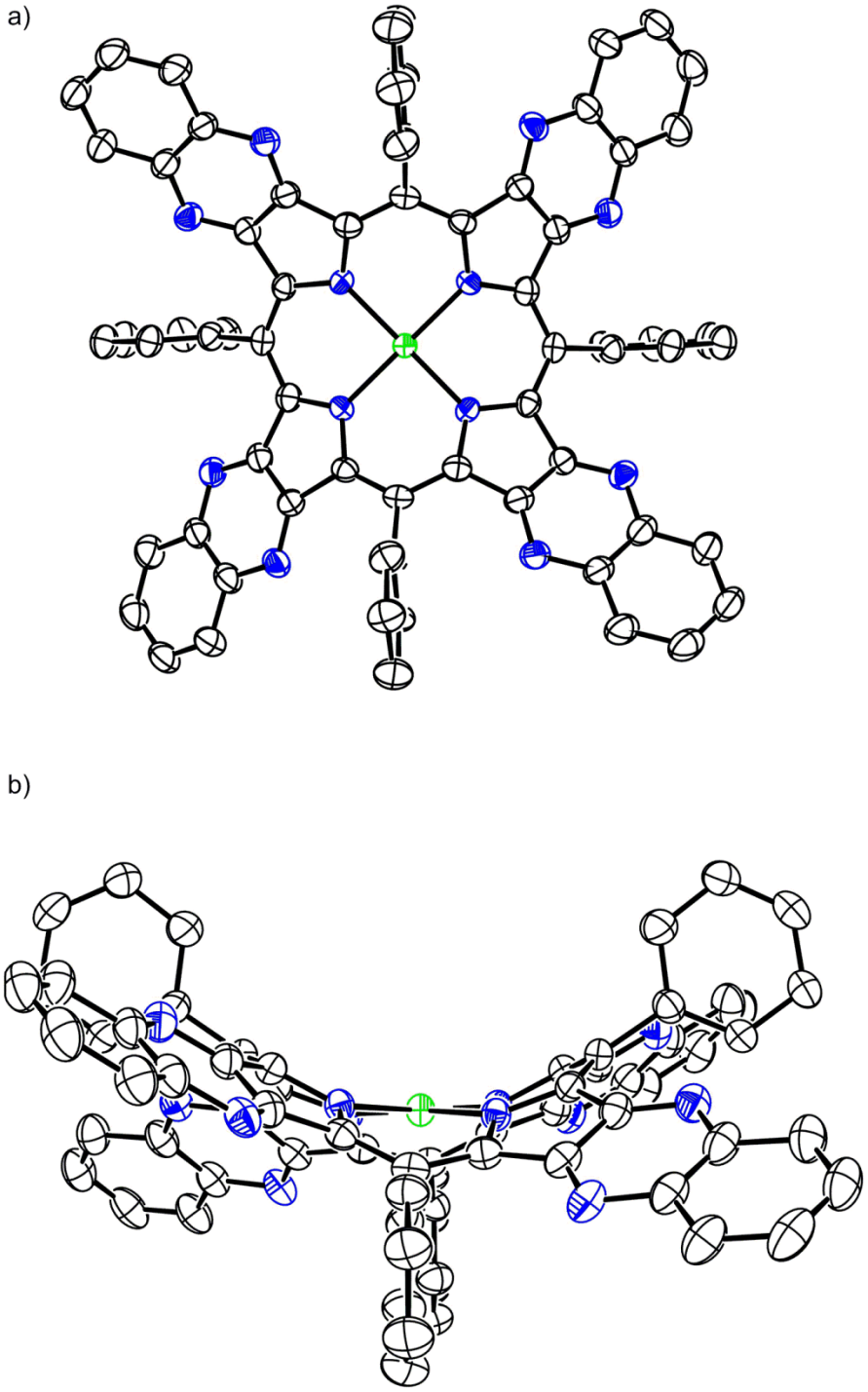

Figure S51. X-ray crystal structure of **7Ni**. (a) Top view, (b) side view. The thermal ellipsoids are 50% probability level. *tert*-Butyl groups and solvent molecules are omitted for clarity.

Table S5. Crystal data and structure refinement for **7Ni**

Identification code	exp_125_sq	
Empirical formula	$C_{100}H_{100}N_{12}Ni$	
Formula weight	1528.62	
Temperature	100.01(10) K	
Wavelength	1.54184 Å	
Crystal system	Tetragonal	
Space group	P-421c	
Unit cell dimensions	a = 21.8548(8) Å	α = 90°.
	b = 21.8548(8) Å	β = 90°.
	c = 9.0971(5) Å	γ = 90°.
Volume	4345.1(4) $Å^3$	
Z	2	
Density (calculated)	1.168 Mg/m^3	
Absorption coefficient	0.731 mm^{-1}	
F(000)	1624	
Crystal size	0.3 x 0.01 x 0.01 mm^3	
Theta range for data collection	4.046 to 66.590°.	
Index ranges	-26<=h<=26, -25<=k<=26, -10<=l<=4	
Reflections collected	28758	
Independent reflections	3835 [R(int) = 0.1398]	
Completeness to theta = 66.590°	100.0 %	
Absorption correction	Semi-empirical from equivalents	
Max. and min. transmission	1.00000 and 0.06285	
Refinement method	Full-matrix least-squares on F^2	
Data / restraints / parameters	3835 / 222 / 322	
Goodness-of-fit on F^2	1.044	
Final R indices [I>2sigma(I)]	R1 = 0.0630, wR2 = 0.1652	
R indices (all data)	R1 = 0.0776, wR2 = 0.1803	
Absolute structure parameter	-0.05(6)	
Extinction coefficient	n/a	
Largest diff. peak and hole	0.377 and -0.312 e.$Å^{-3}$	

a)

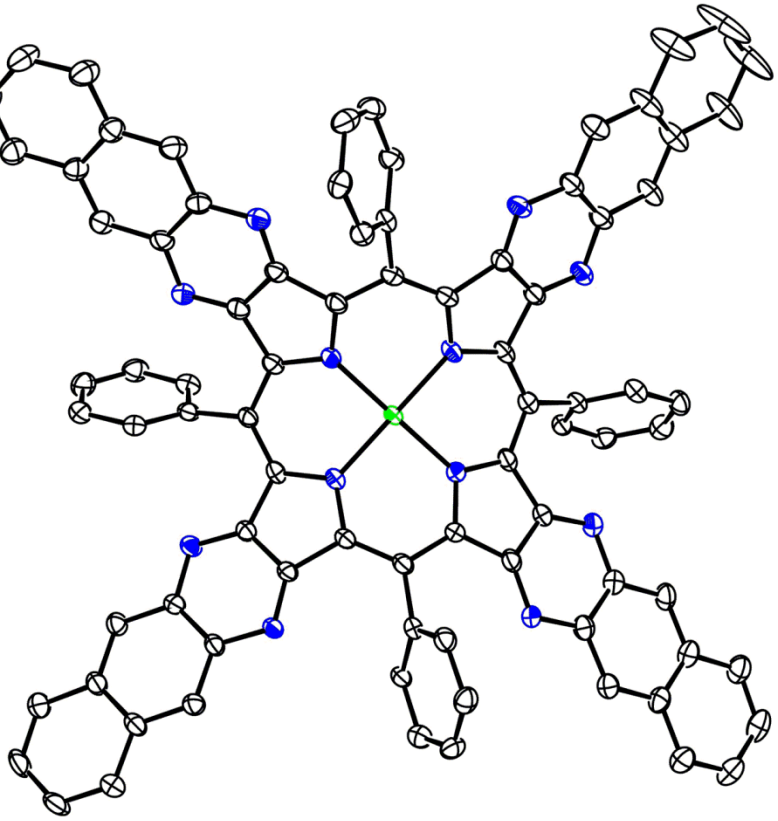

b)

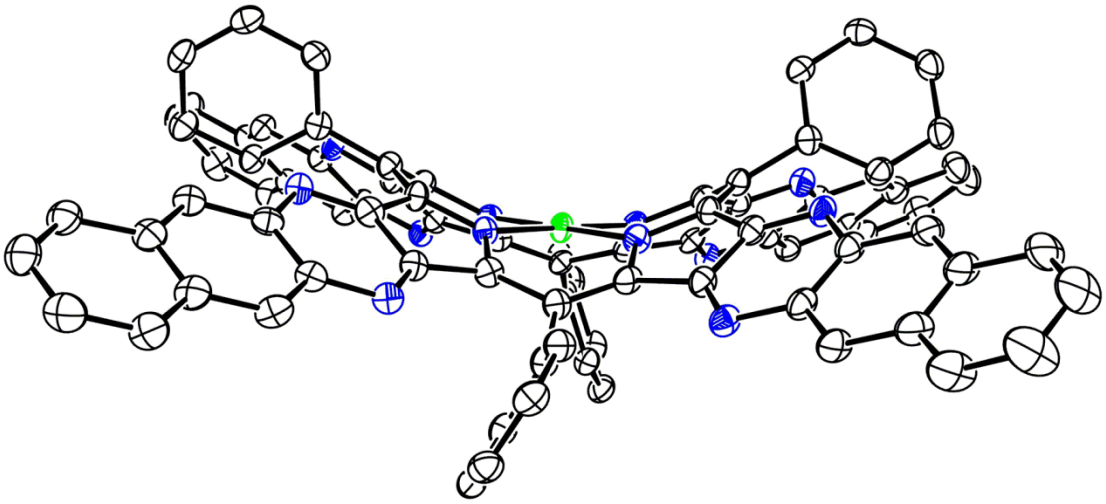

Figure S52. X-ray crystal structure of **8Ni**. (a) Top view, (b) side view. The thermal ellipsoids are 50% probability level. *tert*-Butyl groups and solvent molecules are omitted for clarity.

Table S6. Crystal data and structure refinement for **8Ni**

Identification code	exp_367_sq	
Empirical formula	$C_{116}H_{108}N_{12}Ni$	
Formula weight	1728.85	
Temperature	100.01(10) K	
Wavelength	1.54184 Å	
Crystal system	Monoclinic	
Space group	P 1 21/n 1	
Unit cell dimensions	a = 9.47195(18) Å	α = 90°.
	b = 33.8469(6) Å	β = 92.7229(17)°.
	c = 34.0796(6) Å	γ = 90°.
Volume	10913.5(4) $Å^3$	
Z	4	
Density (calculated)	1.052 Mg/m^3	
Absorption coefficient	0.635 mm^{-1}	
F(000)	3664	
Crystal size	0.1 x 0.1 x 0.01 mm^3	
Theta range for data collection	4.109 to 66.600°.	
Index ranges	-11<=h<=11, -40<=k<=40, -40<=l<=40	
Reflections collected	146801	
Independent reflections	19282 [R(int) = 0.0839]	
Completeness to theta = 66.600°	100.0 %	
Absorption correction	Semi-empirical from equivalents	
Max. and min. transmission	1.00000 and 0.33519	
Refinement method	Full-matrix least-squares on F^2	
Data / restraints / parameters	19282 / 491 / 1217	
Goodness-of-fit on F^2	1.056	
Final R indices [I>2sigma(I)]	R1 = 0.0677, wR2 = 0.1849	
R indices (all data)	R1 = 0.0897, wR2 = 0.1962	
Extinction coefficient	n/a	
Largest diff. peak and hole	1.802 and -0.532 $e.Å^{-3}$	

a)

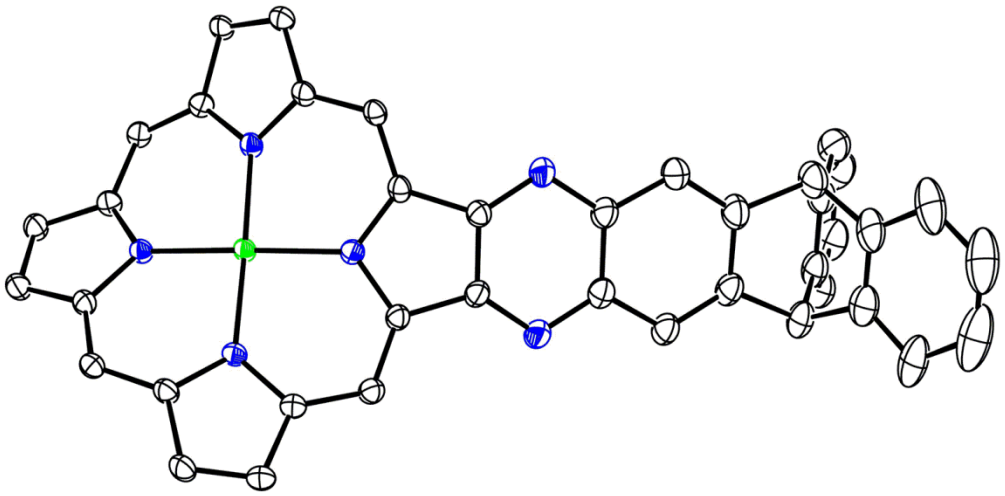

b)

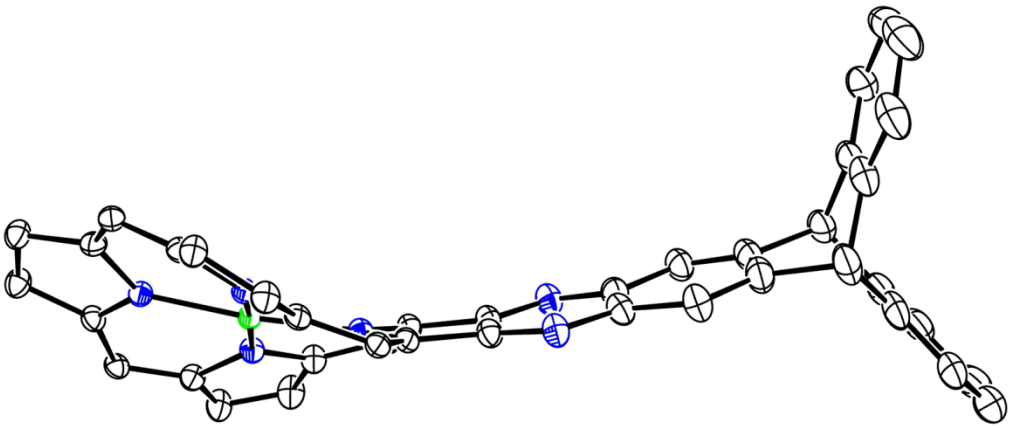

Figure S53. X-ray crystal structure of **9Ni**. (a) Top view, (b) side view. The thermal ellipsoids are 30% probability level. 3,5-di-*tert*-butylphenyl groups and solvent molecules are omitted for clarity.

Table S7. Crystal data and structure refinement for **9Ni**

Identification code	exp_375_sq	
Empirical formula	$C_{103}H_{110}N_6Ni$	
Formula weight	1490.67	
Temperature	100.00(10) K	
Wavelength	1.54184 Å	
Crystal system	Triclinic	
Space group	P-1	
Unit cell dimensions	a = 14.9984(3) Å	α=103.3287(16)°.
	b = 15.1050(3) Å	β= 95.3569(16)°.
	c = 19.2933(4) Å	γ= 97.8627(16)°.
γ		
Volume	4177.68(14) $Å^3$	
Z	2	
Density (calculated)	1.185 Mg/m^3	
Absorption coefficient	0.724 mm^{-1}	
F(000)	1596	
Crystal size	0.3 x 0.2 x 0.2 mm^3	
Theta range for data collection	4.061 to 66.596°.	
Index ranges	-16<=h<=17, -17<=k<=17, -22<=l<=22	
Reflections collected	58314	
Independent reflections	14724 [R(int) = 0.0562]	
Completeness to theta = 66.596°	99.9 %	
Absorption correction	Semi-empirical from equivalents	
Max. and min. transmission	1.00000 and 0.71397	
Refinement method	Full-matrix least-squares on F^2	
Data / restraints / parameters	14724 / 0 / 1078	
Goodness-of-fit on F^2	1.043	
Final R indices [I>2sigma(I)]	R1 = 0.0777, wR2 = 0.2250	
R indices (all data)	R1 = 0.0936, wR2 = 0.2433	
Extinction coefficient	n/a	
Largest diff. peak and hole	1.473 and -0.547 e.$Å^{-3}$	

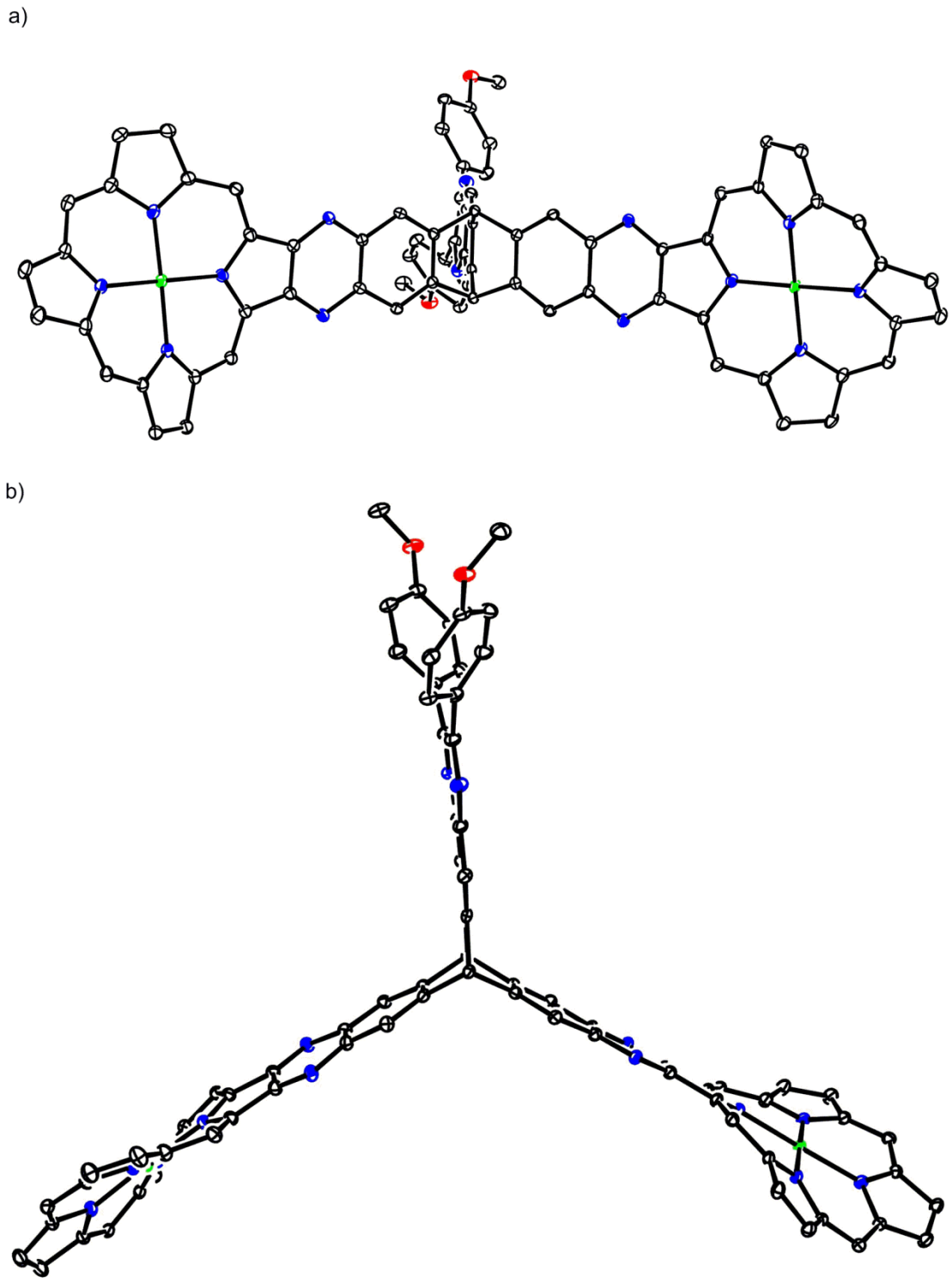

Figure S54. X-ray crystal structure of **10Ni**. (a) Top view, (b) side view. The thermal ellipsoids are 30% probability level. 3,5-di-*tert*-butylphenyl groups and solvent molecules are omitted for clarity.

Table S8. Crystal data and structure refinement for **10Ni**

Identification code	exp_548_sq	
Empirical formula	$C_{188}H_{202}N_{14}Ni_2O_2$	
Formula weight	2807.04	
Temperature	100.01(10) K	
Wavelength	1.54184 Å	
Crystal system	Triclinic	
Space group	P-1	
Unit cell dimensions	a = 16.7663(2) Å	α = 78.6397(9)°.
	b = 23.8905(3) Å	β = 87.1794(10)°.
	c = 28.1890(3) Å	γ = 78.6812(10)°.
Volume	10854.1(2) $Å^3$	
Z	2	
Density (calculated)	0.859 Mg/m^3	
Absorption coefficient	0.545 mm^{-1}	
F(000)	3000	
Crystal size	0.2 x 0.2 x 0.1 mm^3	
Theta range for data collection	3.575 to 66.601°.	
Index ranges	-17<=h<=19, -28<=k<=28, -33<=l<=33	
Reflections collected	154157	
Independent reflections	38297 [R(int) = 0.0383]	
Completeness to theta = 66.601°	99.9 %	
Absorption correction	Semi-empirical from equivalents	
Max. and min. transmission	1.00000 and 0.82446	
Refinement method	Full-matrix least-squares on F^2	
Data / restraints / parameters	38297 / 693 / 1904	
Goodness-of-fit on F^2	1.055	
Final R indices [I>2sigma(I)]	R1 = 0.0669, wR2 = 0.1761	
R indices (all data)	R1 = 0.0768, wR2 = 0.1833	
Extinction coefficient	n/a	
Largest diff. peak and hole	1.013 and -0.532 e.$Å^{-3}$	

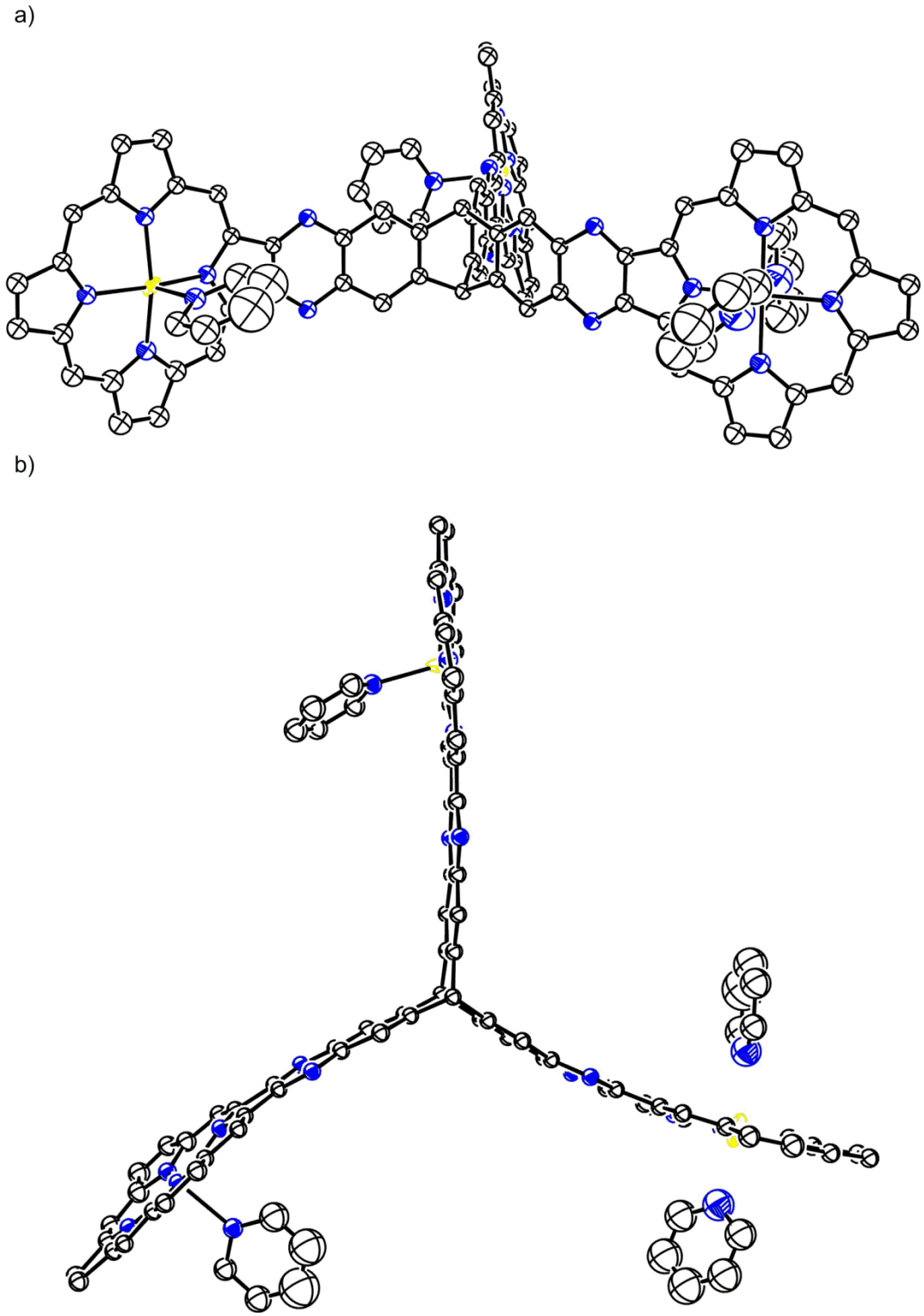

Figure S55. X-ray crystal structure of **12Zn**. (a) Top view, (b) side view. The thermal ellipsoids are 30% probability level. Hydrogen atoms, 3,5-di-*tert*-butylphenyl groups and solvent molecules are omitted for clarity.

Table S9. Crystal data and structure refinement for **12Zn**

Identification code	exp_424_sq	
Empirical formula	$C_{263}H_{293}N_{21}Zn_3$	
Formula weight	3944.28	
Temperature	100.01(10) K	
Wavelength	1.54184 Å	
Crystal system	Triclinic	
Space group	P-1	
Unit cell dimensions	a = 23.4051(8) Å	α = 98.679(2)°.
	b = 25.6957(5) Å	β = 90.766(2)°.
	c = 26.3918(7) Å	γ = 91.045(2)°.
Volume	15685.9(7) $Å^3$	
Z	2	
Density (calculated)	0.835 Mg/m^3	
Absorption coefficient	0.591 mm^{-1}	
F(000)	4216	
Crystal size	0.3 x 0.2 x 0.02 mm^3	
Theta range for data collection	3.907 to 66.600°.	
Index ranges	-27<=h<=27, -30<=k<=30, -31<=l<=31	
Reflections collected	219999	
Independent reflections	55376 [R(int) = 0.1043]	
Completeness to theta = 66.600°	99.9 %	
Absorption correction	Semi-empirical from equivalents	
Max. and min. transmission	1.00000 and 0.56448	
Refinement method	Full-matrix least-squares on F^2	
Data / restraints / parameters	55376 / 2046 / 3084	
Goodness-of-fit on F^2	1.184	
Final R indices [I>2sigma(I)]	R1 = 0.1253, wR2 = 0.3490	
R indices (all data)	R1 = 0.1888, wR2 = 0.3994	
Extinction coefficient	n/a	
Largest diff. peak and hole	1.435 and -0.624 e.$Å^{-3}$	

Density Functional Theory (DFT) calculations

DFT calculations were carried out at the B3LYP/6-31G(d)(C,H,N) level using the Gaussian 09 package.

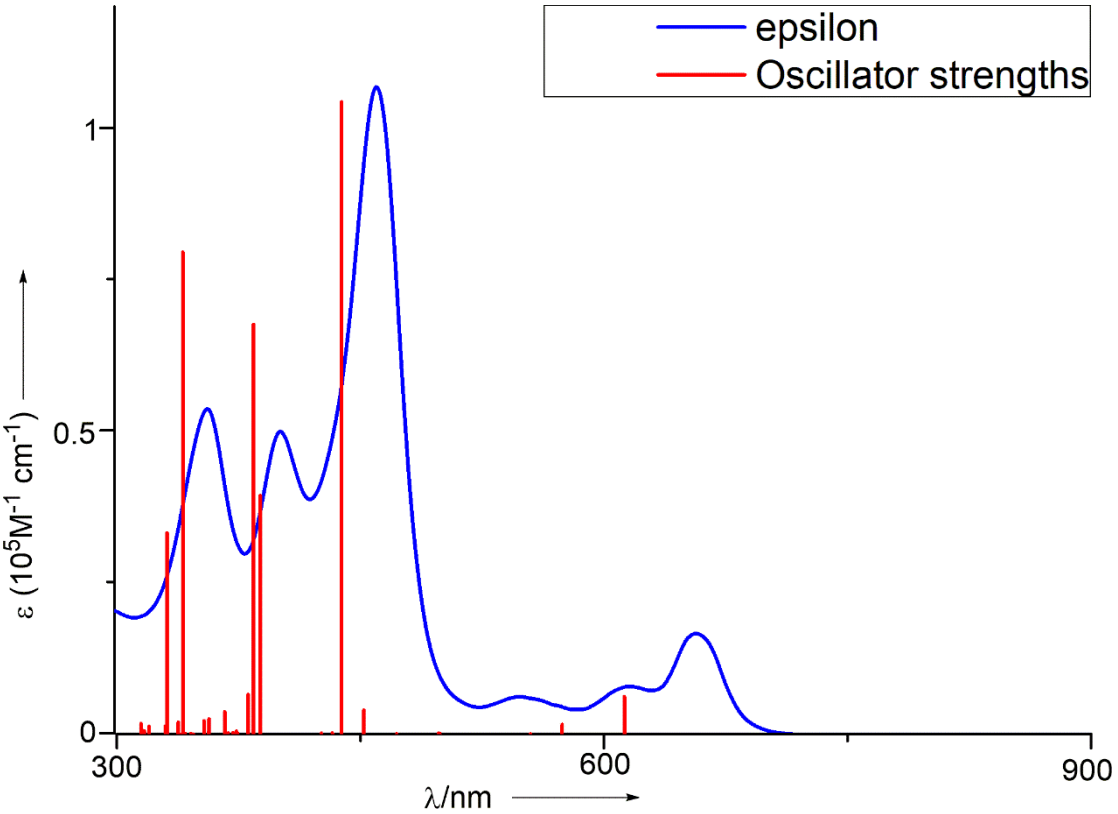

Wavelength (nm)	Oscillator Strengths	Major Transitions
613	0.062	HOMO-1→LUMO+1 (11%); HOMO→LUMO (88%)
574	0.0158	HOMO-1→LUMO (63%); HOMO→LUMO+1 (27%)
438	1.0430	HOMO-1→LUMO (24%); HOMO→LUMO+3 (19%); HOMO→LUMO+1 (55%)
388	0.3933	HOMO-1→LUMO+3 (69%)
384	0.6759	HOMO-1→LUMO+1 (48%); HOMO→LUMO+3 (34%)
341	0.7953	HOMO-4→LUMO+2 (91%)
331	0.3316	HOMO-18→LUMO (65%); HOMO-14→LUMO (18%)

Figure S56. Calculated vertical transitions and major transitions of **5Ni** calculated by TD-DFT using B3LYP employing the 6-31G(d) basis set.

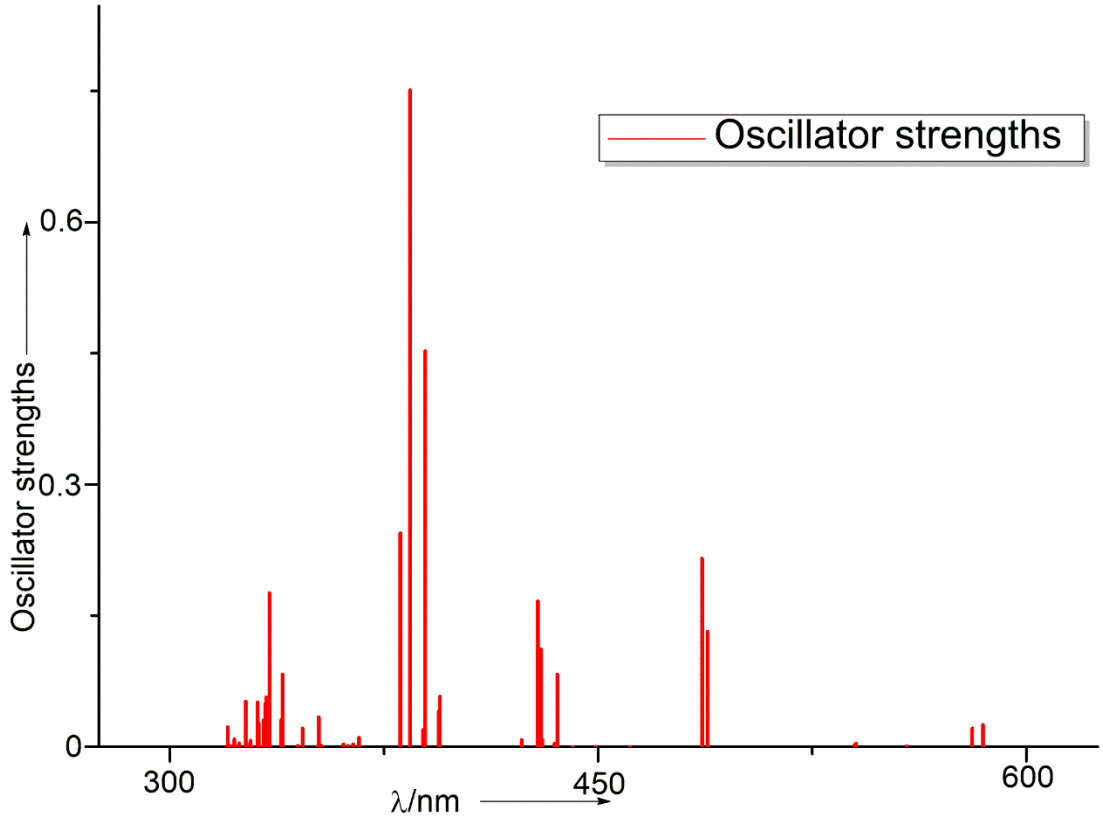

Wavelength (nm)	Oscillator Strengths	Major Transitions
585	0.0251	HOMO-1→LUMO+1 (25%); HOMO→LUMO (74%)
581	0.0212	HOMO-1→LUMO (32%); HOMO→LUMO+1 (66%)
488	0.1317	HOMO-1→LUMO+1 (45%); HOMO→LUMO (14%); HOMO→LUMO+2 (37%)
486	0.2152	HOMO-1→LUMO (45%); HOMO→LUMO+1 (19%); HOMO→LUMO+3 (29%)
430	0.1117	HOMO-2→LUMO+1 (37%); HOMO→LUMO+3 (15%)
429	0.1665	HOMO-2→LUMO+1 (12%); HOMO-1→LUMO+3 (28%); HOMO→LUMO+2 (24%)
389	0.4526	HOMO-1→LUMO+1 (10%); HOMO-1→LUMO+3 (44%); HOMO→LUMO+2 (15%)
384	0.7509	HOMO-1→LUMO (10%); HOMO→LUMO+2 (37%); HOMO→LUMO+3 (15%)

Figure S57. Calculated vertical transitions and major transitions of **5Ni'** calculated by TD-DFT using B3LYP employing the 6-31G(d) basis set.

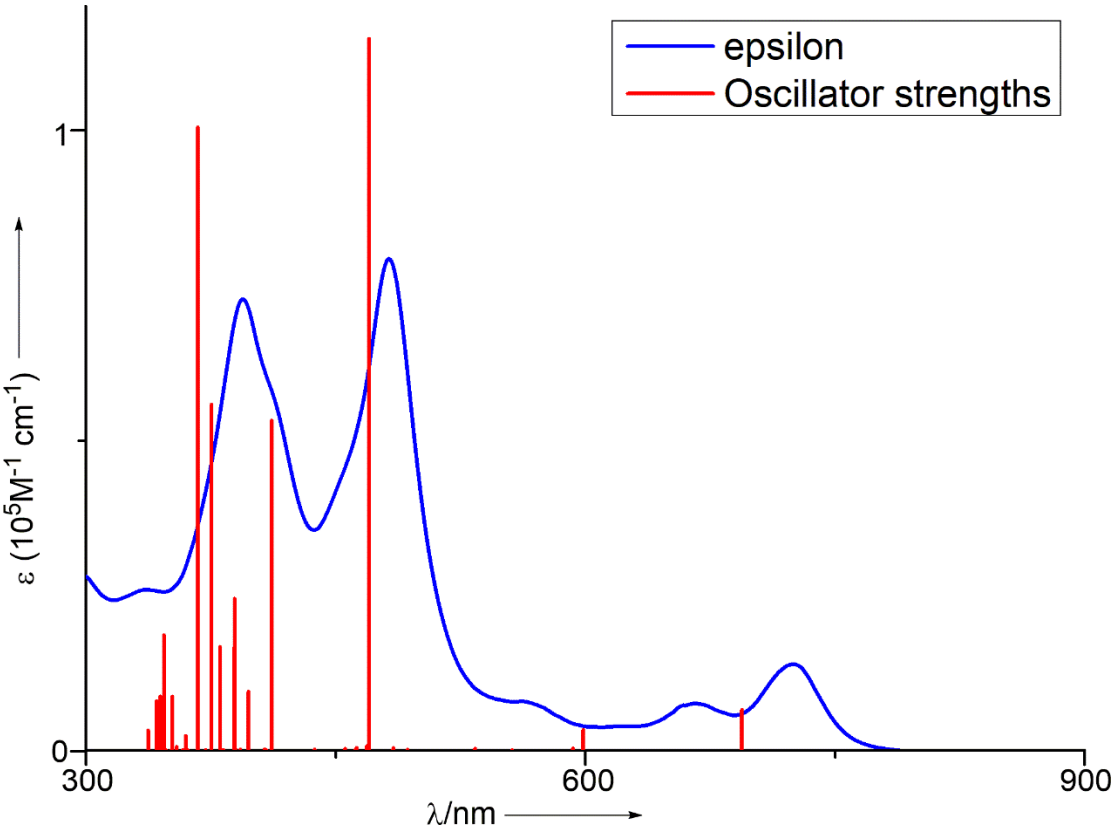

Wavelength (nm)	Oscillator Strengths	Major Transitions
694	0.0651	HOMO→LUMO (95%)
599	0.0327	HOMO-1→LUMO (73%); HOMO→LUMO+2 (23%)
470	1.1454	HOMO-1→LUMO (19%); HOMO-1→LUMO+3 (20%); HOMO→LUMO+2 (59%)
412	0.5303	HOMO-3→LUMO+2 (10%); HOMO-1→LUMO+3 (68%); HOMO→LUMO+2 (12%)
389	0.2420	HOMO-7→LUMO (15%); HOMO-5→LUMO+1 (20%); HOMO-4→LUMO+1 (19%); HOMO-1→LUMO+2 (22%)
389	0.1648	HOMO-7→LUMO (13%); HOMO-5→LUMO+1 (29%); HOMO-1→LUMO+2 (24%)
381	0.1663	HOMO-10→LUMO (89%)
376	0.5565	HOMO-11→LUMO (51%); HOMO-6→LUMO+1 (15%); HOMO-3→LUMO+2 (20%)
367	1.0025	HOMO-11→LUMO (21%); HOMO-6→LUMO+1 (53%)

347	0.1853	HOMO-18→LUMO (22%); HOMO-3→LUMO+3 (59%)

Figure S58. Calculated vertical transitions and major transitions of **6Ni** calculated by TD-DFT using B3LYP employing the 6-31G(d) basis set.

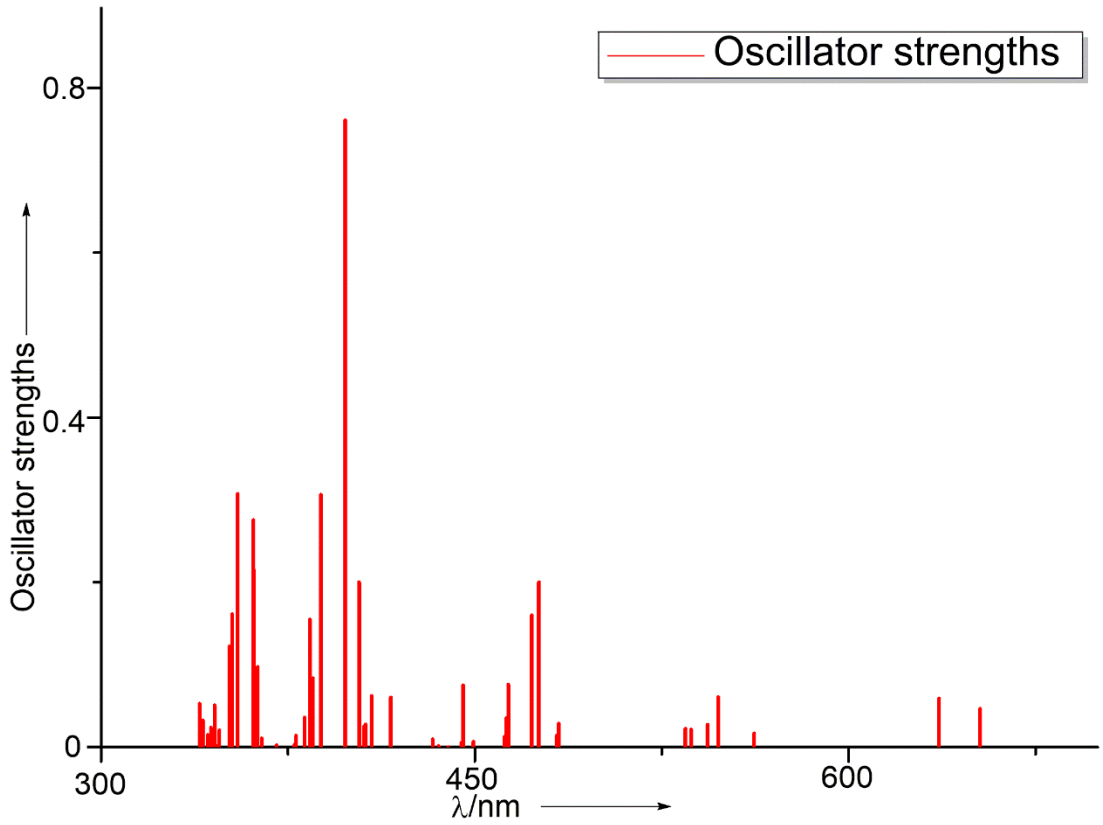

Wavelength (nm)	Oscillator Strengths	Major Transitions
653	0.0467	HOMO→LUMO (91%)
636	0.0593	HOMO-1→LUMO(11%); HOMO→LUMO+1 (87%)
476	0.2004	HOMO-2→LUMO (21%); HOMO-1→LUMO (11%); HOMO-1→LUMO+3 (15%); HOMO→LUMO+2 (38%)
473	0.1603	HOMO-2→LUMO+1 (30%); HOMO-1→LUMO+1 (11%); HOMO-1→LUMO+2 (17%); HOMO→LUMO+3 (33%)
404	0.2003	HOMO-1→LUMO+2 (22%); HOMO→LUMO+4 (52%)
398	0.7608	HOMO-3→LUMO+2 (10%); HOMO-1→LUMO+3 (47%); HOMO→LUMO+2 (14%)
388	0.3064	HOMO-6→LUMO+1 (28%); HOMO-5→LUMO (14%); HOMO-2→LUMO+2 (25%); HOMO-1→LUMO+2 (10%)
384	0.1550	HOMO-2→LUMO+3 (88%)

361	0.2161	HOMO-3→LUMO+2 (33%); HOMO-3→LUMO+3 (11%)
361	0.2756	HOMO-4→LUMO+3 (16%); HOMO-3→LUMO+2 (16%); HOMO-3→LUMO+3 (22%)
355	0.3074	HOMO-11→LUMO+1 (13%); HOMO-6→LUMO+3 (38%); HOMO-5→LUMO+2 (26%)
353	0.1615	HOMO-6→LUMO+2 (23%); HOMO-5→LUMO+2 (47%)
351	0.1223	HOMO-6→LUMO+3 (36%); HOMO-5→LUMO+2 (29%); HOMO-3→LUMO+2 (13%)

Figure S59. Calculated vertical transitions and major transitions of **6Ni'** calculated by TD-DFT using B3LYP employing the 6-31G(d) basis set.

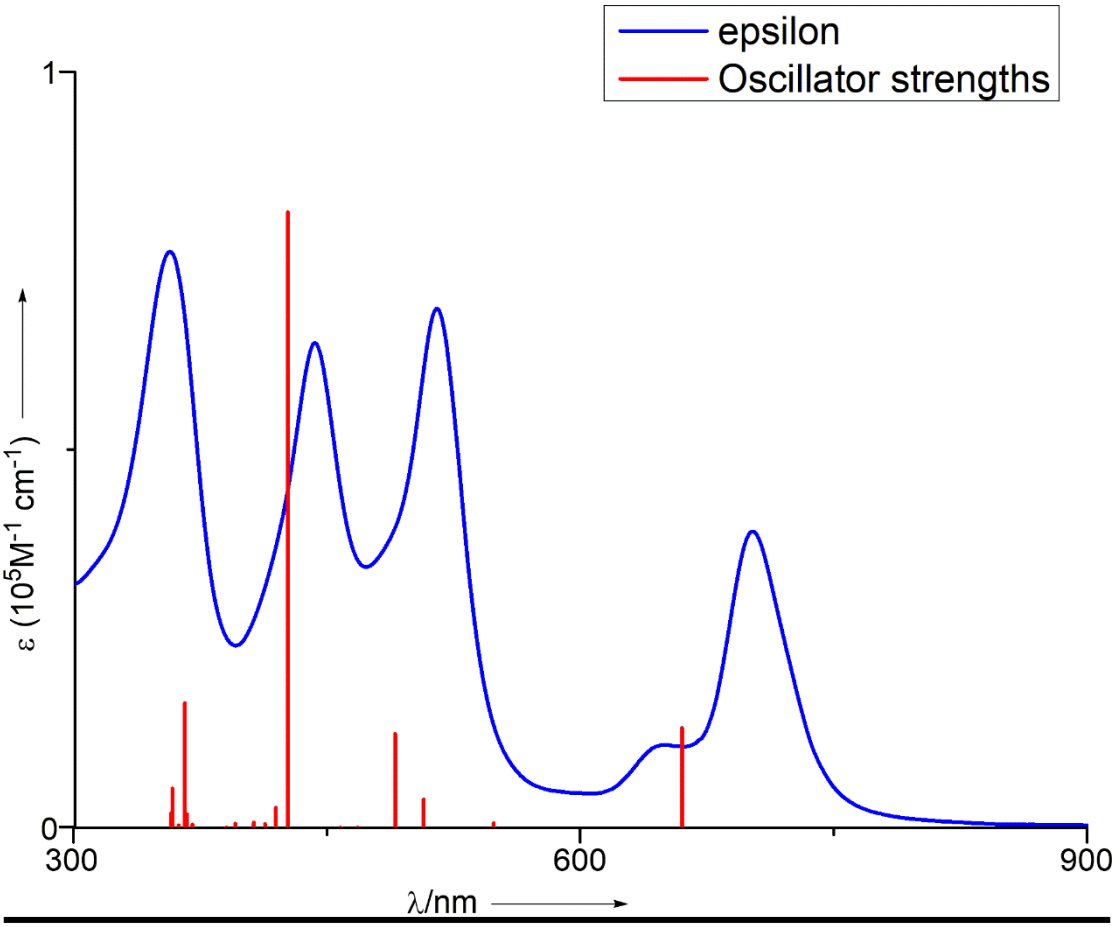

Wavelength (nm)	Oscillator Strengths	Major Transitions
660	0.1321	HOMO-1→LUMO+1 (12%); HOMO→LUMO (87%)
660	0.1321	HOMO-1→LUMO (12%); HOMO→LUMO+1 (87%)
490	0.1243	HOMO-1→LUMO+1 (37%); HOMO→LUMO+4 (31%)

490	0.1243	HOMO→LUMO (37%); HOMO→LUMO+5 (31%)
427	0.8146	HOMO-1→LUMO+1 (25%); HOMO→LUMO+4 (55%)
427	0.8146	HOMO-1→LUMO (25%); HOMO→LUMO+5 (55%)
366	0.1650	HOMO-8→LUMO (10%); HOMO-1→LUMO+5 (56%)
366	0.1650	HOMO-8→LUMO+1 (10%); HOMO-1→LUMO+4 (56%)

Figure S60. Calculated vertical transitions and major transitions of **7Ni** calculated by TD-DFT using B3LYP employing the 6-31G(d) basis set.

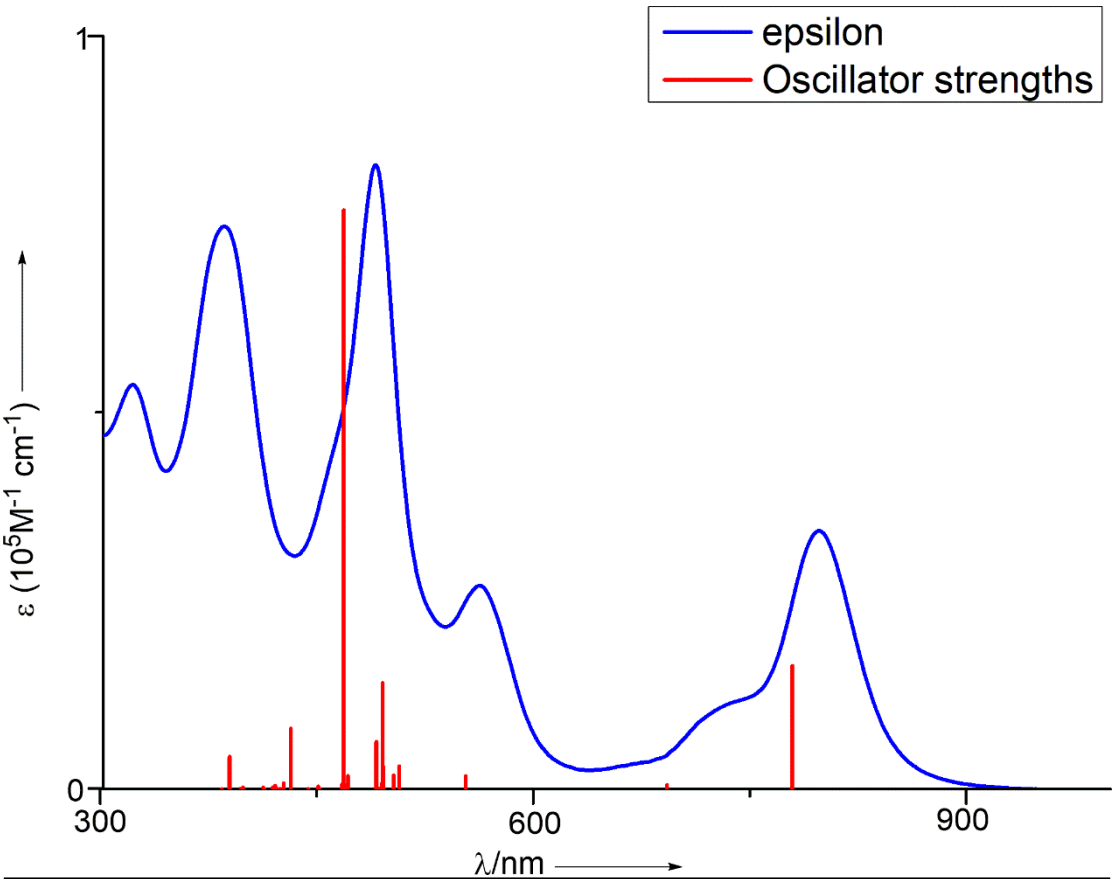

Wavelength (nm)	Oscillator Strengths	Major Transitions
780	0.1640	HOMO→LUMO (94%)
779	0.1640	HOMO→LUMO+1 (94%)
496	0.1411	HOMO-5→LUMO (24%); HOMO-4→LUMO+1 (16%); HOMO-1→LUMO (11%)
496	0.1395	HOMO-5→LUMO+1 (24%); HOMO-4→LUMO (17%); HOMO-1→LUMO+1 (11%)

469	0.7693	HOMO-5→LUMO (28%); HOMO-1→LUMO (21%); HOMO→LUMO+4 (12%) HOMO→LUMO+5 (12%)
469	0.7531	HOMO-5→LUMO+1 (27%); HOMO-1→LUMO+1 (20%); HOMO→LUMO+4 (13%); HOMO→LUMO+5 (12%)

Figure S61. Calculated vertical transitions and major transitions of **8Ni** calculated by TD-DFT using B3LYP employing the 6-31G(d) basis set.

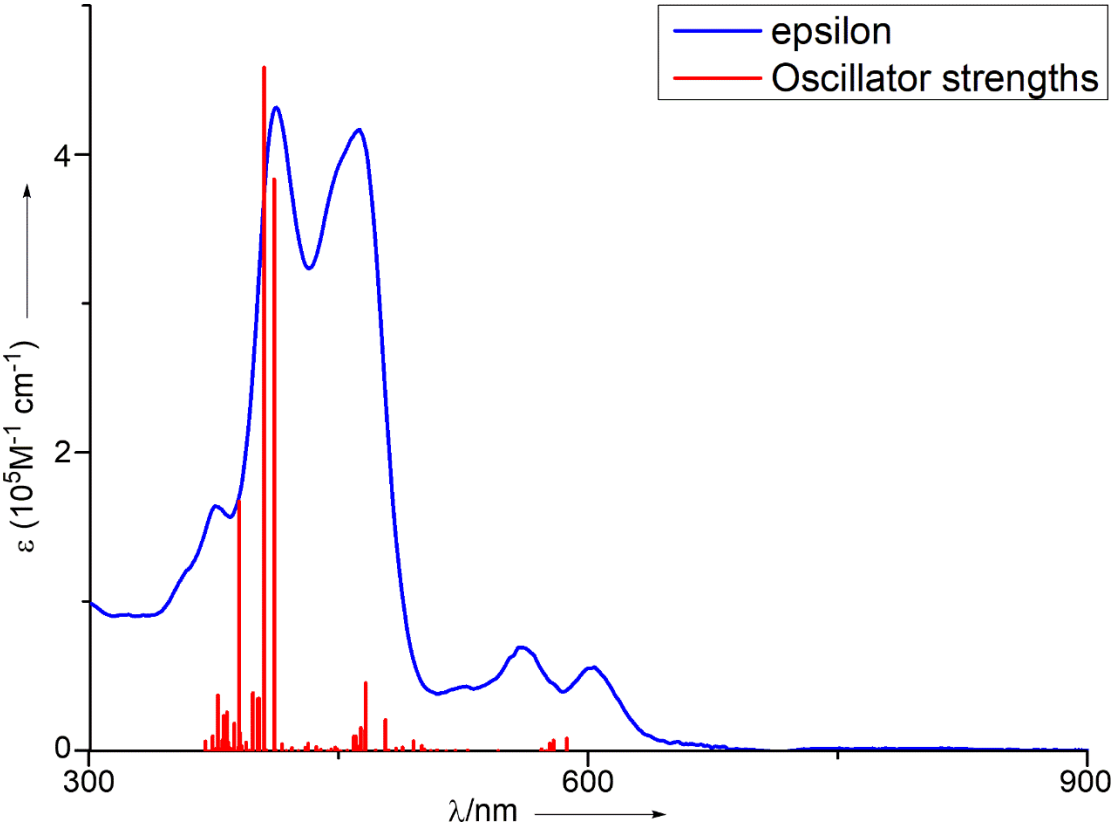

Wavelength (nm)	Oscillator Strengths	Major Transitions
466	0.297	HOMO-2→LUMO+6 (12%); HOMO-1→LUMO+2 (10%) HOMO-1→LUMO+6 (21%); HOMO-1→LUMO+7 (18%)
411	2.4932	HOMO-3→LUMO+5 (32%); HOMO→LUMO+7 (21%)
405	2.9809	HOMO-5→LUMO+3 (17%); HOMO-4→LUMO+4 (14%); HOMO-2→LUMO+6 (11%)
402	0.2306	HOMO→LUMO+10 (63%)
401	0.2267	HOMO-10→LUMO+1 (21%); HOMO-10→LUMO+2 (25%)
399	0.2539	HOMO-3→LUMO+7 (38%); HOMO→LUMO+5 (18%)
390	1.0887	HOMO-5→LUMO+6 (27%); HOMO-4→LUMO+7 (10%); HOMO-2→LUMO+3 (15%)

378	0.2437	HOMO-4→LUMO+10 (79%)

Figure S62. Calculated vertical transitions and major transitions of **12Ni** calculated by TD-DFT using B3LYP employing the 6-31G(d) basis set.

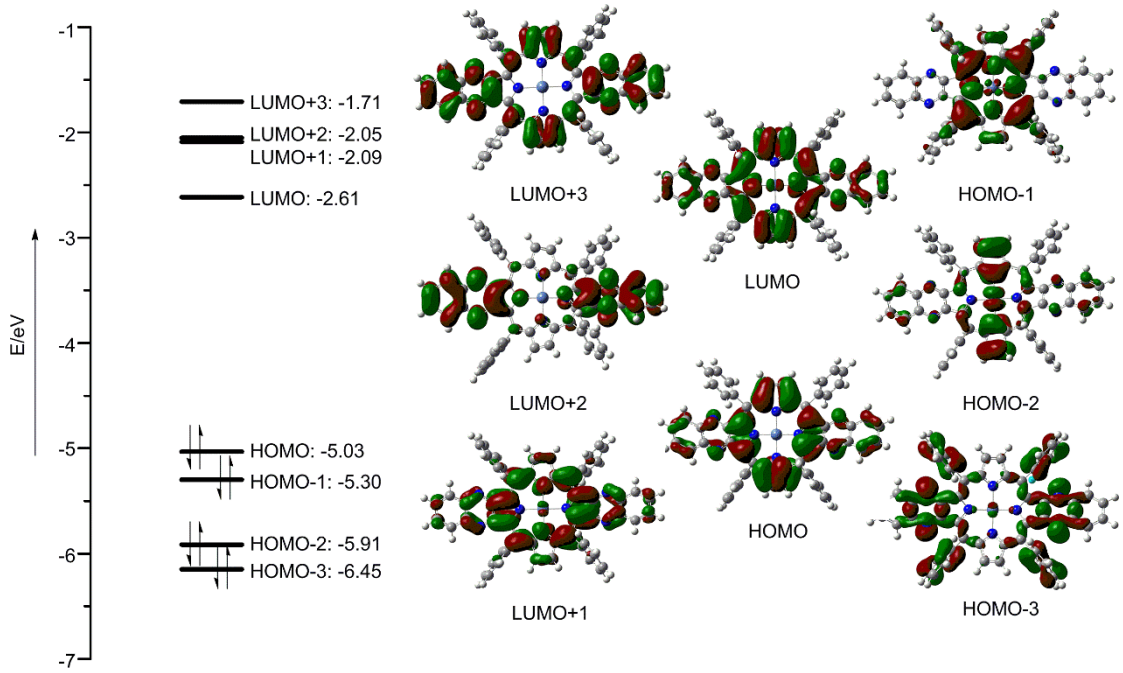

Figure S63. Energy diagram and selected Kohn–Sham orbitals of **5Ni**.

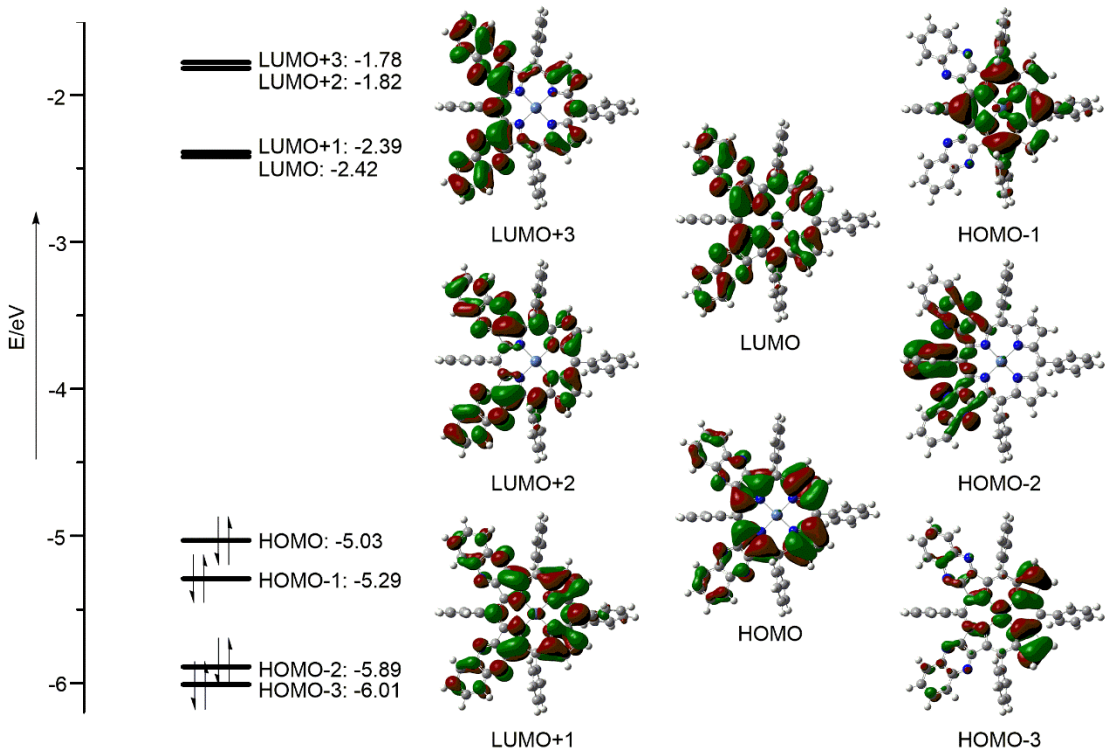

Figure S64. Energy diagram and selected Kohn–Sham orbitals of **5Ni'**.

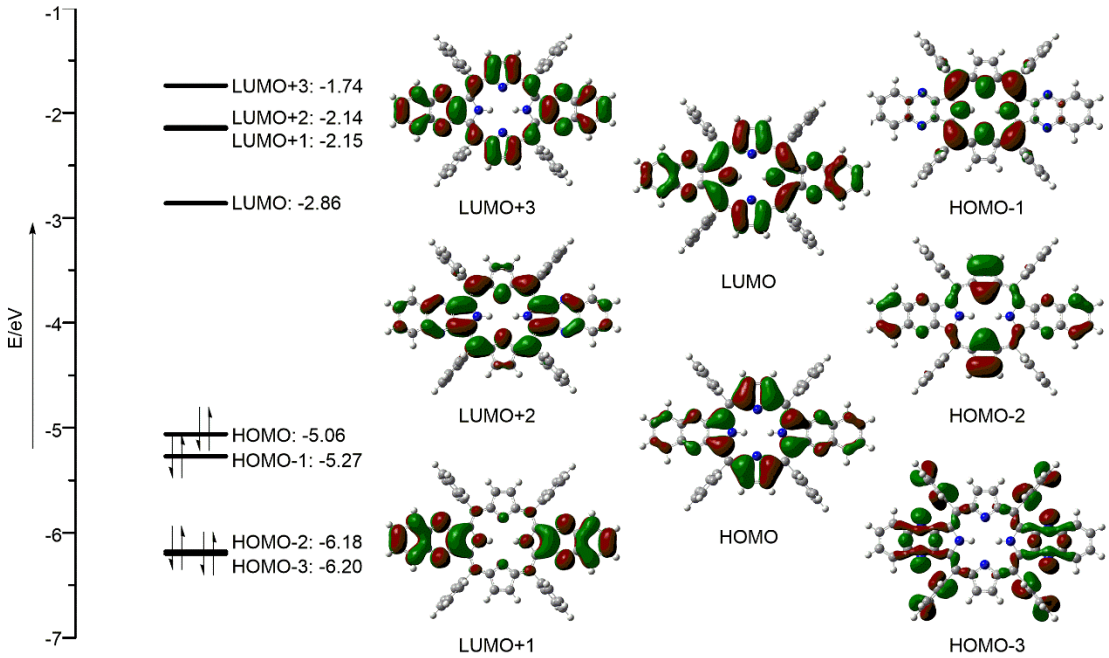

Figure S65. Energy diagram and selected Kohn–Sham orbitals of **5H**.

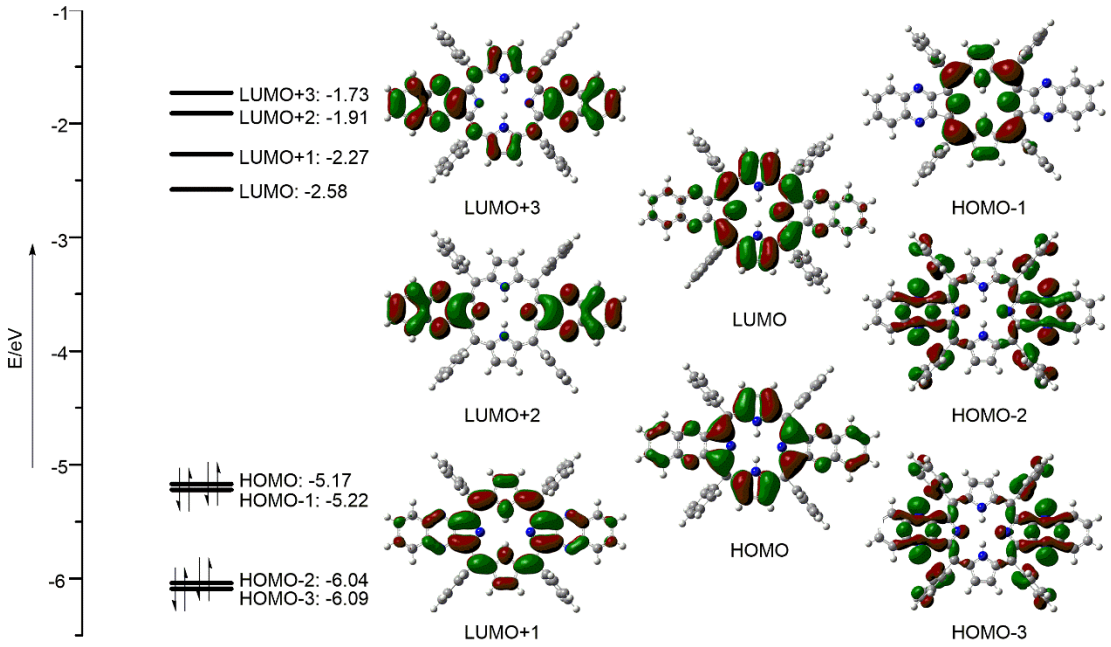

Figure S66. Energy diagram and selected Kohn–Sham orbitals of **5H'**.

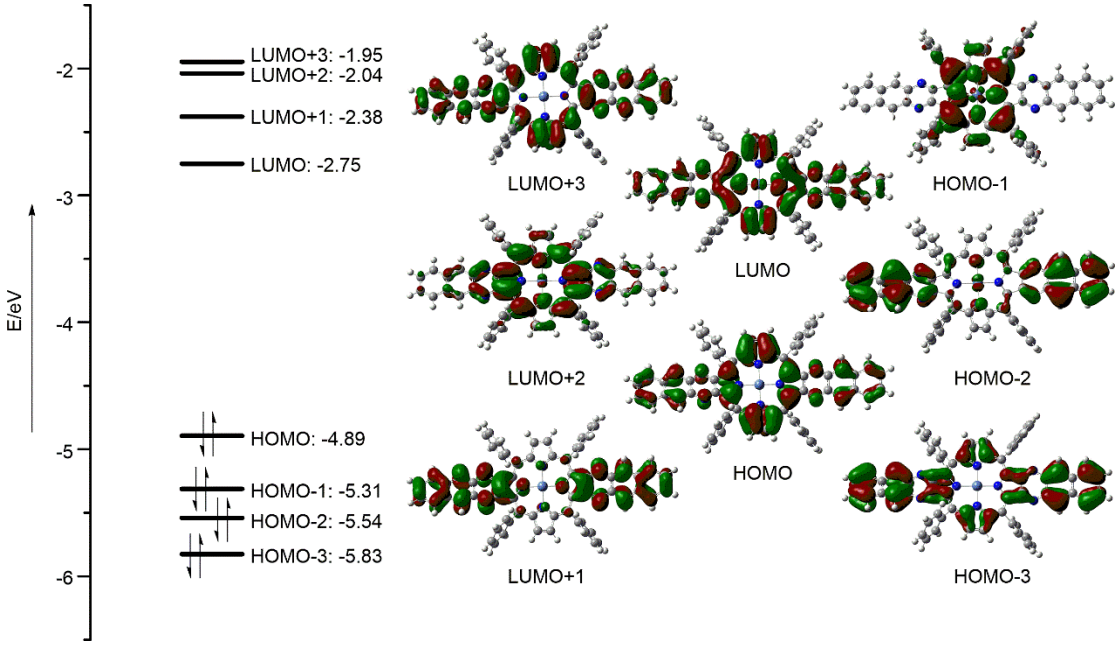

Figure S67. Energy diagram and selected Kohn–Sham orbitals of **6Ni**.

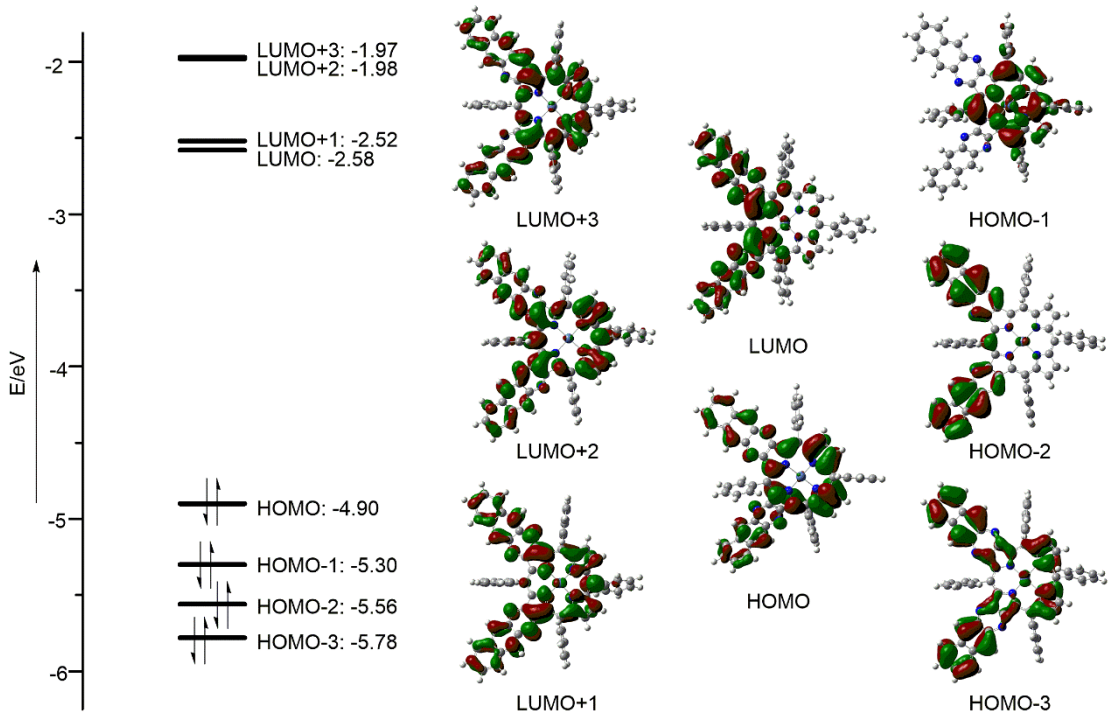

Figure S68. Energy diagram and selected Kohn–Sham orbitals of **6Ni'**.

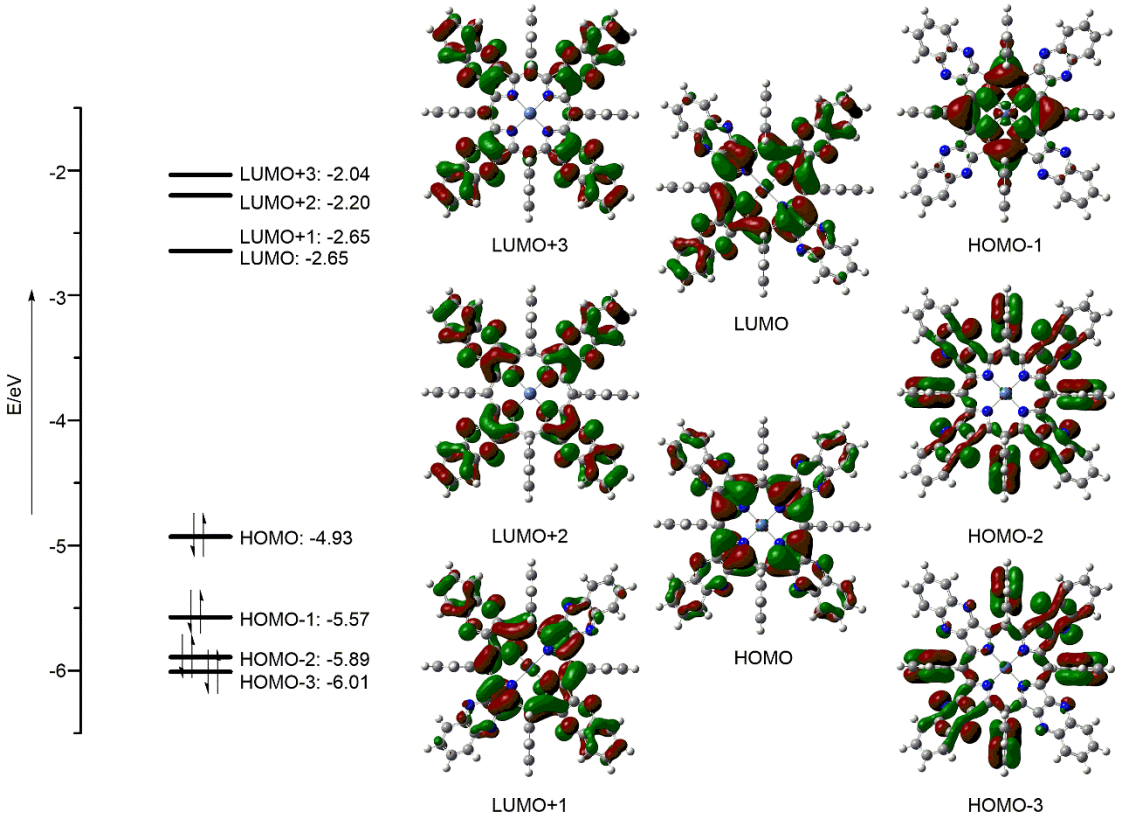

Figure S69. Energy diagram and selected Kohn–Sham orbitals of **7Ni**.

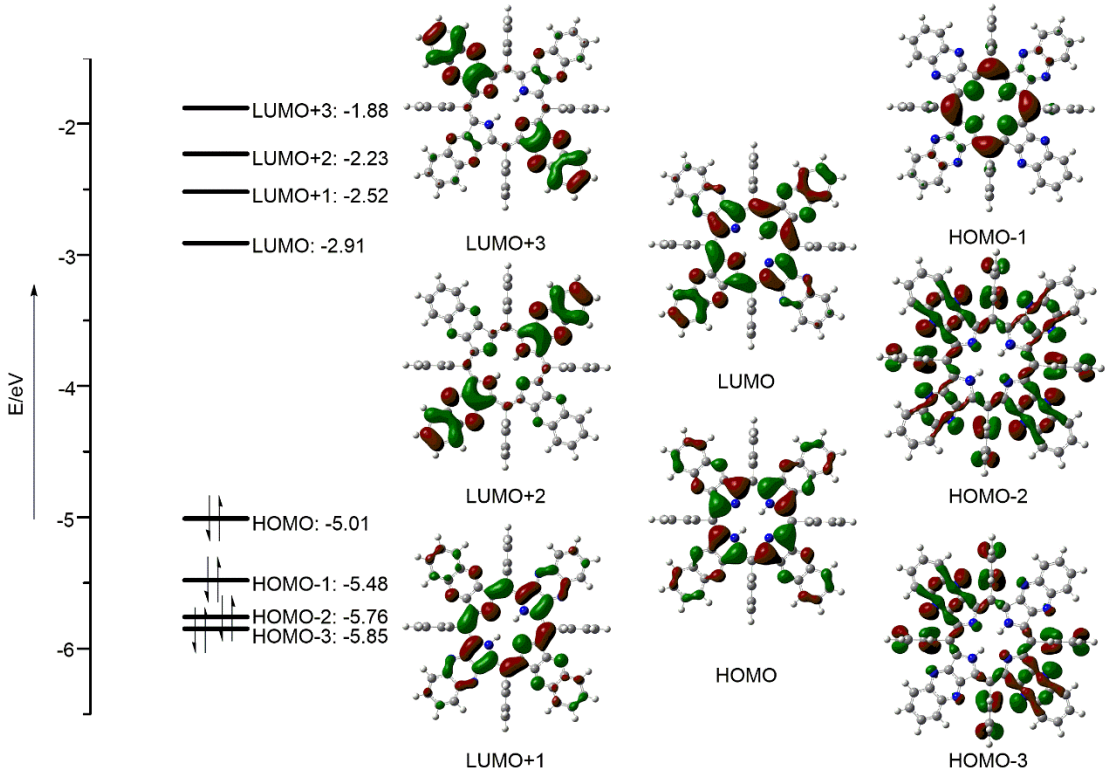

Figure S70. Energy diagram and selected Kohn–Sham orbitals of **7H**.

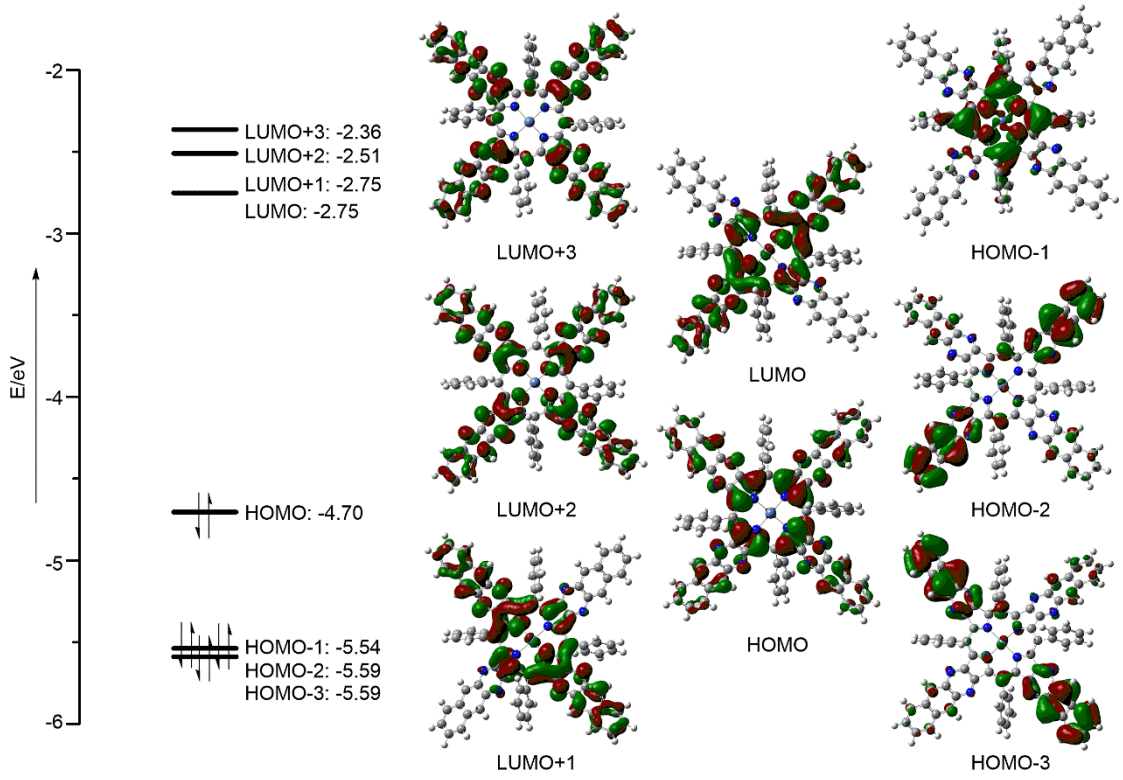

Figure S71. Energy diagram and selected Kohn–Sham orbitals of **8Ni**.

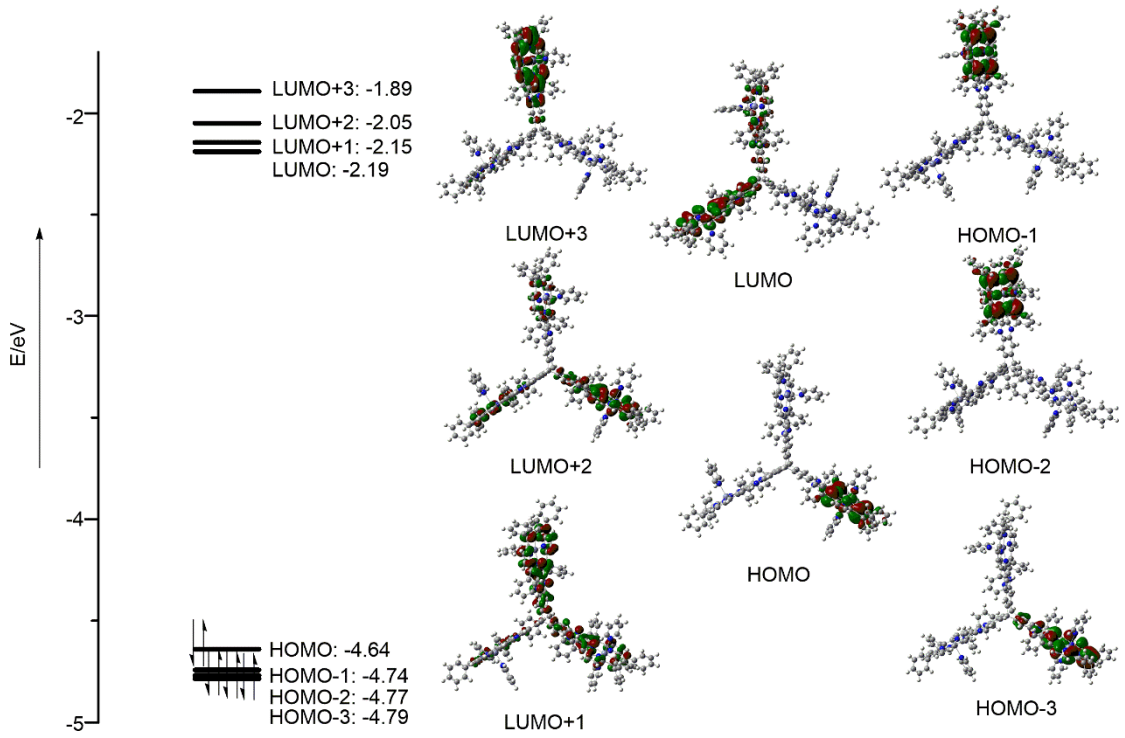

Figure S72. Energy diagram and selected Kohn–Sham orbitals of **12Ni**.

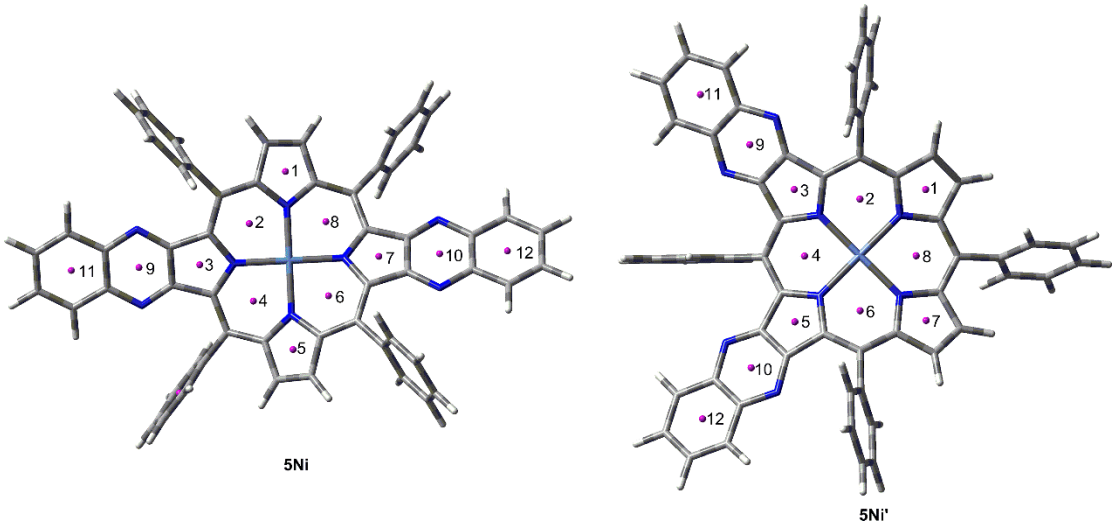

Ring of 5Ni	NICS(0) value / ppm	**Ring of 5Ni'**	NICS(0) value / ppm
1	-6.9102	1	-7.2244
2	-16.3188	2	-15.8892
3	-0.4045	3	0.1196
4	-16.5558	4	-16.0439
5	-6.9252	5	0.0330
6	-16.4016	6	-15.8291

7	-0.4178	7	-7.1573
8	-16.3562	8	-15.6082
9	-8.3340	9	-8.1737
10	-8.2973	10	-8.1588
11	-9.7713	11	-9.6640
12	-9.7977	12	-9.6379

Figure S73. Calculated NICS values of **5Ni** and **5Ni'**.

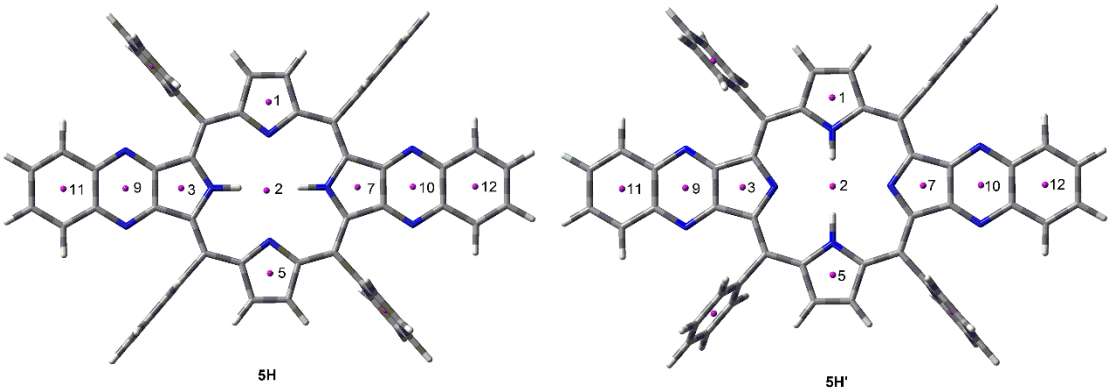

Ring of 5H	NICS(0) value / ppm	**Ring of 5H'**	NICS(0) value / ppm
1	-2.0594	1	-12.6667
3	-4.0872	3	3.5952
5	-2.1632	5	-12.6532
7	-4.0607	7	3.5679
2	-13.4603	2	-13.6956
9	-9.8103	9	-7.2550
10	-9.8043	10	-7.2316
11	-9.9806	11	-9.6295
12	-9.9913	12	-9.6562

Figure S74. Calculated NICS values of **5H** and **5H'**.

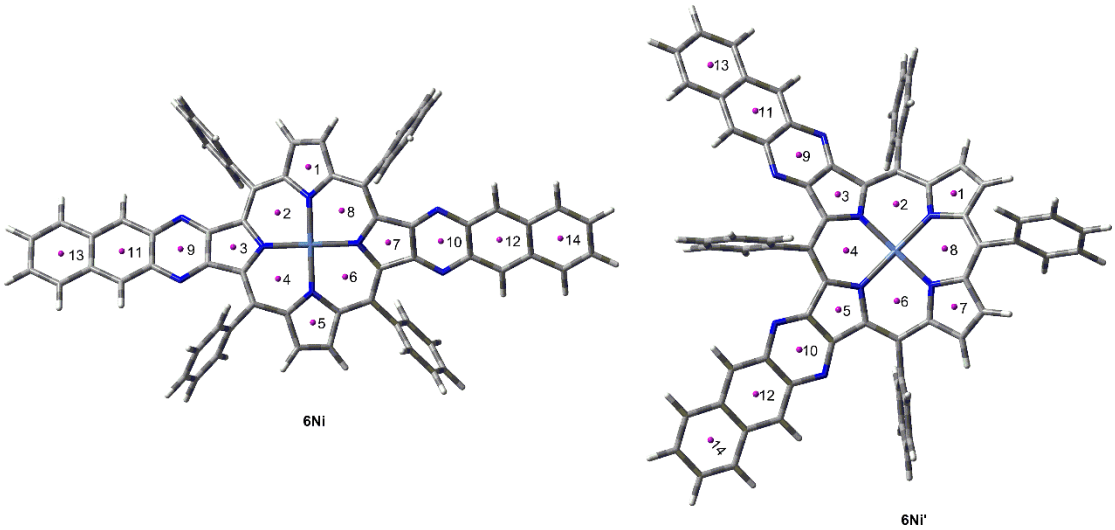

Ring of 6Ni	NICS(0) value / ppm	**Ring of 6Ni'**	NICS(0) value / ppm
1	-6.9027	1	-7.2566
2	-15.6450	2	-15.1790
3	1.4705	3	1.9021
4	-15.8558	4	-15.5111
5	-7.0121	5	2.0572
6	-16.1683	6	-15.0316
7	1.3328	7	-7.2393
8	-16.0294	8	-14.8311
9	-7.4736	9	-7.1858
10	-7.3032	10	-7.1108
11	-12.9369	11	-12.7525
12	-12.8931	12	-12.7635
13	-8.8655	13	-8.7783
14	-8.9048	14	-8.8627

Figure S75. Calculated NICS values of **6Ni** and **6Ni'**.

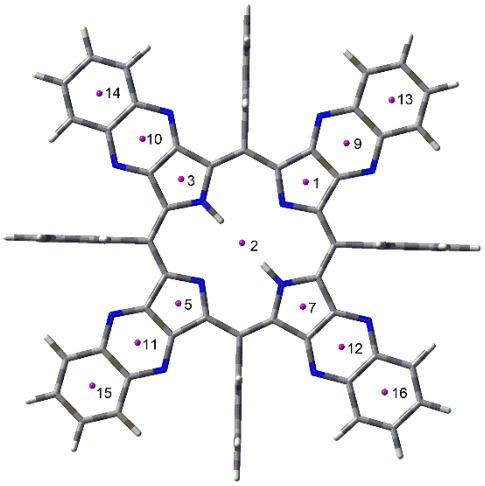

7H

Ring of 7H	NICS(0) value / ppm	**Ring of 7H**	NICS(0) value / ppm
1	3.5052	3	-4.2199
5	3.5046	7	-4.2198
2	-12.5702	9	-7.4142
10	-9.9086	11	-7.4140
12	-9.9087	13	-9.3731
14	-9.7025	15	-9.3729
16	-9.7026		

Figure S76. Calculated NICS values of **7H**.

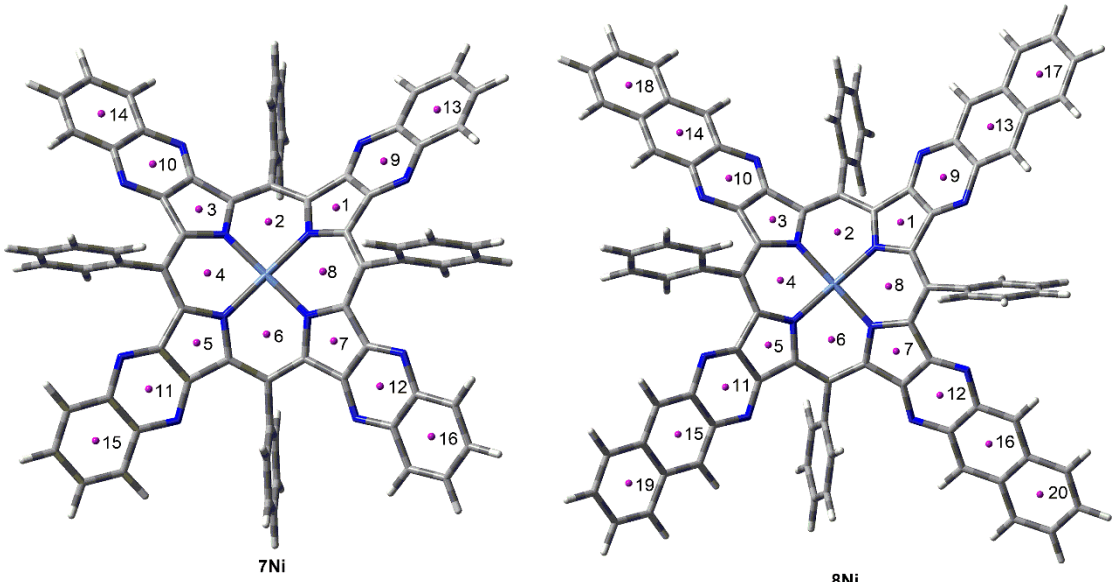

Ring of 7Ni	NICS(0) value / ppm	**Ring of 8Ni**	NICS(0) value / ppm
1	-1.2817	1	0.6198
2	-14.8445	2	-13.9754
3	-1.2816	3	0.3538
4	-14.8446	4	-13.7352
5	-1.2816	5	0.6615
6	-14.8447	6	-13.8249
7	-1.2814	7	0.6164
8	-14.8448	8	-14.0064
9	-8.3624	9	-7.3937
10	-8.3623	10	-7.4238
11	-8.3621	11	-7.4299
12	-8.3623	12	-7.4691
13	-9.5148	13	-12.7307
14	-9.5148	14	-12.6954
15	-9.5149	15	-12.6935
16	-9.5148	16	-12.6942
		17	-8.8472
		18	-8.7337
		19	-8.7621
		20	-8.7091

Figure S77. Calculated NICS values of **7Ni** and **8Ni**.

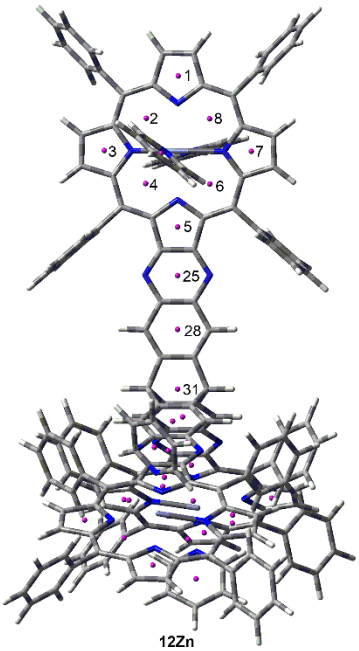

12Zn

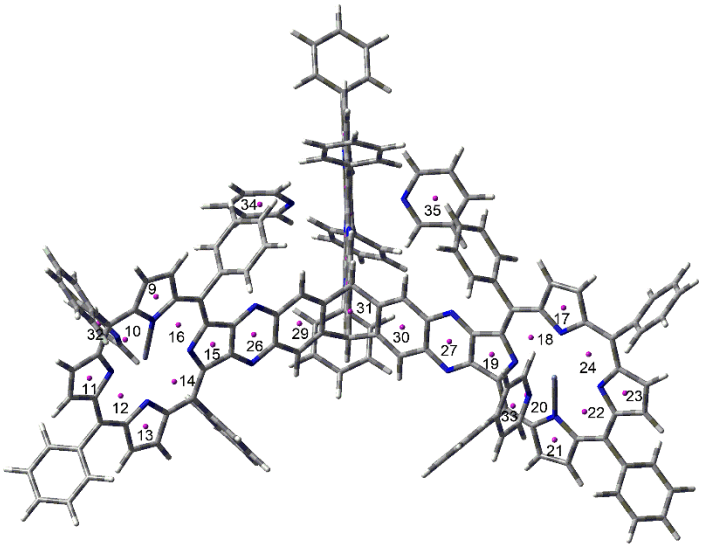

12Zn

Ring of 12Zn	NICS(0) value / ppm	**Ring of 12Zn**	NICS(0) value / ppm
1	-6.1535	19	1.2953
2	-14.5388	20	-15.0484
3	-5.9966	21	-7.0963
4	-14.5741	22	-14.7567
5	1.2008	23	-7.0427
6	-14.5961	24	-14.8208
7	-6.8156	25	-8.0216
8	-14.8239	26	-8.2283
9	-6.8979	27	-8.1486
10	-14.8529	28	-9.1626
11	-7.1219	29	-9.0434
12	-14.7622	30	-9.3093
13	-6.9336	31	3.7639
14	-14.9016	32	-11.8904
15	1.1506	33	-11.8542
16	-14.8176	34	-12.1732
17	-6.9342	35	-12.1772
18	-14.7804		

Figure S78. Calculated NICS values of **12Zn**.

Singlet Oxygen Production

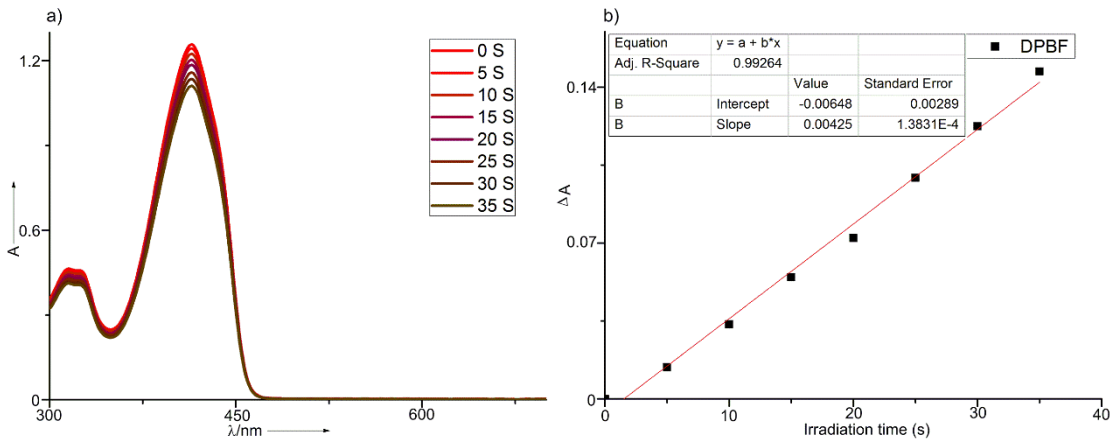

Figure S79 Changes in the absorption spectra of **DPBF** (6.3×10^{-5} mol/L) at 414 nm upon irradiation (λ_{irr} = 450-460 nm). b) Plot of change in absorbance of **DPBF** at 414 nm *vs* irradiation time.

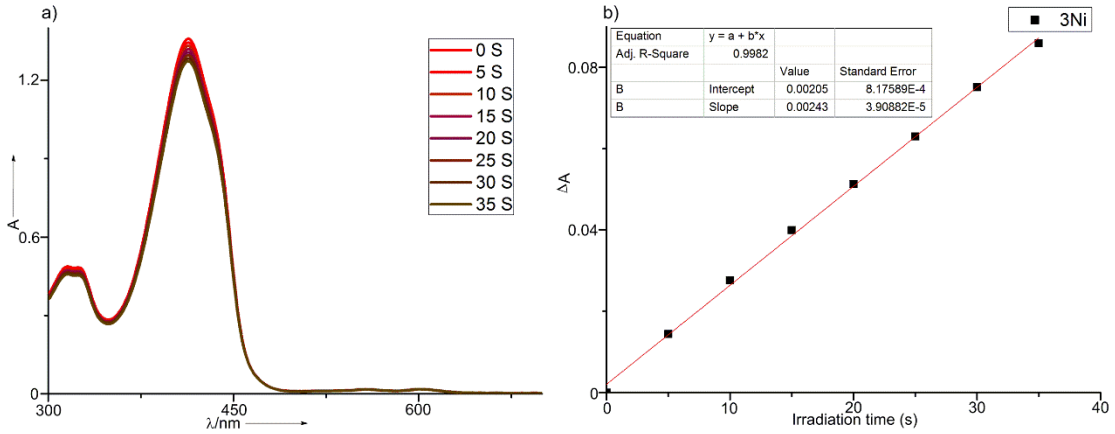

Figure S80 Changes in the absorption spectra of **DPBF** (6.3×10^{-5} mol/L) at 414 nm upon irradiation (λ_{irr} = 450-460 nm) in the presence of **3Ni** (1.3×10^{-6} mol/L). b) Plot of change in absorbance of **DPBF** at 413 nm *vs* irradiation time in the presence of **3Ni**.

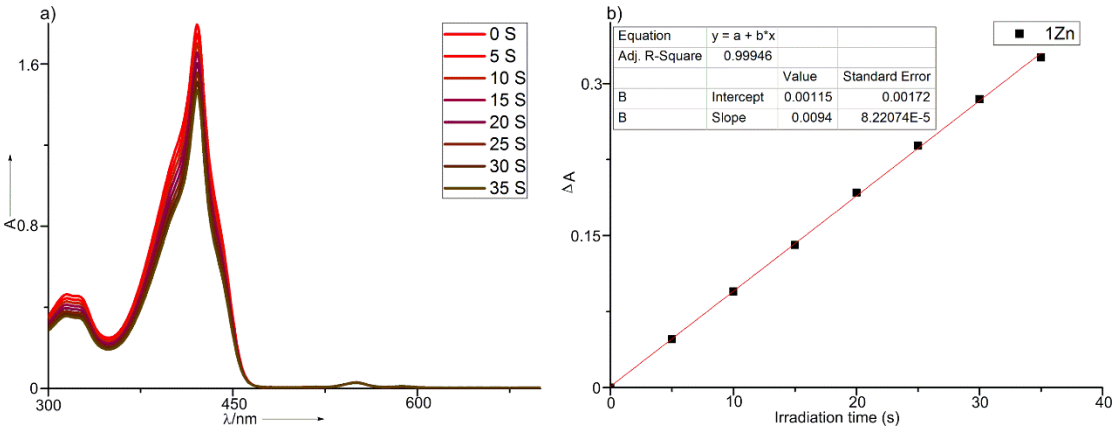

Figure S81 Changes in the absorption spectra of **DPBF** (6.3×10^{-5} mol/L) at 414 nm upon irradiation (λ_{irr} = 450-460 nm) in the presence of **1Zn** (1.3×10^{-6} mol/L). b) Plot of change in absorbance of **DPBF** at 421 nm *vs* irradiation time in the presence of **1Zn**.

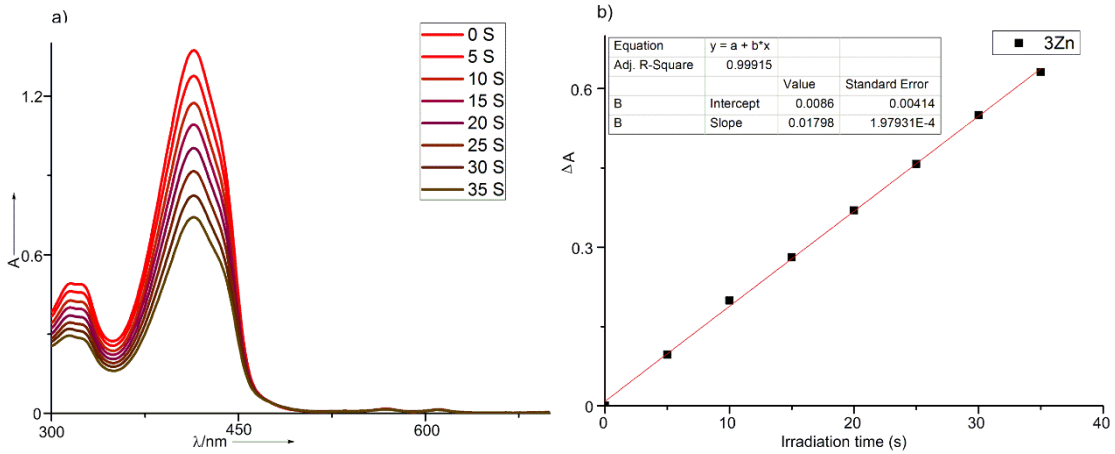

Figure S82. a) Changes in the absorption spectra of **DPBF** (6.3×10^{-5} mol/L) at 414 nm upon irradiation (λ_{irr} = 450-460 nm) in the presence of **3Zn** (1.3×10^{-6} mol/L). b) Plot of change in absorbance of **DPBF** at 414 nm *vs* irradiation time in the presence of **3Zn**.

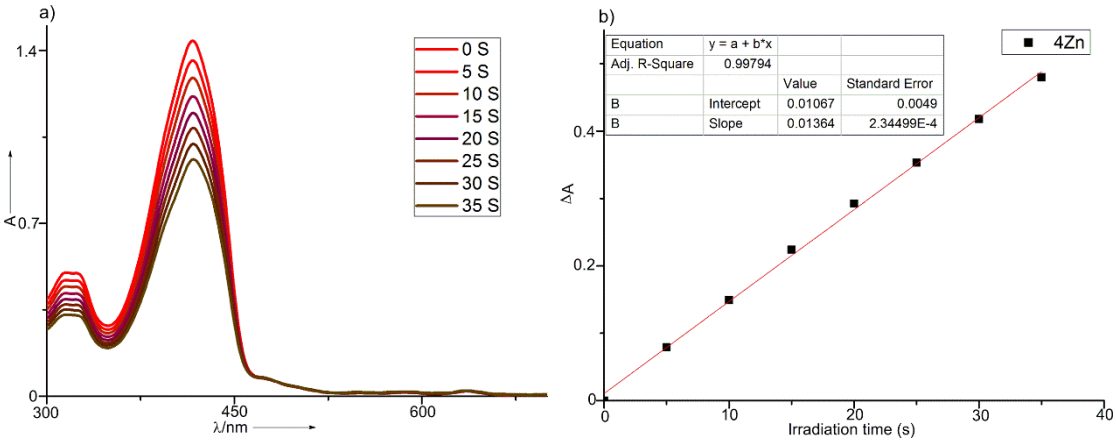

Figure S83. a) Changes in the absorption spectra of **DPBF** (6.3×10^{-5} mol/L) at 414 nm upon irradiation (λ_{irr} = 450-460 nm) in the presence of **4Zn** (1.3×10^{-6} mol/L). b) Plot of change in absorbance of **DPBF** at 417 nm *vs* irradiation time in the presence of **4Zn**.

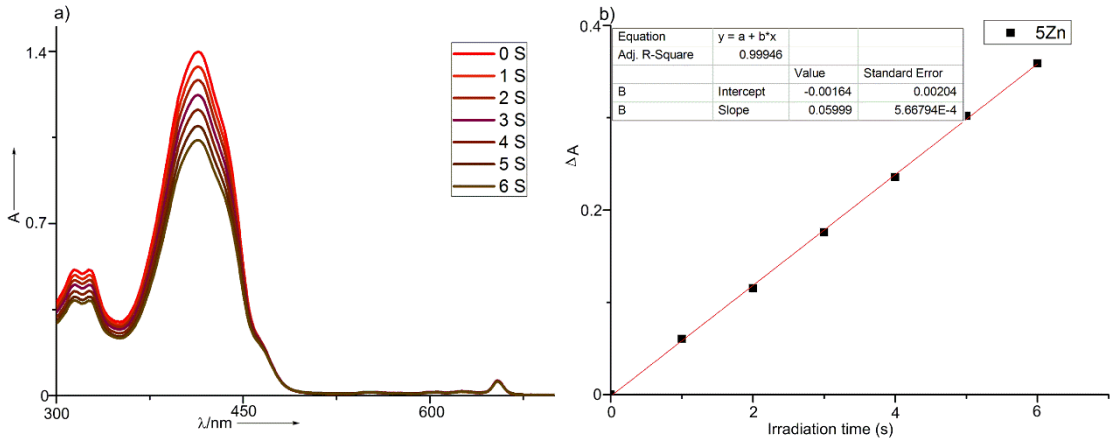

Figure S84. a) Changes in the absorption spectra of **DPBF** (6.3×10^{-5} mol/L) at 414 nm upon irradiation (λ_{irr} = 450-460 nm) in the presence of **5Zn** (1.3×10^{-6} mol/L). b) Plot of change in absorbance of **DPBF** at 414 nm *vs* irradiation time in the presence of **5Zn**.

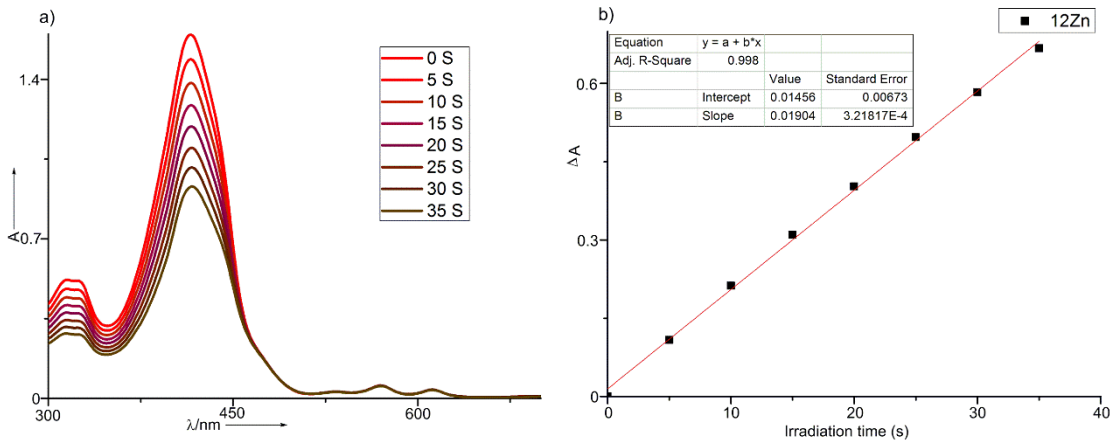

Figure S85. a) Changes in the absorption spectra of **DPBF** (6.3×10^{-5} mol/L) at 416 nm upon irradiation (λ_{irr} = 450-460 nm) in the presence of **12Zn** (1.3×10^{-6} mol/L). b) Plot of change in absorbance of **DPBF** at 414 nm *vs* irradiation time in the presence of **12Zn**.

Electrocatalytic Hydrogen Evolution Reaction

1.0 mg of rGO was mixed with 1 mL of isopropyl alcohol containing 0.2% nafion and the mixture sonicated in an ultrasonic bath for 30 min to produce a homogeneous mixture of concentration 1 mg/mL. The surface of the glassy carbon electrode (GCE) was polished with 0.05 µm alumina and rinsed with doubly distilled water in the ultrasonic bath to remove any adhered Al_2O_3 particles. The electrodes were rinsed with ethanol and dried under room temperature for ca. 5 min. Three 3 µL of the rGO/isopropyl alcohol/nafion suspensions were drop cast on the surface of the GC electrode and allowed to dry at room temperature. 10 µL aliquots of 0.2 mM dichloromethane solutions of **3Ni** to **10Ni** and **12Ni** were added dropwise to the rGO/nafion-coated electrodes and dried at room temperature for 1 h. The electrodes were stored in MilliQ water in the dark.

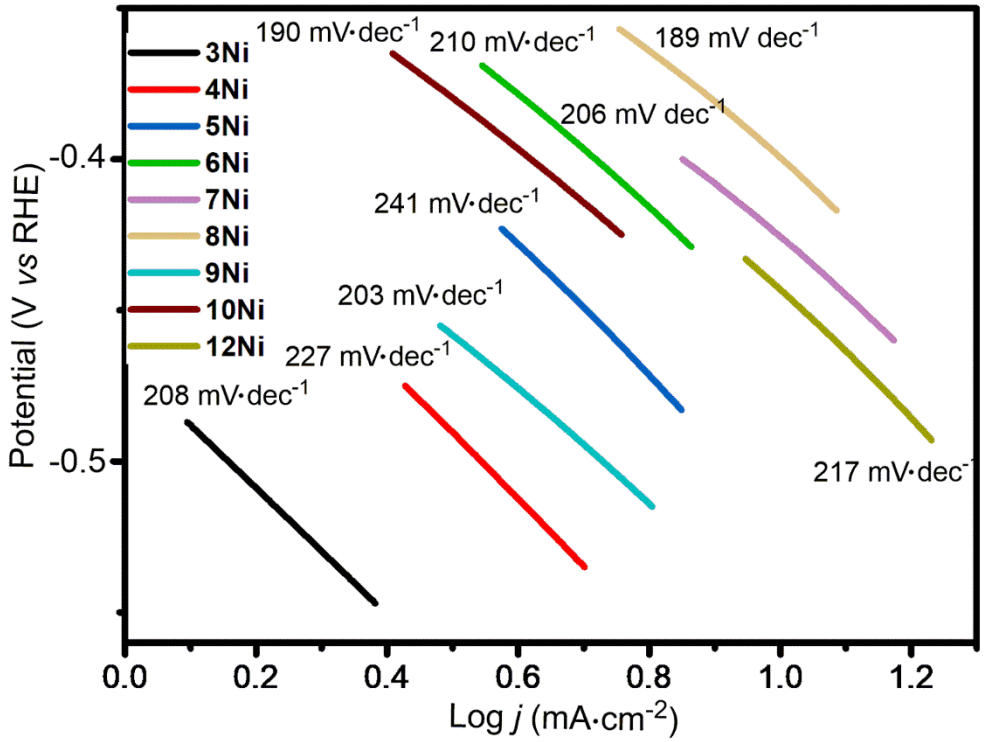

Figure S86. Calculated Tafel slops of **3Ni**/rGO to **10Ni**/rGO and **12Ni**/rGO.

Table S10. Onset potentials and Tafel slope values of **3Ni**/rGO to **10Ni**/rGO and **12Ni**/rGO

Compound	**3Ni**	**4Ni**	**5Ni**	**6Ni**	**7Ni**	**8Ni**	**9Ni**	**10Ni**	**12Ni**
Onset Potentials (mV)	-450	-380	-315	-295	-293	-262	-377	-300	-291
Tafel Slops (mV/dec)	208	227	241	210	206	189	203	190	217

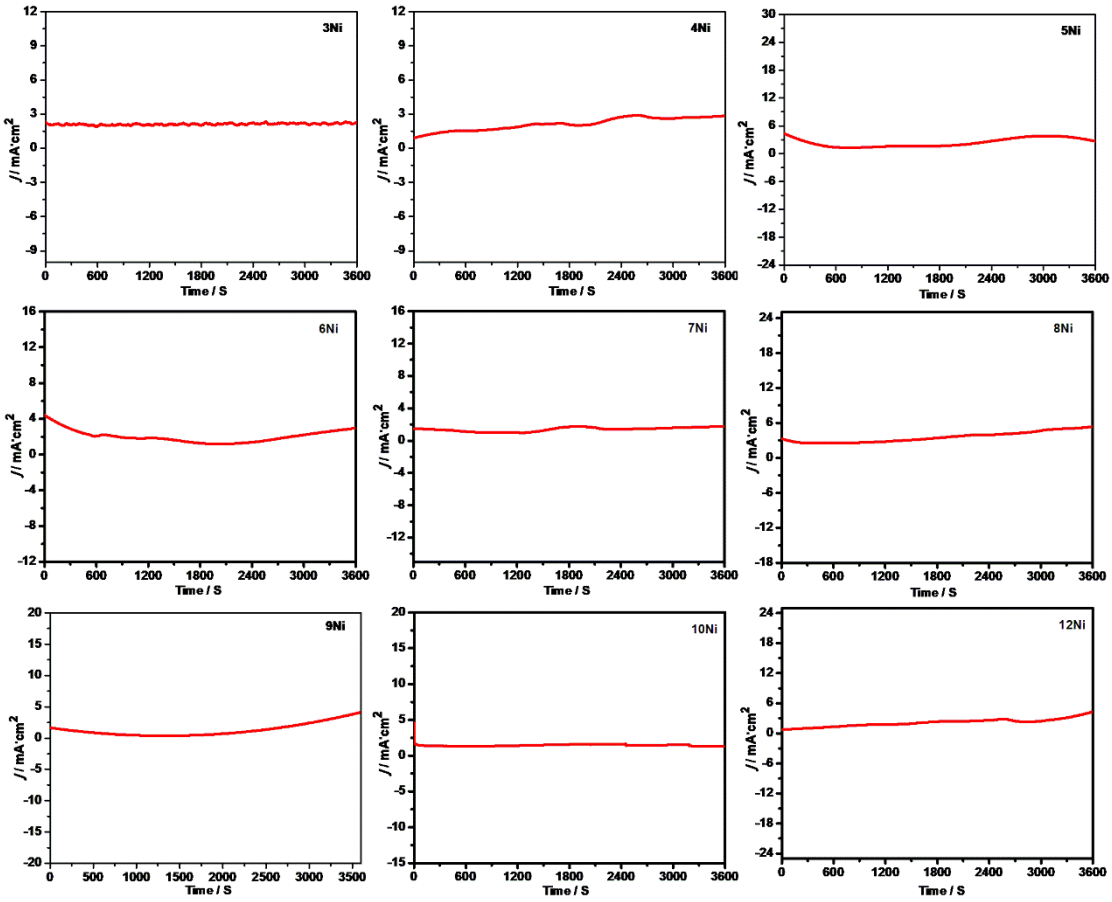

Figure S87. *i-t* curves of **3Ni**/rGO to **10Ni**/rGO and **12Ni**/rGO in 0.5 M H_2SO_4.

References

[1] (*a*) K.-L. Li, C.-C. Guo and Q.-Y. Chen, Efficient one-pot regioselective synthesis of 2,3-dibromo-5,10,15,20-tetra-arylporphyrins from 5,10,15,20-tetraarylchlorins, *Synlett*, 2009, 2867-2871; (*b*) R. Deshpande, L. Jiang, G. Schmidt, J. Rakovan, X Wang, K. Wheeler and H. Wang, A concise approach to the synthesis of opp-dibenzoporphyrins through the Heck reaction, *Org. Lett.*, 2009, **11**, 4251-4253; (*c*) L. Jiang, R. A. Zaenglein, J. T. Engle, C. Mittal, C. S. Hartley, C. J. Ziegler and H. Wang, Water-soluble ionic benzoporphyrins, *Chem. Commun.*, 2012, **48**, 6927-6929.

[2] (*a*) N. G. White and M. J. MacLachlan, Soluble tetraaminotriptycene precursors, *J. Org. Chem.*, 2015, **80**, 8390-8397; (*b*) J. H. Chong and M. J. MacLachlan, Robust non-interpenetrating coordination frameworks from new shape-persistent building blocks, *Inorg. Chem.*, 2006, **45**, 1442-1444; (*c*) M. Mastalerz, S. Sieste, M. Ceninć and I. M Oppel, Two-step synthesis of hexaammonium triptycene: an air-stable building block for condensation reactions to extended

triptycene derivatives, *J. Org. Chem.*, 2011, **76**, 6389-6391.

[3] (*a*) T. Khoury and M. J. Crossley, A strategy for the stepwise ring annulation of all four pyrrolic rings of a porphyrin, *Chem. Commun.*, 2007, 4851-4853; (*b*) M. J. Crossley, C. S. Sheehan, T. Khoury, J. R. Reimers and P. J. Sintic, Construction of building blocks for extended porphyrin arrays by nitration of porphyrin-2,3-diones and quinoxalino[2,3-b]porphyrins, *New J. Chem.*, 2008, **32**, 340-352.

[4] O. V. Dolomanov, L. J. Bourhis, R. J. Gildea, J. A. K. Howard and H. Puschmann, OLEX2: A complete structure solution, refinement and analysis program *J. Appl. Cryst.*, 2009, **42**, 339-341.

[5] L. J. Bourhis, O. V. Dolomanov, R. J. Gildea, J. A. K. Howard and H. Puschmann, The anatomy of a comprehensive constrained, restrained refinement program for the modern computing environment-Olex2 dissected, *Acta Cryst.*, 2015, **A71**, 59-75.

[6] G. M. Sheldrick, Crystal structure refinement with SHELXL *Acta Cryst.*, 2015, **C71**, 3-8.